Study of the interaction between GPI2 and GPI19 in GPI anchor biosynthesis and their effects on Ras1 in *Candida albicans*

Thesis submitted to Jawaharlal Nehru University

for the award of degree of

DOCTOR OF PHILOSOPHY

V.A.PRATYUSHA

SCHOOL OF LIFE SCIENCES
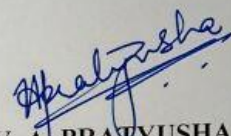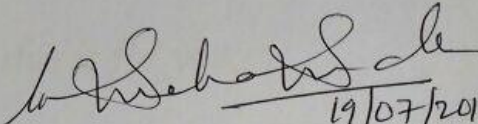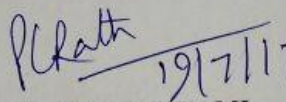
JAWAHARLAL NEHRU UNIVERSITY

NEW DELHI-110067

INDIA

2017

SCHOOL OF LIFE SCIENCES
JAWAHARLAL NEHRU UNIVERSITY
NEW DELHI-110067 INDIA

CERTIFICATE

The research work reported in this thesis entitled **"Study of the interaction between GPI2 and GPI19 in GPI anchor biosynthesis and their effects on Ras1 in *Candida albicans*"** has been carried out in the School of Life Sciences, Jawaharlal Nehru University, New Delhi-110067, India. This work is original and has not been submitted so far, in part or in full, for award of any degree or diploma of any university.

V. A. PRATYUSHA
(Candidate)

19/07/2017
PROF. SNEHA SUDHA KOMATH
(Supervisor)

19/7/17
for **PROF. S.K. GOSWAMI**
(Dean)

Dedicated

to

Amma

Amma and nanna, this is for you.

Acknowledgement

This is my small step in thanking the people involved in the completion of my Ph.D thesis. Firstly I would like to acknowledge my mother and the almighty without whose support I would never have been able to give shape to this thesis.

I would like to acknowledge my Ph.D supervisor, Prof. Sneha Sudha Komath for mentoring me throughout the course of this study. Working with her has taught me how to think in a scientific and an unbiased manner. She has been a source of constant motivation for me. Her never say die attitude, especially in times of failed experiments, has taught me that perseverance will always payoff in the long run. Her ever approachable nature made working with her so much more easy and comfortable. Being available at all times for your students is a rare quality and ma'am, I was fortunate that I could complete my doctoral studies under your guidance.

I would also like to thank Dr. Sobhan Sen for graciously allowing me to do a major part of this study in his lab. All the FCS experiments were done in his lab and he gave me complete freedom to do my experiments there whenever I needed to. Firoz sir has always helped me in my experiments and in troubleshooting them. He has also managed to comfort me when I used to get anxious in between the experiments. I would also like to thank Nibedita mam for helping me with the FCS experiments initially, also not to forget Kiran sir, Shweta and Kavita for being there if I needed any help.

I would also like to acknowledge mydoctoral committee members, Prof. S. Gourinath,Prof. A.K Saxena. Dr. B. K. Biswal and Dr. Apurba Kumar Sau from NII for providing valuable inputs for my thesis work.

I would like to thank the present and former deans of the School of Life Sciences, Prof. Neera Bhalla Sarin, Prof. B. N.Mallick, Prof. B. C. Tripathy and Prof. S. K. Goswami.

I would like to acknowledge all the CIF staff for their support and keeping the CIF functional at all times.

I would now like to acknowledge all my labmates, who have been with me, through this long journey. Bhawna, Faiz, Soraya, Priyanka, Usha, Kalpana, Anshuman, Tarun, Sudisht, Shazia, Anupriya, Pramita and Subhash have all been very cooperative and supportive. Subhash deserves a special mention for helping me with my experiments at a crucial time.

Being in a high pressure lab has its own set of advantages and disadvantages. Yes, it is true that you get to learn a lot, both scientifically as well as in terms of working under stress and in co-ordination with other lab members. But in times of such severe stress, when there is also a lot of negativity bound to bearound you, you need a solid support system to keep you going till the end and. Few people in the lab I feel are more than just my labmates. Apart from working together, we have managed to

strike a bond offriendship that I wish goes beyond the walls of JNU. Snehlata, Preeta and Anshumanare foremost amongst those. Snehlata and me have come a long way from attending lab meetings together in the first year to lending a shoulder to each other to cry on during difficult times of Ph.D. Preeta came into the lab like a breath of fresh air and though it took a few months for us to become close, but now, there's no looking back. Anshuman,is one of the few people who can crack me up in a split second, to say the least. They have helped me remain calm throughout, especially during the last stages and I look forward to seeing them daily now.

Tarun and Sudisht also deserve mention for bringing the much needed comic relief and also giving suggestions regarding my experiments.

I would also like to thank all the lab attendants, Umesh, Bharat, Ved and especially Deepak for helping us by maintaining the lab in a proper order.

I would also like to acknowledge my Ph.Dbatch mates especially Sudhaker, Prabu, Gopi, Gunjan and Suchi for helping me with reagents and their inputs whenever I needed their helpand Kishore and Wasi for little pep talks in between. I would also like to mention all the M.Sc students who worked along with me and in the lab and all the project students and post docs who were there in the lab during my tenure as a Ph.D student, Rohini, Dominic, Prerna Sharma, Prerna Chaudhary, Namita, Shafaque. Dominic has been the most amazing senior I ever worked with and his enthusiasm towards science and his energy is just infectious. He made working in the lab so much fun.

My sole pillar of strength throughout this journey has been my mother. Amma, I would never have been able to even remotely complete this thesis, had it not been for you. Keeping her own dreams and aspirations aside for me, Amma, you are the epitome of perfection and personification of God for me. This thesis would be absolutely incomplete if I do not mention my hero, my father.Nanna, I know, you are always with me in spirit and are showering your blessings upon me

I would like to mention Padma aunty and Uncle for being with me through thick and thin. Chaitu and Udbhav, spending time with you both is so therapeutic! I would also like to mention Parul, my childhood friend, or rather; my soul sister who I know can call and rant about anything, anytime. Ravi aunty and Uncle have also supported me throughout my study. I would also like to mention my mava, who has also been very supportive of me pursuing higher studies.

I would also like to acknowledge my friends for being with me throughout. Poorti and Kritika, Oh those hanging out sessions. A chat session with you all wherein I can pour my heart is enough to relieve my stress. These are people I can tell anything, and I know they won't be judgemental about me and help mewith all they can. Arundhoti (Aru) and Divya, I wish we met more often. but alas, Ph.D woes yet again! But still, believe me, not even a single day went by, when I didn't think of you two. Roopsee and Raghav, though we are separated by continents now, chatting with you both is something that I always look forward to. If only we could meet more often. I would also like to mention Prakriti, my school friend from kindergarten who has been with me throughout.

V.A. Pratyusha

Table of contents

Abbreviations

°C	Degree centigrade
ALS	Agglutinin like Sequence
AMP	Adenosine monophosphate
APS	Ammonium persulphate
Arg	Arginine
ATP	Adenosine triphosphate
BCA	Bicinchonic acid
Ca	*Candida albicans*
cAMP	Cyclic AMP
Cys	Cysteine
Cyto D	Cytochalasin D
cDNA	Complementary DNA
CHO	Chinese hamster Ovary
CIp10	Candida Integrating plasmid 10
ddA	Dideoxy adenosine
ddT	Dideoxy thymidine
DNA	Deoxyriboucleic acid
dNTP	Deoxynucleoside triphosphate
Dol-P-Man	Dolichol-Phosphate-Mannose
E.Coli	*Escherichia coli*
ECL	Enhanced Chemiluminiscence
EDTA	Ethylene disodium tetraacetate
ER	Endoplasmic Reticulum
Etn-P	Ethanolamine-phosphate
EhPIG-L	*Entamoeba histolytica* PIG-L
FBS	Fetal Bovine Serum
fl	Femtolitre
FP	Forward primer
GPI	Glycosylphosphatidylinositol
GlcN	Glucosamine
Gly	Glycine
GlcNAc	*N*-acetylglucosamine
GlcNAc-PI	*N*-acetylglucosamine-phosphatidylinositol
GPI-GnT	GPI-*N*-acetylglucosaminyltransferase
GlcN-PI	Glucosamine-phosphatidylinositol
GAA1	GPI anchor attachment 1
GTP	Guanosine triphosphate
GDP	Guanosine diphosphate
GAPs	GTPase Activating Proteins
GEFs	Guanine nucleotide Exchange Factors

GC-MS	Gas Chromatography Mass Spectrometry
h	hours
HVR	Hypervariable
H-Ras	Harvey-Ras
Jas P	Jasplakonilide
K-Ras	Kirsten-Ras
Lys	Lysine
M	Molar
Man	Mannose
MAP Kinase	Mitogen Activated Protein Kinase
MOPS	3-(N-morpholino)propanesulfonic acid
mRNA	Messenger RNA
N-Ras	Neuroblastoma-Ras
OD	Optical Density
PI	Phosphatidylinositol
PGAP1	Post GPI anchor Attachment to Protein 1
PBS	Phosphate Buffer Saline
PCR	Polymerase chain Reaction
PIG	Phosphatidylinositol glycan
RAS	Rat Sarcoma
RP	Reverse primer
RT-PCR	Real Time Polymerase chain Reaction
RNA	Ribonucleic acid
RPM	Rotations per minute
Sec	Second
Ser	Serine
Sc	*Saccharomyces cerevisiae*
S.D.	Standard deviation
SD	Synthetic Defined medium
SDS	Sodium dodecyl sulphate
SH3	SRC Homology 3 Domain
Thr	Threonine
Thy-1	Thymocyte-1 cell surface antigen
TE	Tris EDTA
TEMED	Tetramethylethylenediamine
UDP	Uridine diphosphate
VSG	Variant surface glycoprotein
YEPD	Yeast extract peptone dextrose

List of Figures

List of Tables

Table no.	Table title	Page no.
Table I	List of *Candida albicans* strains used in this study	55
Table II	List of plasmids used in this study	57
Table III	List of primers used in this study	58
Table IV	Nomenclature followed in this study	70

Chapter 1

Introduction

1.1*Candida albicans: a brief overview*

Candida albicans is a dimorphic opportunistic fungal pathogen having two morphological forms, the yeast form and the filamentous hyphal form which is required for attachment to the host cell during the invasion process(Jones and Sudbery, 2010). It is a normal commensal organism in the human gut flora, but it causes about 50-90% of the *Candida* infections in immunocompromised human(Martins *et al*., 2014). Systemic fungal infections, commonly known as fungemias, can cause mortality in immunocompromised patients. Many *Candida albicans* infections are also hospital-acquired, sometimes forming biofilms on implants and other devices.*Candida albicans* is the major worldwide cause of invasive candidiasis, accounting for over half of all cases. It starts off as white patches in the affected areas, usually mouth, tongue, nails or vagina in women and can spread to the entire body causing invasive candidiasis if not controlled timely and can be quite fatal also. The incidence of candidiasis is quite high in people whose immune system is already compromised, like in AIDS/HIV, or infants with low birth weight or during critical care after a surgery. The current line of treatment includes drugs targeting the ergosterol biosynthesis pathway in *Candida albicans*, like amphoterecin B, fluconazole, clotrimazole and when the disease is widespread, drugs like caspofungin and micafungin are commonly used. The treatment is usually prolonged ranging from 4-12 weeks at least. *Candida albicans* accounts for 40.9% of the total fungal infections in Brazil (Mendes Giannini *et al*., 2013). In European countries, an analysis showed that more than half of the cases of candidaemia were causedby *Candida albicans*(Yapar, 2014). In India also, the situation is no less different. A study from Aligarh, India reported that about 20% of the tested women were positive for *Candida* species, and among them, about 41% had a *Candida albicans* infection (Ahmad and Khan, 2009).Another study revealed that of about 10% patients in a hospital who had *Candida* infections,about 30% had *Candida albicans* infection(Chander *et al*., 2013). Also, lack of proper medical care

and facilities in many parts of rural India make matters worse, especially for women, in whom high incidences of vulvovaginal candidiasis have been reported. All these aspects make *Candida albicans* a very important organism to study. But strangely, it has not yet been explored much as a model organism for research and also in terms of its invasive and disease causing properties. *Candida albicans* invades the host through proteins present on it cell surface. It has a rigid cell wall that is of paramount importance for maintaining its structural integrity and its interaction with the outer environment. The cell wall is mainly composed of chitin and polysaccharides, enriched in the outer layer and mannoproteins which are more prominent in the inner layer. The chitin is present cross linked to glucans, specifically the β-1,3 glucan. β-1,6 glucan is also present to provide branching to the linkages. The cell wall proteins are attached to this fibrillar network of polysaccharides. The most abundant class of cell wall proteins is the GPI anchored proteins; wherein proteins are linked to β-1,6-glucan through a glycophosphatidylinositol (GPI) anchor. The other class of proteinswhich are less abundant are the Pir (*p*roteins with *i*nternal *r*epeats) proteins which are attached to the β-1,3 glucan through their glutamine residues (Chaffin, 2008). Proteins involved in virulence and invasion of the human host in *Candida albicans* are expressed on the cell surface, in the hyphal form, which is required for adhesion to the host cell wall. Carbohydrates, present in the cell wall, on the other hand regulate the host innate immune response through PAMPs (Pathogen associated Molecular Patterns). Upon invasion, the hyphal form induces damage to the cell and activates pathways that lead to formation of the inflammasome. MAP Kinase (Mitogen Activated Protein) mediated cytokine response is alsoinduced, leading to recruitment of neutrophils, which subsequently help in controlling the spread of the infection (Gow and Hube, 2012). Most of these virulence factors and other proteins on the cell surface of *Candida albicans* which act as antigens like Hwp1, Ecm33, Als3 etc., are GPI anchored proteins. These GPI anchored proteins are involved in a variety of functions like biofilm

formation, adhesion and invasion. Mutants lacking GPI anchored proteins in *Candida albicans* have been shown to display alterations in azole resistance, in the Protein Kinase C mediated cell wall integrity pathway, in filamentation etc (Plaine *et al*., 2008; Victoria *et al*., 2010; Yadav *et al*., 2014b). The number of GPI anchored proteins in *Candida albicans* is around twice that found in *Saccharomyces cerevisiae* (Plaine *et al*., 2008).

1.2 *GPI anchor biosynthesis*

GPI (Glycophosphatidylinositol) anchor is an important post translational modification in eukaryotes to anchor proteins to the cell wall or the plasma membrane. About 10-20% of the eukaryotic membrane proteins are GPI anchored (Eisenhaber *et al*., 2003). It is a complex multistep pathway occurring mostly in the endoplasmic reticulum (ER) with sequential addition of each of the components resulting in the formation of a precursor GPI anchor. Proteins destined to be GPI anchored have a C terminal signal sequence. The preformed GPI anchor is attached to the ω site of the signal sequence. Once the GPI anchor is attached it is further remodeled both in the ER and the Golgi during its transport to the cell surface. In organisms that lack a cell wall, the GPI anchored proteins are finally localized on the outer leaflet of the plasma membrane. In organisms with a cell wall, many of these GPI anchored proteins may be further covalently cross-linked to chitin in the the wall via β-glucans. The various steps involved in the biosynthesis of the GPI anchor in the ER are depicted in Figure 1.1.
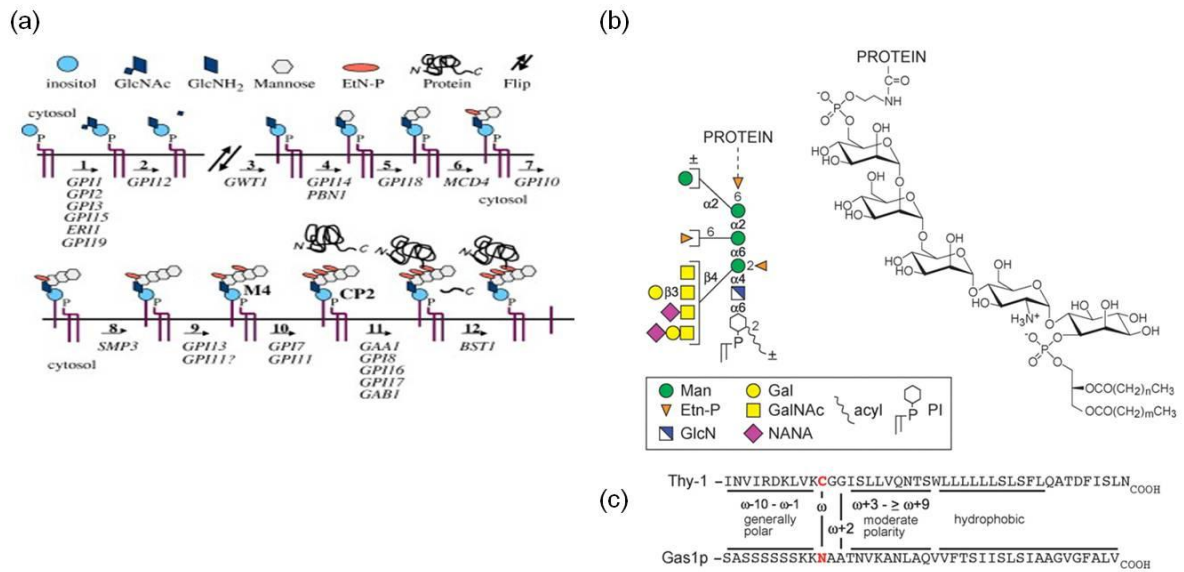
Figure 1.1: A brief overview of GPI anchor biosynthesis in yeast.(a) GPI anchor biosynthesis in yeast (Pittet and Conzelmann, 2007). **(b)** The core structure of the GPI glycolipid anchor and **(c)** shows the ω site and the GPI anchor signal sequence of two GPI anchored proteins, Thy-1 and Gas1 (Orlean and Menon, 2007).

Although some studies on GPI anchor biosynthesis have been done in trypanosoma, yeast and mammals, there is still a lot to be explored. Initial studies in the field of GPI anchor began with the knowledge of the Variant Surface Glycoprotein (VSG) coat in trypanosome (Grab*etal*., 1987). VSG is the main protein present in abundance (about 10 million) on the surface of trypanosome, forming a 12-15 nm thick coat on the surface. Because of this, the host immune system is not able to reach the antigenic epitopes on the plasma membrane. Moreover, theorganism keeps on switching the VSG and expresses its different forms, further preventing host recognition. Groups working on this problem were intrigued as to how this protein isattached to the plasma membrane but becomes soluble upon lysis. This was explained by the discovery of the GPI specific phospholipase-C by Cardoso de Almeida and Turner in 1983(Cardoso de Almeida and Turner, 1983). They showed that when they isolated VSG under denaturing conditions, it still retained its amphipathic properties responsible for membrane insertionIt has a dimyristoylphosphatidylinositol moiety and galactose (Gal)side chain. Initial description of the GPI anchor core as well as the lipid remodeling that occurs

afterwards was given by studies in *T. brucei*(Masterson *et al.*, 1989) Initial studies were done by complementation assays of mammalian and yeast genes, which restored the GPI anchored proteins onto the cell surface. This is also the basis for the nomenclature of these genes involved in the GPI anchor biosynthesis pathway. The genes are named according to the class of genes complementing a particular pathway like PIG-A, PIG-C and so on. Presented below is an overview of the different steps of the GPI anchor biosynthesis pathway.

1.2.1 PI-GlcNAc transfer

The first step is the addition of GlcNAc to phosphatidylinositol(PI). This particular step occurs on the cytosolic face of the ER (Figure 1.2). UDP-GlcNAc serves as the donor. This reaction is catalyzed by a complex of six subunits in yeast andfungi,namely Gpi1, Gpi2, Gpi3, Gpi15, Gpi19 and Eri1, known as the GPI-GnT complex (Glycosylphosphatidylinositol-*N*-acetylglucosamine transferase). This is the first and committed step of the pathway. Let us look at the different subunits of the complex.
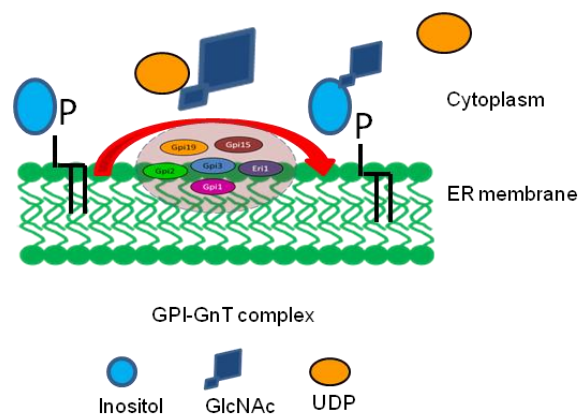
Figure 1.2:A schematic representation showing the first step of GPI anchor biosynthesis in *Candida albicans*. The GPI-GnT complex, consisting of six subunits catalyzes the attachment of GlcNAc from UDP-GlcNAc to PI (Phosphatidyl inositiol). This reaction takes place on the cytosolic side of the ER.

Gpi3/PIG-A

The yeast ScGpi3, a 452 amino acid protein is the putative catalytic subunit of this complex. Photoaffinity labeling studies have shown that that it binds UDP-GlcNAc with its glycosyltransferase motif (Kostova *et al.*, 2000). It is also known as Spt14 and is essential for the viability of the organism. Mutation of this gene increases the doubling time of yeast. Also, because no GPI anchor is formed in such cells, there is accumulation at the ER of proteins destined to be GPI anchored , like ScGas1, ScAga1 and ScCwp1(Vossen *et al.*, 1997). The human homolog of yeast ScGpi3 is PIG-A.A deficiency of PIG-A in humans causes Paroxysmal Nocturnal Hemoglobinurea or PNH which is a fatal disease. Patients with this disorder have abnormal populations of the different hematopoietic cells which are deficient in the surface expression of various GPI anchored proteins like CD59, CD55 (also known as Decay Accelating Factor or DAF) and other complement regulatory proteins. Thiscauses intravascular hemolysis, leading to presence of hemoglobin and hemosiderin in the urine, which causes red discoloration of the urine It is an X-linked gene in humans thereby raising the incidences of the disease in males. Both ScGpi3 and PIG-A have a large cytosolicsegment and a single transmembrane domain and are members of the glycosyltransferase family. Studies are going on in our lab to characterize the *Candida albicans* CaGpi3. *CaGPI3* heterozygous mutant shows decreased GPI-GnT activity (Jain. P., 2016) and a hypofilamentous phenotype. This mutant also shows increased *CaERG11* transcript levels which could be correlated with the azole resistance phenotype displayed by this mutant.

Gpi2/PIG-C

The yeast ScGpi2 gene was first identified by complementation analysis of a series of temperature sensitive yeast mutants that were defective in incorporating [^{3}H]inositol in their system and in their GPI anchors (Leidich *et al.*, 1995). It is a highly hydrophobic ER

membrane protein having 269 amino acids with about six transmembrane domains wherein both theN and the C termini are on the cytosolic side. Mammalian PIG-C was identified based on complementation of Class C cells, which were defective in the first step of GPI anchor biosynthesis, with the human homologue of yeast ScGpi2 (Inoue *et al.,* 1996). This complementation restored the surface expression of GPI anchored proteins in Class C mutants, thus proving that PIG-C is indeed the homologue of yeast Gpi2.*Candida albicans* mutants wherein one allele of *CaGPI2* is disrupted have extremely low GPI-GnT activity and display a hypofilamentous phenotype (Yadav *et al*., 2014b)which can be correlated with reduced virulence. It also shows higher ergosterol levels and azole resistant phenotype. *CaGPI2* does not complement the growth defect of the yeast *ScGPI2* mutant. However, complementation of *ScGPI2* into the *Cagpi2* heterozygous mutant complements filamentation to some extentand reverses azole resistance, but not GPI anchor biosynthesis and cell wall integrity (Yadav *et al*., 2014a). The conditional null generated is inviable (Yadav *et al*., 2014b).

Gpi1/PIG-Q

Initial studies on Gpi1 were done in the yeast *Saccharomyces cerevisiae* by Orlean group (Leidich and Orlean, 1996). These were the first isolated yeast *GPI* mutants, hence the name*Scgpi1* mutant and the corresponding gene was named *ScGPI1*(Leidich *et al*., 1994). The *Saccharomyces cerevisiae*ScGpi1 is a 609 amino acid protein residing in the ER havingsix transmembrane domains. These mutants grew slowly at 25°C and their growth was blocked at 37°C. ScGpi1 is, however not essential for cell viability. As expected, they show a decrease in the level of GPI anchored proteins on the cell surface and are defective for [3H]Inositol incorporation into protein, and for GPI anchor-dependent transport and processing of a model protein(Leidich and Orlean, 1996). These *Scgpi1* mutants also showed

a hyperfilamentation phenotype (Sobering *et al.*, 2004). In mammals however, the ScGpi1 homologue, hGPI1 is a multi transmembrane 581 amino acid protein(Leidich *et al.*, 1995) having a polar N-terminus with a tyrosine phosphorylation site. The region corresponding to amino acids 280-560 is reported to be hydrophobic. It has a polar N terminus and also a tyrosine phosphorylation site. When hGPI1 was disrupted, GPI anchor biosynthesis was reduced but not completely blocked. Some characterization of the *Candida albicansCaGPI1*has been done in our lab. *Cagpi1* heterozygous mutant showed an azole resistant and hypofilamentous phenotype, similar to the *Cagpi2* mutant. This was also correlated with higher *CaERG11* and low *CaRAS1* levels (Yadav. B., 2013).

Gpi15/PIG-H

ScGpi15, another subunit of the GPI-GnT complex, was in fact one of the first GPI-GnTsubunits to be discovered in *Saccharomyces cerevisiae*. It has about 24% sequence homology

with its human counterpart (Yan *et al.*, 2001). It consists of 212 amino acids with two hydrophobic stretches. Depletion of ScGpi15 in yeast lowers *in vitro* GlcNAc-PI synthetic activity, which proved it to be a subunit of the GPI-GnT complex. PIG-H is the human functional orthologue of ScGpi15.It is a 188 amino acid protein possessing two transmembrane domains with its N and the C termini facing the cytosolic side (Kamitani *etal*., 1993). The authors also show that mutants of *PIG-H* have decreased GPI-GnT activityand less than 1% of normal GPI anchor levels. The *Candida albicans* homologue, CaGpi15 is also an essential subunit. . This is able to complement the yeast ScGpi15 mutant (Kumar, P., 2010). *CaGPI15* mutants have been found to be hypofilamentous and have lower *CaERG11*levels, correlating with an azole sensitive phenotype. Studies are going on in this regard in our lab (Jain, P., 2016).

Gpi19/PIG-P

The yeast ScGpi19, another essential subunit of the GPI-GnT complex, was identified based on homology studies with its human counterpart. ScGpi19 shares about20% sequence similarity with its human homolog (Watanabe *et al*., 2000). Conditional *gpi19* mutants in yeast showa decrease in the GPI-GnT activity and lower levels of GPI anchored protein levels on the cell surface(Newman *et al.*, 2005). This article also reported that these mutants show a hyper filamentous phenotype and agar invasion, which are also phenotypes of hyperactive Ras. The human homolog of yeast ScGpi19 is the PIG-P protein. The *PIG-P*gene, which resides on chromosome 21, is also known as DSCR5, for Down Syndrome Critical Region 5(Ferrando-Miguel *et al*., 2003). PIG-P is overexpressed twofold in fetal Down Syndrome' brain tissue, which tells us that proper GPI anchoring is an importantrequirement for brain development. Also,*PIG-P* is the only DSCR gene expressed in tongue tissue, and it could be that this is responsible for the pathophysiology of tongue malformation in DS patients. In *Candida albicans* also, the CaGpi19 subunit is essential and hence studies have been done on the conditional null mutant(Victoria *et al*., 2010). As expected, it shows a marked decrease in the GPI anchored Ecm33-GFP levels. The sequence similarity between CaGpi19 and ScGpi19 is only 35%, with a few conserved residues in the predicted transmembrane regions. CaGpi19 has extra 151 amino acids at its N terminus which are not present in the yeast and human orthologues. These extra residues at theN-terminus probably interfere in the formation of the intact GPI-GnT complex in yeast as can be seen from the fact that the full length CaGpi19 cannot restore the viability of a conditionally lethal ScGpi19 mutant, whereas the viability is restored upon truncation ofthese residues (Victoria *et al*., 2010). The *Cagpi19* conditional null mutant shows lower ergosterol levels,azole sensitivity, and a loosely packed membrane relativeto the wild type; which is

explained by lower transcript levels of *CaERG11*, which encodes lanosterol 14-αdemethylase (Victoria. S., 2010) and lower levels of *ERG11*, (Victoria *et al.*, 2012). Also, similar to yeast, it shows phenotypes of hyperactive Ras, i.e., hyperfilamentous phenotype even at room temperature and consequently, higher PKA activity. This particular mutant also shows higher CFW staining indicating the presence of more chitin in its cell wall (Victoria*et al.*, 2010).

Eri1/PIG-Y

ERI1 encodes a 68 amino acid long hydrophobic protein that, which was shown to be required for GPI anchor biosynthesis by Levin group (Sobering *et al.*, 2003, 2004). Microsomes isolated from an *eri1*null mutant exhibited defects in the transfer of GlcNAc tothe acceptor PI. It was initially discovered in yeast as Endoplasmic Reticulum-associated Ras Inhibitor 1. Mutants lacking a functional ScEri1 protein seemed to have a hyperactivated ScRas, which led to hyperfilamentation and agar invasion, proving that ScEri interacts negatively with ScRas.Eri1 has 2 long hydrophobic segments which could be the potential transmembrane regions. The report also showed that the *Sceri1*nullmutants also have decreased GPI anchored proteins at the surface, as they are deficient in the maturation of GPI-anchored proteins at the ER. The authors hypothesize that when a stimulus is received, ScEri1 disengages ScRas from the ER and ScRas then goes to the plasma membrane and then the downstream signaling proceeds (Sobering *et al.*, 2004). The mammalian homologue PIG-Y has 22% sequence identitywith ScEri1 and has a similar hydropathy profile as ScEri1(Murakami, 2005). However, no association of PIG-Y with any of the human Ras family members was seen when both the proteins were co-transfected into Daudi cells. *Caeri1*heterozygous disruption mutant made in*Candida albicans* shows a reduction of about 50% in GPI-GnT activity. This mutant also hashigher transcript levels of *CaGPI2* and is hyperfilamentous (Priyanka Jain, unpublished work).

Inter-subunit interactions within the GPI-GnT complex and its cross-talk across pathways

The six subunits described above come together to form the GPI-GnT complex which catalyzes the first step of the GPI anchor biosynthesis pathway. However, how each subunit interacts with the other subunits and other pathways in the cell, is not fully known till now. Some initial reports show physical association between different subunits of the GPI-GnTcomplex in humans and yeast. For instance, in humans, PIG-Y has been shown to bind to PIG-A, but to no other component of the PI-GlcNActransferasecomplex(Murakami, 2005).Immunoprecipitaton studies were done using HA-PIG-Y and tagging the other subunits of the GPI-GnT complex with GST and sequential transfection in human JY5 and JY25 cell lines. PIG-Y could not be co-precipitated in PIG-A deficient JY5 cell with any other subunit of the GPI-GnT complex.Extrapolating these results to *Saccharomyces cerevisiae* would suggest that the interaction of yeastScEri1 with ScGpi2 may also be mediated by ScGpi3 during infections and other events. However, no physical interaction was observed between PIG-Y and members of the Ras family in the mammalian system as was seen in *Saccharomyces cerevisiae*(Sobering *et al*., 2003), suggesting that such simple extrapolations of interactions seen from one system cannot be made in another. hGpi1 is thought to stabilize the interaction between PIG-A, PIG-C and PIG-H in the mammalian system (Hong *et al*., 1999).When hGpi1 was disrupted inhuman F9 carcinoma cells, even though PIG-A and PIG-H continued to interact with each other, but the complex of PIG-C with PIG-A and PIG-H was nearly undetectable. Also, disrupting *hGPI1* brought down the protein levels of PIG-C and PIG-H.hGpi1, therefore, stabilizes the interaction of PIG-C with the other subunits and formation of a stable GPI-GnTcomplex. In *Saccharomyces cerevisiae*, a large scale split ubiquitin based assay also showed a physical interaction between ScGpi2 and ScGpi19 (Miller *et al*., 2005) which was also validated byco-immunoprecipitation studies in

yeastwhich showed an association of ScGpi19-HA with FLAG-ScGpi2(Newman *et al.*, 2005).Similar studies are being carried out in *Candida albicans*in our lab. In *Candida albicans*, our lab was the first to report a crosstalk between the GPI anchor biosynthesis pathway and the ergosterol pathway via *CaGPI19*(Victoria *et al.*, 2012). We have shown that deletion of *CaGPI19* causesdownregulation of *CaERG11* leading to lower levels of ergosterol and disruption of *CaGPI2* leads to repression of the CaRas1 signaling pathway and giving rise to a hypofilamentous pathway (Yadav *et al.*,2014b). Additionally, there is a negative regulation between *CaGPI2* and *CaGPI19*. Disruption of one causes increase in the transcript levels of the other gene. Deletion of *CaGPI19* decreases the levels of *CaGPI2* which in turn increases the CaRas1 signaling pathway in the mutant, giving rise to a hyperfilamentous pathway. Similarly, disruption of *CaGPI2* causes upregulation of *CaGPI19* which in turn increases the ergosterol levels inside the cell, thus making *CaGPI2* heterozygous mutant azole resistant (Yadav *et al.*, 2014b). As mentioned earlier, another subunit of the same complex, *CaGPI15* has also been studied in our lab extensively (Jain. P., 2016 and Kumar. P., 2010). It appears to be a master regulator of this whole complex, as disruption of a single allele of this gene causes a decrease in the transcript of all the other subunits and overexpression of *CaGPI15* causes an increase in the transcript levels of all the other subunits of the GPI-GnT complex. Data from our lab hasshown that disruption of *CaGPI19* in the *CaGPI15* heterozygous background increases the azole sensitivity of the *CaGPI15* heterozygote and overexpression of *CaGPI19* reverses itsazole sensitivity. Similarly, disruption of *CaGPI2* in the *CaGPI15* heterozygousbackground further reduces the filamentationof the *CaGPI15* heterozygote and overexpression of*CaGPI2* makes it hyperfilamentous. These studies tell us that *CaGPI2* and *CaGPI19* act downstream of *CaGPI15*.Our lab has also showed that overexpression of *CaGPI19*, either in wild type or in a *Cagpi2* heterozygous mutant, increases the transcript levels of *CaGPI15*. When one allele

of *CaGPI19* is disrupted in the *Cagpi2* heterozygous background, *CaGPI15* transcript levels drop down significantly. Similarly, overexpression of *CaGPI2*, either in wild type or in a *Cagpi19* heterozygous mutant, increases the transcript levels of *CaGPI15*. When one allele of *CaGPI2* is disrupted in the *Cagpi19* heterozygous background, *CaGPI15* transcript levels drop down significantly. Also overexpression of *CaGPI15* increases the transcript levels of both *CaGPI2* and *CaGPI19*, though the negative co-regulation between the two is still maintained. These studies show that *CaGPI2* and *CaGPI15* independently activate each other; similarly *CaGPI19* and *CaGPI15* independently activate each other (Jain, P., 2016)

1.2.2 GlcNAc-PI de-N-acetylase Gpi12/PIG-L

This enzyme catalyzes the second step of the pathway, i.e. removal of the acetyl group from GlcNAc-PI to form GlcN-PI. It is a de-*N*-acetylase. It also occurs on the cytosolic side of the ER. It has been studied in human and rats and in lower eukaryotes also (Nakamura *et al*., 1997). It is an essential enzyme and mutants lacking this particular enzyme are inviable in mammals as well as yeast (Watanabe *et al*., 1999). PIG-L can catalyze conversion of different substrates with different specificities. Ferguson and group studied the mechanism of PIG-L in trypanosoma and HeLa cell line (Urbaniak *et al*., 2005). They found out that as the size of the N-acyl group (from acetyl to propionyl to butyryl and so on) increases, the substrate specificity of the enzyme drops down, both in trypanosoma and in humans (HeLa cell free systems). Also, the trypanosomal PIG-L can catalyze the conversion of substrates with more hydrophobic side chains better than the human one. It has been reported in our lab that unlike the other de-N-acetylases studied so far, the Entamoeba PIG-L works via an acid base mechanism with an optimum pH of 5.5. Also, it is metal stimulated but not metal dependent, wherein externally added divalent cations like Mn^{2+}, Zn^{2+} enhance the basal catalytic activity of the enzyme (Ashraf *et al*., 2011, 2013). Studies on the *Candidaalbicans*

*CaGPI12*are going on in the lab currently and it shows a different activity profile (Yadav. U., 2016). Unlike the Entamoeba PIG-L, it has an optimum pH at 7.5 and highest activity at 30℃. *Cagpi12* conditional null is azole sensitive and also shows cell wall defects like clumping and sensitivity to cell wall disrupting agents. Also, downregulation of *CaGPI12* makes the strain hypofilamentous. CaGpi12 also has two conserved motifs HPDDE and HXXH which are found in other de-acetylases. Our lab has studied the role of these residues by making site directed mutants of each of these residues and transforming them into the *Cagpi12* conditional null mutant. When H77, D80, E81, H190 or H193 were mutated, the strain was unable to grow, indicating that these residues might be important for the activity of CaGpi12. The corresponding residues are also found to be important in MshB and rat PIG-L. (McCarthy *et al*., 2004; Urbaniak *et al*., 2005). On the other hand, when P78 and H190 residues were mutated, the strains showed a slower growth compared to the wild type. This could be because of the fact that as in case of rat PIG-L, these residues could be important for substrate recognition, but not critical (Urbaniak *et al*., 2005). The exact roles of all of these residues needs to be explored still.

1.2.3 GlcN-PI acyltransfer

The third step in GPI anchor biosynthesis is the acylation of inositol at the C2 position of the inositol ring. This acylation makes the GPI anchors resistant to PI-PLC (Pittet and Conzelmann, 2007). In yeast, it is catalyzed by ScGwt1. Acyl-CoA acts as the donor for acyl group in yeast, where the acyl group is usually palmitoyl group. However, it has been seen that cells deficient in this enzyme also produce GPI lipids. Inhibitors have been developed against ScGwt1 since a long time and have been successful in inhibiting GPI anchor biosynthesis. The first inhibitor to be developed was BIQ, 1-[4-butylbenzyl]isoquinoline). This was developed as part of a phenotype screening assay wherein cell wall localization of

yeast GPI-mannoprotein was monitored(Tsukahara *et al*., 2003). This was also the firstinhibitor to be developed against yeast cell wall GPI anchored proteins. This compound is thought to bind at the substrate binding pocket of Gwt1 and inhibit its action. This was modified and a more potent inhibitor called E1210, 3-(3-{4-[(pyridin-2-yloxy)methyl]benzyl}isoxazol-5-yl)pyridin-2-amine was developed(Watanabe *et al*., 2012). Not only is the E1210 effective against *Candida albicans*, but other pathogenic fungi also, like *Aspergillus* spp.,and other molds, such as *Fusarium* and *Scedosporium* spp. E1210 inhibits only the fungal enzyme selectively, with an IC50 of 0.3 -0.6 µM, but not the mammalian enzymes, which makes it a potent drug candidate.Other inhibitors likeGepinacin G365 and G884 were also developed against this enzyme.Like E1210, these also bind to the substrate binding pocket of the enzyme and a G132R mutation at this site confers resistance to these chemicals. G365 lacks yeastactivity. Like gepinacin, G884 displayed appreciable(>10-fold) selectivity to its fungal target versus the human counterpart (Mann *etal*., 2015).

1.2.4 Addition of mannoses and phosphorylethanolamines

Acylation of inositol is followed by the addition of mannoses and phosphorylethanolamines.It occurs in a sequential manner. The first mannosylation (α1-4 bond) occurs on the luminal side of the ER and has a conserved DXD motif found in many Dol-P-Man utilizing enzymes. Dolicholphosphomannose (Dol-P-Man) acts as the mannose donor. In yeast the enzyme is ScGpi14 and its human homolog is PIG-M. It is an essential subunit. In humans, PIG-X forms a complex with PIG-M, thereby stabilizing the enzyme. PIG-X is also an essential subunit and is required for the activity of PIG-M. This is the only known example of a heterodimeric mannosyltransferase so far (Pittet and Conzelmann, 2007). Both PIG-M and PIG-X are integral transmembrane proteins. ScPbn1 is the functional homologue of PIG-X in

Saccharomyces cerevisiae and is also involved in the processing of the preprotein of the yeast vacuolar hydrolase protease B (Ashida *et al*., 2005). In *Candida albicans*, *Cagpi14* conditional null mutant shows a defective filamentation phenotype even though the cAMP dependent PKA pathway is unaltered (Singh *et al*., 2016). Studies from our lab have shown that in these mutants, the Hog1 pathway is affected which is responsible for hypofilamentation and cell wall biogenesis defects in this mutant. Addition of the second mannose (α1-2 bond) is done by PIG-V or ScGpi18 (Orlean and Menon, 2007). It is also added on the lumenal side. It has 2 lumenally oriented conserved hydrophilic regions. It is also an essential gene in humans and *PIG-V* mutants are rescued by complementation with Gpi18. The next step is addition of Etn-P to the first mannose. It is catalyzed by PIG-N in mammals and ScMcd4 in yeast(Orlean and Menon, 2007). The third mannose cannot be added until the Etn-P is added to the first mannose. Defect in this gene or adding an inhibitor of ScMcd4 in yeast results in the accumulation of the Man2 intermediate. EtN-P group added by ScMcd4 is required for the recognition of GPIs by ScGpi10 as wellas by the transamidase complex and this is also involved in ER to Golgi transport of GPI proteins and also inceramide remodeling (Pittet and Conzelmann, 2007).This is catalyzed by a complex of PIG-N, PIG-O and PIG-F. Gpi13 and PIG-O, and its functional homologue in yeast, ScGpi13 are also required for addition of EtN-P to the third mannose. Defects in PIG-O in humans has some clinical implications also in humans like hyperphosphatasia, intractable epilepsy and mental retardation (Krawitz *et al*., 2012; Nakamura *et al.*, 2014). In yeast, this step cannot be completed until the fourth mannose in added. That is why, Smp3, which encodes the fourth mannosyltransferase in yeast and *Candida albicans* is essential (Grimme *et al*., 2001).As already explained, the addition of the third mannose by PIG-B (and its yeast homologue ScGpi10) requires recognition of EtnP (Ethanolamine phosphate). The pattern of hydrophobic residues remains the same. There are some species-specific differences also, like

PIG-F is essential in humans, as it stabilizes hGPI7, whereas, in yeast, there is addition of fourth mannose even in Scgpi11 (the yeast counterpart of PIG-F) mutants. There are some views that there is more to ScGpi11 than just stabilizing ScGpi7, like stabilizing ScGpi13 in yeast, which is not an essential function in humans (Orlean and Menon, 2007). YW3548, a terpenoid lactone is a GPI anchor biosynthesis inhibitor that has been identified some time back. It blocks the addition of the third mannose (Sütterlin *et al*., 1997). The lactone ring of YW3548 mimics the substrate of the α-1,2 mannosyltransferase. Since this is a highly hydrophobic molecule, it is thought that this inserts itself in the lipid bilayer and binds to the mannosyltransferase. The interesting thing, however is that this inhibitor is highly species specific. It has been shown to inhibit the addition of the third mannose in *Candida albicans* and in human lymphoma cells, but the GPI anchor biosynthesis was unaffected in protozoans like *T.brucei*, *P.falciparum*, *P.primaurelia* and *T.gondii*even after using 40 times the concentration that was used in *Candida albicans.* Another class of terpenoid lactone ringbased inhibitors from natural product extracts against *Candida albicans* CaMcd4 have been recently developed, named M743 and its semi-synthetic analogue M720 (Mann et al., 2015).They probably act by binding at the C-terminal region of the protein and lie within the C-terminal region of transmembrane11 (G792C) or within a cytosolic loop (Q679P) or ER luminal domain (F800L andP810L) based on the predicted topology of the protein as all the mutationsthat are resistant to these inhibitors map to these regions.

1.2.5 GPI-Transamidase

Once the GPI-anchor precursor is synthesized, the next step is to transfer the preformed GPI anchor to the protein. This is catalyzed by the GPI-transamidase complex (Figure 1.3). It is an enzyme complex of 5 subunits: PIG-K/Gpi8, GPAA1/Gaa1, PIG-T/Gpi16, PIG-S/Gpi17 and PIG-U/Gab1. The fungal homologues are written next to the human subunits.
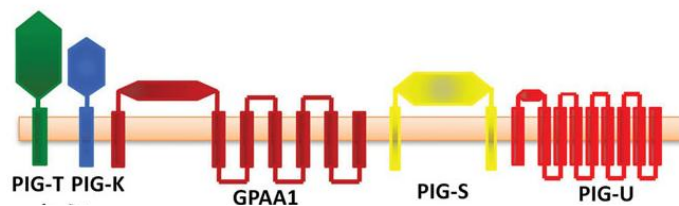
Figure 1.3:A schematic diagram showing the GPI transamidase complex along with its various subunits on the ER membrane. (Gamage and Hendrickson, 2013)

Homologs of human Gaa1, PIG-K and PIG-T are conserved in eukaryotes. The complex has been purified through immunoprecipitation in yeast (Fraering *et al*., 2001) and in humans (Pittet and Conzelmann, 2007). All the subunits are essential in yeast. These subunits are hypothesized to attack the ω site of the GPI signal sequence in a nucleophilic manner. The GPI anchoring signal sequence consists of the GPI anchor attachment site, which is known as the ω-site (usually residues with small side chains like cysteine, serine). The residues immediately after the ω site are hydrophilic, usually residues with short side chains like glycine, alanine etc., followed by a hydrophobic region, which is important for transport ofthe GPI anchored proteins to the cell surface. The GPI anchored proteins are retained in the ER in case of any mutations in the hydrophobic region of the signal sequence ((Pittet and Conzelmann, 2007).PIG-K is thought to be the catalytic subunit of the transamidase complex in humans as it shows serine protease activity(Fraering *et al*., 2001). ScGaa1 interacts with the GPI anchor signal sequence, specifically the C-terminal part and stabilizes it via P609 residue present in the last transmembrane helix. (Vainauskas, 2003). PIG-T, another subunit of the complex, is an N-glycosylated protein with a C-terminal transmembrane domain. According to a report, PIG-T is required for stabilizing the transamidase complex and forms a carbonyl intermediate between the protein and ScGpi8. (Ohishi *et al*., 2000). Depletion of ScGpi16, its yeast homologue results in accumulation of the complete GPI anchor in the ER. ScGpi17, on the other hand is essential for transamidase activity in yeast, but its exact role is still unknown (Zhu *et al*., 2005). The final subunit of this complex is PIG-U. It is highly

hydrophobic and has around eight to ten transmembrane helices. Mutants of *PIG-U* in humans show defective formation of cell surface GPI-anchored proteins (Hong *et al.*, 2003). Its yeast homologue is ScGab1. Both PIG-U and ScGab1 have a slight similarity to fatty acid elongase proteins, hence can be speculated to have a lipid binding role. ScGab1 has been shown to form a complex with ScGpi17 (Orlean and Menon, 2007). The authors also show that depletion of ScGab1 leads to formation of actin-bars, structures having Actin depolymerizing factor/Cofilin that are always associated with the perinuclear ER in neurodegenerative cells, speculating that ScGab1 might be involved in the ER-actin interaction (Grimme, 2004) .Mostly prion proteins like PrP, which are GPI anchored in their toxic scrapie (PrP^{Sc}) form, have been studied in the context of transamidase reaction. The scrapie form of these proteins is misfolded and is present at the cell surface by virtue of its GPI anchor, and accumulation ofthe misfolded PrP^{Sc} causes many neurodegenerative diseases like Creutzfeldt-Jakob disease(CJD) in humans, Bovine spongiform encephalopathy (BSE) in cows, and scrapies insheep (Prusiner, 1998). Inhibiting transamidation for these proteins can help to reduce their expression, and promote their retrotranslocation to the ER where they can be degraded via the ER associated degradation(ERAD) pathway. This can be an effective therapeutic strategy to control the toxicity of the disease causing PrP prion proteins, if applied selectively to these proteins (Ashok and Hegde, 2008).

1.2.6 Modifications of the GPI anchor after attachment to the target protein

After synthesis of the GPI anchor, some remodeling occurs where the GPI lipids are replaced by other lipids. Studies on this lipid remodeling have been particularly difficult because of the need to isolate early GPI intermediates. Recently, a GPI inositol deaylase has been discovered in trypanosome which deacylates the inositol after attachment to the protein (Pittet and Conzelmann, 2007). Proteins having similarity to this protein in mammals, like

acyloxyacyl hydrolyases, could serve a similar function. In yeast, it has been seen that diacylglycerol is not present on the GPI lipids, instead, a ceramide moiety is present, of mainly 26 carbon length. This was studied in *Saccharomyces cerevisiae* by metabolic labeling in which the uptake of tritiated DHS ($[^3H]$DHS) was monitored. This showed that a ceramide remodalase activity introducing ceramide with C26 was present only in the Golgi. ScGup1 was one such protein which was shown to participate in the synthesis of C26:0 diacylglycerol(Pittet and Conzelmann, 2007).PGAP1, an inositol deacylase, is another protein which is involved in remodeling of the GPI anchor after they are attached to the proteins. GPI anchored proteins can beremoved by PI-PLC treatment from the cell surface of normal, but notPGAP1-deficient cells(Pittet and Conzelmann, 2007; Tanaka, 2004). PGAP1 has 6 transmembrane domains, a lumenal hydrophilic domain and a lipase motif also. The yeast homologue of PGAP1 is ScBst1. Cells lacking this protein get blocked in the ER to Golgi transport step. It is also required for ER associated degradation of misfolded proteins.PGAP2/ScCwh43 is another integral membrane remodeling protein studied in mammals and yeast respectively. Deficiency of this protein causes conversion of the diacylglycerolipids to their lyso form, after which they get to the plasma membrane and are cleaved by PLD, and secreted outside the cell (Pittet and Conzelmann, 2007).

PGAP3 is involved in the generation of the lyso forms of GPI anchored proteins in humans (Maeda *et al*., 2007). It has many conserved serine and histidine residues that are found in the members of PLA_2 family. The yeast homolog of PGAP3 is ScPer1, and both of these cancomplement the function of each other. Deficiency of PGAP3 is known to cause hyperphosphatasia and mental retardation due to impaired GPI anchor maturation in humans (Howard *et al*., 2014).

After this lipid remodeling is complete, the GPI anchored proteins exit the ER through COPII coated vesicles and reach the cell surface via the Golgi. Proteins without the anchor (which

are otherwise destined to be) eventually get degraded in the ER (Eisenhaber *et al.,* 2003; Pittet and Conzelmann, 2007).

As already explained, mutants of the GPI biosynthetic pathway in *Candida albicans*, especially the GPI-GnT complex, show either a hypofilamentous or a hyperfilamentous phenotype, which can be due to the alteration in the activity of CaRas1 signaling pathway. Filamentation, or hyphal formation is controlled in *Candida albicans* through the CaRas1 signaling pathway mainly. Also, most of the GPI anchored proteins which act as virulence factors or aid in attachment and invasion to the human host, like CaHwp1, CaAls3, CaAls5, are expressed in the hyphal form of *Candida albicans.* Let us look in a little detail as to howthese Ras proteins actually function and regulate the hyphal morphogenesis in *Candida albicans*.

1.3 *Ras signaling*

Ras signaling is a major signal transduction pathway in eukaryotes. The Ras proteins are a family of small GTPases which, in their GTP bound active state, transmit signals to the downstream transcription factors by interacting with effector proteins. Ras signaling forms a major signaling network inside the cells.They are involved in cell proliferation, differentiation, and metabolism, and are mutated in approximately 30% of human cancers. (Shields *et al.,* 2000) . Ras mutations are found in 90% of the pancreatic cancers (Prior and Hancock, 2012). There are 3 types of Ras in humans, H-Ras, K-Ras and N-Ras. K-Ras is most frequently mutated in cancers while H-Ras is the least mutated. Rho and Rab proteins also associate with the Ras protein to activate the downstream signaling network.

1.3.1 *Ras structure and function in mammals*

Ras is a membrane anchored inner membrane protein which is tethered to the membrane bilayer via lipid modifications like palmitoylation and farnesylation(Piispanen *et al.*, 2011). The palmitoylation occurs at the Cys287 residue whereas farnesylation occurs at the C288residue. In its inactive state, Ras is bound to GDP, through some key residues like Lys161 and Lys164 (Hall *et al.*, 2002). Upon activation, during which the GDP is replacedby GTP, this interaction is replaced by Lys169 and Arg170.
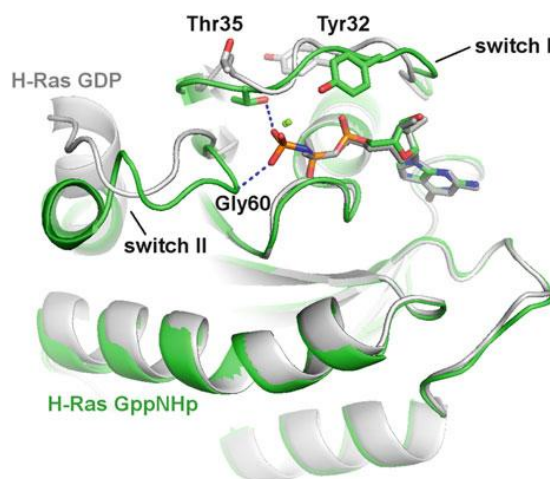
Figure 1.4:Structure of Ras protein. Cartoon showing the change in conformation in Ras potein upon nucleotide exchange from GDP to GTP. Gray color shows the conformation in the GDP bound state and the green denotes the GTP bound form (Wittinghofer, 2014).

A lot of study has been done on Ras structure and function. Studies on mammalian Ras have shown that the switch I (amino acids 30-38) and the switch II (amino acids 59-67) regions of Ras proteins undergo a conformational change upon GTP binding (Figure 1.4)(Rajalingam *etal.*, 2007). Switch I region has a conserved threonine residue for sensing the GTP γ phosphate and contacting the magnesium ion. The switch II region has a conserved glycine residue (G60 in H-Ras), which is also involved in sensing the γ phosphate and the action of GEFs. Mutations in the switchIII region and the hypervariable regions modulate the Ras signaling to a high extent as they affect the reorientation of Ras upon activation on the

membrane. A Fluorescence Correlation Spectroscopy(FCS) study has shown that mammalian Ras dimerizes on supported membranes(Lin *et al*., 2014). Also, it has been reported that upon activation, Ras proteins organize themselves into nanoclusters of about 6-8 molecules whichlead to downstream signaling pathway (Abankwa *et al*., 2007). This nanoclustering is controlled by scaffold proteins like Galectin-1 (Gal-1), galectin-3 and neurophosmin.Mutations like R128A and R135A decrease H-ras^{G12V} nanoclustering. Different forms of Ras have also been reported to localize in specific regions of themembrane bilayer. This is due to the difference in their targeting to the plasma membrane by virtue of differences in the polybasic domain which is crucial for their traffic through the cell. K-Ras does not follow the conventional exocytic pathway and bypasses the Golgi to reach the cell surface, whereas H-Ras and N-Ras enter the exocytic pathway and reach the cell surface via the Golgi. This is supported by studies which show that disruption of the Golgi by addition of Brefeldin A reduced trafficking of GFP having the membrane targeting sequence of H-Ras to the plasma membrane but not that of K-Ras (Apolloni *et al*., 2000) For example, Kras can initiate the signaling only when it is localized in anionic lipid rafts. H-Ras on the other hand, functions in cholesterol rich domains of the plasma membrane. Cholesterol depletion in the plasma membrane using cyclodextrin, compromises H-Ras signaling (Roy *et al*., 1999).

1.3.2*Ras signaling in yeast and fungi*

In *Candida albicans*, two types of Ras are present, CaRas1 and CaRas2. CaRas1 is the major player in *Candida albicans* for controlling the filamentation process. It is through these filamentous structures called hyphae that this fungus attaches to the host cell tissue and invades through. Mutants defective in CaRas1 show defective filamentation, which is further aggravated by deletion of CaRas2(Zhu *et al*., 2009). The authors show that CaRas1 and CaRas2 act in an antagonistic manner to each other in *Candida albicans*, unlike in

Saccharomyces cerevisiae, wherein they serve redundant roles. CaRas1, in *Candida albicans*upon activation, increases cAMP levels, whereas CaRas2 has been shown to decrease cAMPlevels. Together, these two act to maintain a fine balance of cAMP levels so that the cell can respond to hyphal stimuli by transient fluctuations in cAMP levels. In a closely relatedfungus, *Saccharomyces cerevisiae*, it has been shown that a subunit of the GPI-GnT complex,involved in GPI anchor biosynthesis, ScEri1, inhibits the function of ScRas2, i.e. the yeast homologue of CaRas1 (Sobering *et al*., 2004) .*Saccharomyces cerevisiae* mutants defective in ScRas2 show greater GPI-GnT activity The authors propose that ScEri1 engages ScRas in the ER and prevents it from going to the cell membrane. However, the case is completely contradictory in *Candida albicans*. We have seen in our lab that mutants of CaRas1 (which is the functional homologue of Saccharomyces cerevisiae Ras2) show lesser GPI-GnT activity. Also, mutating different subunits of the GPI-GnT complex has different effects on Ras1 activity in *Candida albicans*. *CaGPI19* mutants, for example show hyperfilamentation and greater CaRas1 activity, whereas *CaGPI2* mutants show a hypofilamentous phenotype and lower CaRas1 activity (Victoria *et al*., 2010; Yadav *et al*., 2014b). How exactly this association works and what are the other effects of Ras associating with the GPI-GnT complex *in Candida albicans* and *Saccharomyces cerevisiae* is something that is currently under investigation in our lab. CaRas1 signaling pathway controls filamentation in *Candida albicans* by working through a cAMP dependent PKA pathway. Apart from the CaRas1 signaling pathway, there are some other pathways also that control filamentation, for e.g., the MAPK pathway and theRIM101 pathway. In the MAPK pathway, the kinase involved is Hsf1 which triggers the activation of the transcription factor CaCph1, causing filamentation. Then, proteins like CaTup1, in association with CaNrg1 and CaRfg1, repress CaUme6, which also leads to increased filamentation. On the other hand, the RIM101 pathway controls filamentation in response to a change in the pH of the system. The CaSet3C histonedeacetylase complex, which can deacetylate histone H4 and is composed of the

CaSet3 and CaHos2 subunits, is present at highly transcribed genes and is also important for inhibiting the yeast-to-filament transition in a cAMP/PKA pathway-dependent manner. However, the CaRas1-PKA dependent pathway is the major pathway controlling filamentation in *Candida albicans* in response to a wide range of stimuli.Upon receiving signals like elevated temperatures, CO_2, pH change etc, CaRas1 binds to GTP and forms theactivated Ras1-GTP which interacts with downstream effectors, namely CaCyr1(or CaCdc35) which is the only adenylyl cyclase known in *Candida albicans*. It then causes an increase in the production of cAMP, which in turn triggers the release of the catalytic subunits of Protein Kinase A (PKA) from its regulatory subunits (CaBcy1). PKA then causes filamentation through the transcription factors CaEfg1. This pathway is controlled at various steps to keep the filamentation pathway under check. CaHsp90, the heat shock protein in *Candida albicans*, through CaSgt1, blocks the interaction of CaRas1-GTP with CaCyr1(Inglis and Sherlock, 2013). Cells devoid of CaHsp90 arehyperfilamentous, even at room temperature. The filamentation in the *Candida albicans* cells is, thus, a function of the CaHsp90 levels inside the cells. Also phosphodiesterases like CaPde1 and CaPde2 degrade cAMP and limit the hyphal formation. Conversion of CaRas1-GTP to CaRas1-GDP which is carried out by CaIra2, the only GAP in *Candidaalbicans* is inhibited by CaUbp3, which is a part of the ubiquitinating network in the fungus. Neurofilin is its mammalian homolog and has been studied for its role as a tumor supressor(Shapiro *et al*., 2009). Recent studies have shown that CaRas1 in *Candida albicans* exists in 2 forms, a full length form in hyphae whereas a truncated version that is pre dominant in the yeast form. The cleavage occurs after the N212 residue at the plasma membrane. This cleavage affects the CaRas1-CaCyr1 interaction in*Candida albicans*and strains wherein the cleavage site has been mutated, maintain the hyphal forms for a longer time(Piispanen *et al*., 2013).

1.3.3 *Interaction of Ras with the actin cytoskeleton*

The highly conserved adenylyl cyclase, CaCyr1 also binds to cyclase associated proteins inside the cell. In *Candida*, the only known cyclase associated protein till now is Cap1. It is also the only protein known to interact directly with CaCyr1. It was initially discovered in yeast, and since then, has been extensively studied in *Saccharomyces cerevisiae* and humans, and like Cyr1, Cap1 is also highly conserved in all eukaryotes, which allows us to extrapolate the studies done in yeast to other forms of fungi like *Candida albicans* as well (Fedor-Chaiken *et al*., 1990; Zhou *et al*., 2012). ScCap1 is a dual function protein; on one hand, it interacts with ScCyr1 through its N-terminus, and on the other hand, it interacts with the actin cytoskeletal elements to maintain the proper cytoskeletal network via its carboxyl terminus. ScCap1 in complex with the carboxyl terminus of ScCyr1 can associate with farnesylated ScRas, causing Ras-dependent ScCyr1 activation. It has a proline rich region through which ScCap1 interacts with SH3 domains of some proteins. Then it has a fourth domain responsible for oligomerization of ScCap1. Another report in yeast says that ScCap1 in association with the LRR domain of ScCyr1 (Shima *et al*., 2000) constitutes a Ras bindingsite and farnesylated ScRas binds to this and then the downstream signaling works. However, unmodified ScRas can also bind to ScCap1, but activation requires the addition of a farnesyl group. A change in the cytoskeletal organization has also been shown upon switch from yeastto the hyphal form in *Candida albicans*(Zou *et al*., 2009). CaCap1 has been shown to interact with the actin monomer, the G-actin. G-actin is the monomeric actin whichpolymerizes in a head to tail fashion to form actin filaments. There is a critical concentration of G-actin in the cell, which is about 0.1 μM(Wang *et al*., 2010). Once the G-actinconcentration rises above the critical value, it is released by CaCap1, and forms filaments, and when the concentration is more than the critical value, it is sequestered by CaCap1. CaCap1 has been co-purified with CaCyr1 and G-actin. Addition of actin polymerization inhibitors, latrunculin B or cytochalasin A, did not affect the levels of actin

bound to Cap1, suggesting that it is G-actin that is bound to CaCap1(Wang *et al.*, 2010).Although role of Cap1 has been shown in vesicle trafficking and endocytosis in yeast and some species of *Candida*(Epp *et al.*, 2013; Kaksonen *et al.*, 2005), however, till date, no clear cut interaction of CaRas1 with CaCap1 or any other proteins of the cytoskeletal network in *Candida albicans* has not been shown. A report in *Saccharomyces cerevisiae*, however, proves that the N-terminus of ScSrv2(Cap1 homologue in yeast) facilitates Ras signaling and that stabilization of F-actin filaments leads to Ras hyperactivation(Gourlay and Ayscough, 2006). This is described in detail in Chapter 4 of this study.

1.3.4 *Signaling of Ras from various intracellular organelles*

Another interesting feature about Ras is that it can signal from various locations inside thecell, not only from the plasma membrane (Hancock, 2003).In mammalian systems, Ras has been shown to reside in the ER/Golgi also, interacting with the scaffolding proteins like SNX17 and SNX27. Phosphorylation of Ser181 on K-Ras inhibits its plasma membrane association, causing K-Ras to translocate to the cytosol where it triggers apoptosis(van der Hoeven *et al.*, 2013). In case of *Candida albicans*, it has been shown that mitochondrial inhibitors decrease CaRas1 activity and GTP-binding thereby repressing hyphal formation(Grahl *et al.*, 2015). In human COS-1 and Jurkat T-cells, K-Ras interacts with Bcl-XL in the mitochondria to trigger apoptosis, whereas in cancer cells, antiapoptotic Ras signalling occursin the mitochondria. On the other hand, N-Ras initiates retrograde signaling to the nucleus from the mitochondria (Prior *et al.*, 2012).

1.4 *Objectives of this study*

As described in the previous sections of this chapter, studies are being done in our lab regarding the cross talk amongst different subunits of the GPI-GnT pathway with the CaRas1 signaling pathway in *Candida albicans*. We have reported that *CaGPI2* interacts with CaRas1 signaling pathway and *CaGPI2* and *CaGPI19* negatively interact with each other.

- ❖ This study mainly deals examines how and why CaRas1 signaling pathway is affected in the GPI biosynthetic mutants with our focus on *CaGPI2* and *CaGPI19*.

- ❖ Additionally, we attempted to study the physical interaction between CaGpi2 and CaGpi19 and their dynamics using fluorescence based approaches.

Chapter 2

Materials and Methods

2.1 Materials

2.1.1 *Chemicals/Reagents*

All thechemicals used were of analytical grade and purchased from Sigma Aldrich, Fluka, Merck, Invitrogenor SRL. Growth media were purchased from Himedia, Fisher Scientific and Qualigens. The DNA sequences for designing primers were retreived from Candida Genome Database and NCBI. The primers used for the study were synthesized by Sigma-Aldrich/GCC Biotech/Xceleris Genomics in lyophilized form and reconsituted in sterile TE buffer and used at a working concentration of 2μM. Antibodies and other enzymesand stains were purchased from Genei NEB or Thermo Scientific.

2.1.2 *Plasmids and strains*

The parent strain of *Candida albicans* used in this work is BWP17 and all mutants were generated in this strain only (Wilson *et al*., 1999). SN152 wild type strain was used for BiFC studies. The different plasmids and strains used in this study are listed in Table I and II. All the primers used for this study are listed in table III. The *Candida albicans* mutants were generated using a PCR mediated strategy which is explained in detail in the later section. Lithium acetate method or electroporation was used for transformation of *Candida albicans* strains. All the *Candida albicans* strains were grown at 30°C unless otherwise stated. Strains were grown either in YEPD medium or in synthetic defined (SD) medium with appropriate amino acids according to the auxotrophic status of the mutant/wild type strain. Uridine was addedfor Ura$^-$ strains at a concentration of 12mg/100mL. The composition of the dropout mix used is mentioned in the later part of this chapter.

2.2 The theoretical basis of the major fluorescence methods used in this study

2.2.1 Fluorescence Correlation Spectroscopy (FCS)

The major technique used in this study is fluorescence correlation spectroscopy. This technique was first shown in 1972 by Magde, Elson, and Webb (Elson and Magde, 1974; Magde *et al.*, 1974; Maiti *et al.*, 1997). In FCS, the diffusion of the fluorescent probe is monitored in a small confocal volume, of the order of ~1 fL. The fluorescence signal observed will depend on the diffusion of the particle, when sufficiently diluted. This is because, when the sample is sufficiently dilute, at a time, only one (or few) molecules are there in the confocal volume. Hence, the fluorescence observed depends on the diffusional dynamics of the fluorescent molecule; giving rise to fluctuations in the fluorescence signal. On the other hand, presence of multiple fluorophores, as in a concentrated sample can mask the fluctuations in the fluorescence intensity of each fluorophore, making it difficult to interpret the diffusion of a single molecule Larger the particle, slower will be the diffusion and vice-a-versa (Figure 2.1).
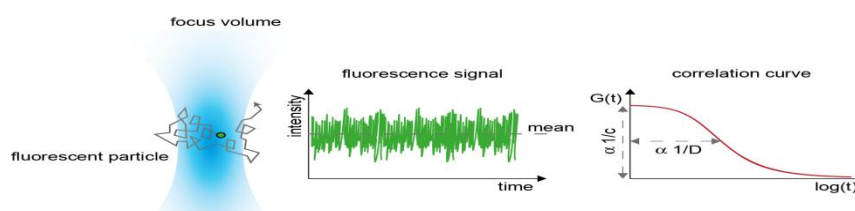
BioQuant (DKFZ-German Cancer Research Centre)

Figure 2.1:A schematic diagram showing how FCS (Fluoroscence Correlation Spectroscopy) works.

This technique can be used directly or indirectly in a number of biological applications. For e.g., aggregation of the fluorescent particle/fluorescently tagged protein under particular conditions will give a slow diffusion time and can be studied. Similarly, if one of the reactants of a reaction is fluorescent, and there is a change in fluorescence in the product,

then fluorescence cross correlation can be used wherein two lasers are employed and we can monitor the formation of the product. The beauty of this technique is that it can be adapted and used across disciplines, from chemical sciences to biological sciences, as per the need. People have studied intercalation of various dyes in DNA (Verma *et al*., 2012) to formation of amyloid β oligomers in case of Parkinson's disease (Garai *et al*., 2007; Sengupta *et al*., 2003) to signaling pathways on modeled membranes (Lin *et al.,* 2014) and uncovered quite a lot of useful information.

FCS differs from other fluorescent techniques in the sense that the main focus is not on theemission intensity, but on the fluctuations in the intensity caused by minute deviations in the system under study. When the technique was developed initially by Elson and Webb, it still had poor signal to noise ration because of inefficient background suppression and low detection efficiency. Rigler and his team combined FCS with confocal detection which is used in most experiments till date (Rigler *et al*., 1993). The incoming laser is strongly focused by a high numerical aperture objective (NA ≥ 0.9) to a diffraction limited stop (Figure 2.2). So, only the few fluorophores in the illuminated region are excited, which significantly improves the signal to noise ratio.
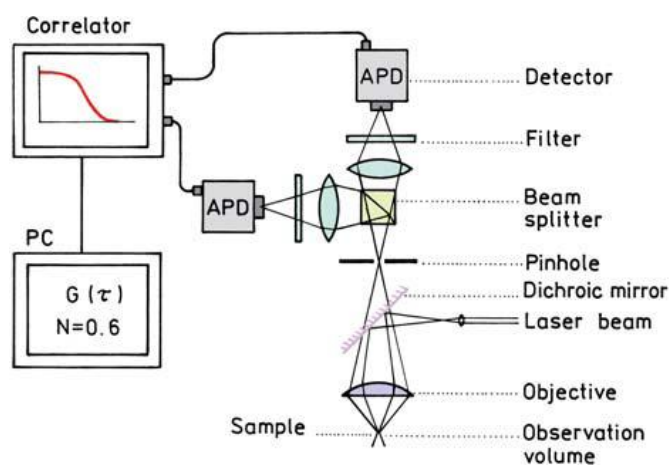
Figure 2.2:A typical FCS set up.(Lakowicz, 1999)

A typical FCS setup consists of a laser which is reflected into an objective by a dichroic mirror (Figure 2.2). The laser beam is focused on the sample, which is dilute enough such that there are about 1-10 particles in the confocal volume of ~1 fL. When the particles crossthe focal volume, they fluoresce and give a peak.This signal reaches the detector, a photomultiplier tube, an avalanche photodiode detector or a superconducting nanowire single-photon detector. The resulting electronic signal can be analyzed as an intensity versus time or special correlator cards can be used to give the autocorrelation (or cross-correlation directly. The parameters of interest can be determined after fitting the autocorrelation curve to the desired mathematical model. Also these days, dual color cross correlation is also used to study systems where diffusion times differ by a very small magnitude by exciting the sample with two different lasers and the fluorescent signal is cross correlated to get a direct measure of the reaction efficiency.

Autocorrelation Analysis

The diffusion of the fluorophores in and out of the confocal volume give rise to fluctuationsin the fluorescence intensity, which is denoted by $\delta I(t)$. Assuming that there is no change inthe laser excitation power during the course of the experiment, these fluctuations are defined as below (Lakowicz, 1999):

$$\delta I(t) = I(t) - \langle I(t) \rangle \dots (i)$$

where $\langle I(t) \rangle = \frac{1}{T} \int_0^T I(t) dt$.

These fluctuations are then correlated with themselves (hence the name autocorrelation), shifted at a time τ later, which is known as the lag time. This is done by a correlator card connected to the FCS setup. The (temporal) autocorrelation function is given by:

$$G(\tau) = \frac{\langle \delta I(t)\delta I(t+\tau)\rangle}{\langle I(t)\rangle^2} \dots (ii)$$

As the time lag τ increases, the autocorrelation drops to zero as the probability that the fluctuations at time t and at time t+τ are caused by independent particles, increases and if τ is small, we tend to get a higher autocorrelation. Now, assuming that the sole reason for fluctuations is a change in the concentration of the fluorophores in the excitation volume, and other parameters like change in laser power, detection electronics, photochemistry etc are unchanged during the course of observation, $I(t)$ can be written as:

$$\delta I(t) = \iiint \Phi(r)\delta C(r,t)dr \dots (iii)$$

where $\Phi(r)$ represents the detection efficiency of the photons emitted and also includes contributions from the optics of the microscope, quantum efficiency of the fluorophore, viscosity of the sample and all other constants. $\delta C(r,t)$ represents change in the concentration of the fluorophore at location r and time t. Equations $(i) - (iii)$ can be solved to express the autocorrelation $G(\tau)$ as:

$$G(\tau) = \frac{1}{V_{eff}\langle C\rangle}\frac{1}{1+\frac{\tau}{\tau_D}}\frac{1}{\sqrt{1+\frac{\tau}{\tau_D}\left(\frac{r_0^2}{z_0}\right)}} \dots (iv)$$

where V_{eff} is the effective confocal volume, which is approximately $\pi^{3/2}\ r_o^2 z_o$ and τ_D corresponds to the translational diffusion time of the molecule. Hence diffusion time can be estimated from this autocorrelation function. Equation *(iv)* can also be used to calculate the concentration of the fluorophore as at τ=0,

$$G(0) = \frac{1}{V_{eff}\langle C\rangle} \dots (v)$$

Thus, the number of particles in the confocal volume at any given point of time, $Veff <C>$ $\equiv N$. As the autocorrelation function is a ratio of variance to its mean (equation *(ii)*), and assuming the fluctuations follow a Poisson distribution,

$$G(0) = \frac{\langle \delta N^2 \rangle}{\langle N \rangle^2} = \frac{N_{eff}}{N_{eff}^2} = \frac{1}{N_{eff}} \dots (vi)$$

As explained earlier equation *(vi)* also shows that more dilute is the sample, greater is the autocorrelation we get. The correlation curves obtained after the FCS measurements are then fit to an appropriate diffusion model to extract out the required information, according to the type of diffusion the fluorophore undergoes. The model that is used to fit the correlation curves depends on the fluorescent probe being used and the problem that is being addressed. For example, small molecules diffusing freely in a solution will undergo 3D diffusion, whereas a fluorescent dye in a lipid bilayer will undergo 2D diffusion (Sengupta *et al.*, 2002). Hence, careful selection of an appropriate diffusion model is essential to interpret the results correctly. Below are mentioned some modifications of FCS which can be used to address even more advanced problems.

Fluorescence cross-correlation spectroscopy

Two colour fluorescence cross-correlation spectroscopy (FCCS) is used to measure interactions by cross-correlating two or more fluorescent laser signals. This distinguishes interactions more sensitively than FCS, particularly when the mass change in the reaction is small. This is particularly useful when studying protein-protein interactions.

FRET-FCS

Here there are two types of fluorescent probes, with a single channel and light is only detected when the two probes are very close, such that there is an interaction between the

two.The FRET signal is weaker than with fluorescence, but has the advantage that there is only signal during a reaction.

Scanning FCS

Here the confocal volume is moved across the sample, thereby scanning the sample for correlation. This is mainly used tracking protein translocation in live cells.

2.2.2 Steady State Anisotropy

Steady state anisotropy is another fluorescence based technique wherein we get to study the immediate microenvironment around a fluorescent probe. The fluorescent probe is excited with vertically polarized light and the horizontal and vertical components of the light emitted is measured (I_{VV} and I_{VH}). Figure 2.3 shows the basic setup used for measuring steady state anisotropy.
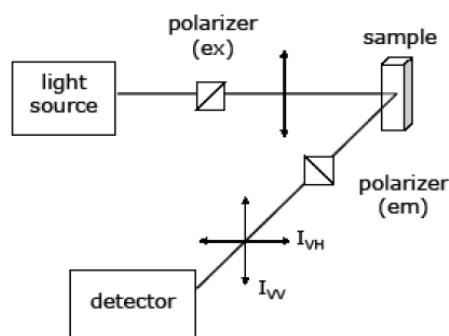
Figure 2.3: Basic setup of an L-shaped fluorimeter used to measure steady state fluorescenceanisotropy.(http://courses.chem.indiana.edu/a316/documents/FluorescenceAnisotropy.pdf)

If the probe is able to rotate freely, as in an isotropic environment, both the horizontal and vertical components of the emitted light are equal; however if that is not the case, as is mostly the case in biological systems, like cell membranes, for example, the probe preferentially emits light in a particular direction, hence giving rise to a difference in the horizontal and

vertical components of the emitted light. Anisotropy (r) is an experimental measure of the fluorescence depolarization. The lower the value of anisotropy, the faster is the rotational diffusion of the probe. In steady state anisotropy, the fluorescent probe is constantly illuminated which provides a steady stream of molecules in the excited state. Equation (vii) is used to calculate the steady state anisotropy:

$$r_{SS} = \frac{I_{VV} - GI_{VH}}{I_{VV} + 2GI_{VH}} \cdots (vii)$$

In the above equation, G represents the correction factor (G= I_{HV}/I_{HH}), i.e the ratio of the light emitted in the verticl direction (I_{HV}) to that in the horizontaldirection (I_{HH}), when the excited light is horizontally polarized.The G-value essentially measures the sensitivity of the detector for detecting vertically and horizontally polarized light. The theoretical maximum value of anisotropy is 0.4 which arises due to a phenomenon called photoselection. Photoselection refers to the selectivity in the excitation of a population of randomly oriented fluorophores whose electric vectors are aligned approximately along the direction of polarized excitation light (Lakowicz, 1999).

2.2.3 Bimolecular Fluorescence Complementation (BiFC)

This is an in vivo technique which is also used widely in many biological systems nowadays to study physical interaction between different proteins of interest. This is somewhat like yeast two hybrid in the sense that the prey and the bait proteins are cloned and expressed with two halves of any fluorescent proteins. The two halves of the fluorescent protein, howevermust be carefully chosen such that they do not spontaneously interact. If the bait and the prey proteins interact physically, they would come closer, leading to formation of the complete fluorescent molecule which would give us fluorescence (Figure 2.4). The fluorescence can be then observed under a fluorescence microscope. This technique is being

used widely nowadays, from mammalian cell lines to plants to fungal systems and is a quick and easy way to screen interacting partners from a large library (Abrahamsson, 1979; Ohad and Yalovsky, 2010).

(Fan *et al*., 2008)
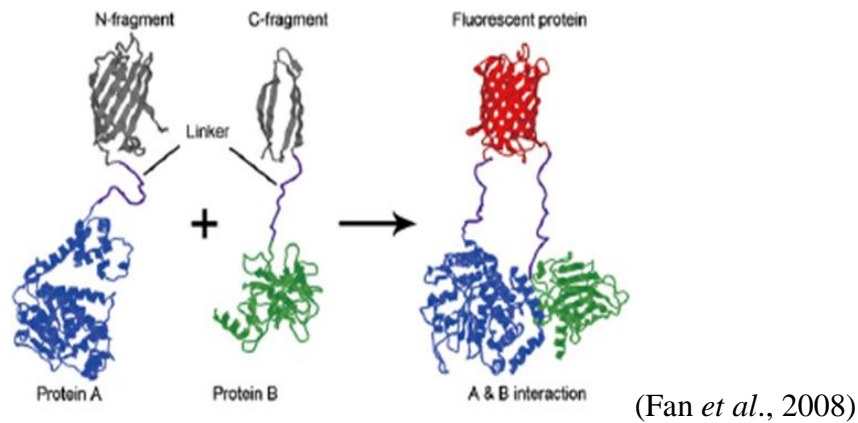
Figure 2.4:Cartoon depicting the technique of Bimolecular Fluorescence complementation.

Having got a brief overview of the different fluorescent techniques, it is clear how versatile these techniques are modulating these techniques according to the needs of the experiment can provide a plethora of information; ranging from pH of the surrounding microenvironment to the exact orientation of the molecule in the cell to the dynamics of a protein in vivo under different conditions to physical interaction between any two proteins of interest to name just a few. Also, membrane proteins which were hitherto difficult to study can now be accessed bythese techniques. Moreover, since the size of a majority of these fluorescent tags are small insize, they do not disturb much of the natural microenvironment of the concerned membrane protein. Also, to study a protein from scratch, or even a membrane protein, FLIM can be performed initially to check for its exact localization; which could be followed by anisotropy to check for its orientation in the membrane, and then FCS and FRET and other techniques. So these fluorescent techniques that are coming up now can provide so much information without using complex techniques like NMR etc.

2.3 Methods

2.3.1 *Generation of mutants in Candida albicans*

Generation of mutants in *Candida albicans* involves homologous recombination. For disruption of any gene or for promoter replacement, the cassette to be replaced with is amplified using appropriate primers which also generate an overhang at both ends for homologous recombination (Figure 2.5). The DNA fragment is then purified using NaCl and absolute ethanol and then transformed into *Candida albicans* using LiAc method or electroporation. Conditional null mutants were created by disrupting one allele of the desired gene with *HIS1/ARG4* marker and placing the second allele under the control of regulatable *MET3* promoter using the *pMET3-URA3-GFP* cassette.
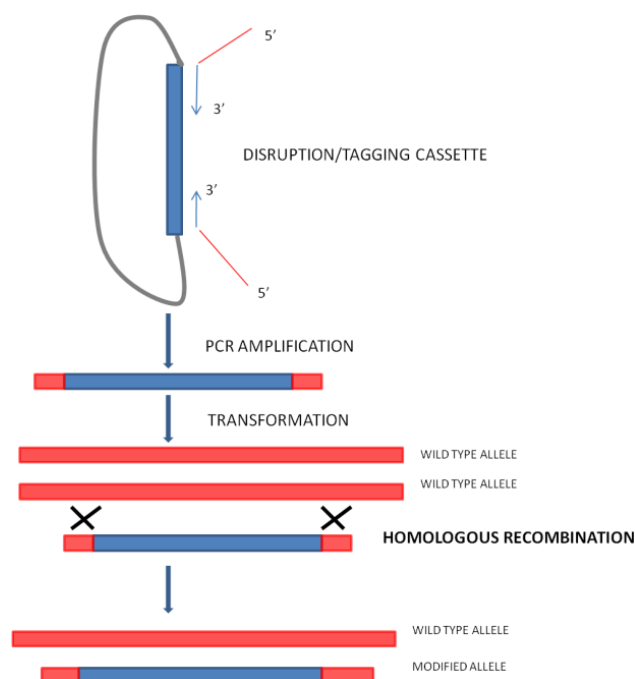
Figure 2.5:PCR mediated strategy involving homologous recombination to create disruption mutants or tag any gene in *Candida albicans*.

To over express any gene, thedesired gene of interest was cloned downstream of theconstitutively active *ACT1* or *ADH1* promoters using the appropriate restriction sites, in

pACT1-GFP or *pEGFP* vectors respectively. The plasmids have a part of the *RPS1* locus in them. Hence, these plasmids weredigested with Stu1 enzymes, which lies in this *RPS1* site, so as to linearize them. The linearized DNA was purified as before and proceeded for transformation, which resulted inthe integration of the plasmid in the *RPS1* locus of the *Candida albicans* genome. Similarly, to tag any gene with RFP at the C-terminal end of the gene, an *mRFP-ARG4* cassette was amplified with appropriate primers and used for homologous recombination.

2.3.2 *Transformation of Candida albicans by lithium acetate method*

Transformation of *Candida albicans* by lithium acetate method was performed using the protocol by Walther and Wendland, 2003. A primary culture was set up in YEPD medium and incubated at 30°C with continuous shaking overnight. Then a secondary culture was set up with 2% innoculum from the primary culture for 5-7 hours till O.D reached 2.0. The cells were then harvested and washed and resuspended in 1 ml of 0.1 M LiAc. In a separate microcentrifuge tube, the purified DNA to be transformed was added along with 10 µL of ssDNA (10 mg/ml). Then about 100 µL of the cells were added and mixed thoroughly and kept at 30°C without any shaking for 30 minutes. To this, then PLATE mix was added (1 volume 50% PEG, 1 volume of 1 M LiAc and 8 volumes of autoclaved sterile water). The mixture was then mixed thoroughly by vortexing and kept at 30°C overnight. Then, heat shock was given to the cells in a water bath at 42 °C for 30-45 minutes. The cells were thenwashed with water and plated on appropriate selective plates. Colonies appeared after 2-3 days. The colonies were then screened by isolating the genomic DNA for the cells and amplifying the desired DNA fragment through PCR.

2.3.3 *Transformation of Candida albicans by electroporation method*

Transformation of *Candida albicans* by electroporation method was performed using the protocol by De Backer *et al*., 1999. Briefly, a 20 ml secondary culture was set up in YEPD medium for 5-7 hours till log phase. Cells were harvested, washed with sterile water and resuspended in 1X TE-LiAC buffer pH 7.5 and kept at 30°C for 1 hour. Then, 150 µl of 1M DTT was added and kept at 30°C for 30 minutes. The cells were then pelleted, washed with water and then washed with 1M sorbitol. The cells were resuspended in 100 µl of 1M sorbitol and transferred to a fresh microcentrifuge tube. The DNA to be transformed was added and mixed by pipetting. This mixture was transferred to a 0.2 mm electroporation cuvette and pulse was given (1.5 kV, 200 Ω). The cells were washed with sorbitol andresuspended in 1ml YEPD medium and kept on shaking at 30°C overnight. The cells were pelleted the following morning and plated on an appropriate selective plate. Transformed coloniesappeared after 2-3 days and screened for integration of the transformed DNA cassette.

2.3.4 *Genomic DNA isolation from Candida albicans*

Genomic DNA was isolated from the colonies obtained after transformation using the protocol from Amberg *et al*., 2006. Briefly, cells pelleted from a 10ml overnight culture were lysed with glass beads, (5 cycles vortexing 1 min each followed by 1 min on ice) and 275 µlof 7M ammonium acetate added to the lysate and boiled at 65°C for 5 minutes and then chilled. 500 µl chloroform was added and centrifuged at 12000 rpm for 15 minues and the upper layer was treated with RNAse for 30 minutes. After another round of extraction with chloroform, the DNA was precipitated by adding isopropanol. The pellet was washed with 70% ethanol and resuspended in water. 2-4 µl of this DNA was used as template for confirmation of positive transformant colonies.

2.3.5 *RNA isolation from Candida albicans*

For isolation of total RNA from *Candida albicans*, 10 ml overnight culture in appropriate media was harvested and the pellet was washed with DEPC treated water, and 1 ml of TRI reagent and 0.8 gm acid-washed glass beads were added to it. The pellet was vortexed thricefor 1 minute each, and kept on ice for 1 minute each. The supernatant was collected in a 2 ml microcentrifuge tubes and to it, 200 µl of chloroform was added, and kept at room temperature for 5-10 minutes. The samples were inverted gently a few times, and centrifuged at 12000 rpm for 5 minutes at 4°C. The upper phase was collected in a fresh 2 ml microcentrifuge tube, and to this 500 µl of chilled isopropanol was added. The tubes were inverted a few times, and centrifuged at 12000 rpm for 15 minutes at 4°C. The pellet was washed in 75% ethanol, air dried, and resuspended in 40 µl of DEPC-treated water and stored at -20°C. The yield and quality of the isolated RNA was measured spectrophotometrically using the NanoDrop® ND-1000 UV-Vis Spectrophotometer using a 1 µl aliquot of the RNA. An absorbance ratio of $A_{260/280}$ of ~2.0 is regarded as a pure sample of RNA. An absorbance ratio of $A_{260/230}$ is used as a secondary measure of nucleic acid purity. This ratio should commonly be in the range of ~1.8-2.0 for a pure sample of RNA. The concentration of thesample RNA is calculated based on the A_{260} value. An A_{260} value of 1.0 corresponds to 40 µg/ml of RNA in water.

2.3.6 *Agarose Gel Electrophoresis of RNA*

For assessing the integrity of the isolated RNA, a 1.5% denaturing agarose gel was prepared by dissolving 0.60 g of agarose in 28.8 g of water (for a 40 ml gel), and once sufficiently cooled, 4 ml of 10X TAE and 7.2 ml formaldehyde was added to it. This was poured on a gel tray that had been cleaned with 10% SDS.

2.3.7 *RNA sample preparation*

To a 2.0 µl aliquot of the isolated RNA, 2.0 µl of 10X TAE, 4.0 µl of formaldehyde, 10.0 µl of formamide and 1.0 µl of EtBr was added. heated at 65°C for 15 minutes and kept for 10 minutes on ice. To this, 5 µl of 50% glycerol was added, loaded in the 1.5% denaturingagarose gel. The gel was run at 80V with 1X TAE running buffer. The integrity of the isolated total RNA was assessed by the presence of distinct 25S, 18S and 5.8S rRNA bands. To rule out any DNA contamination in the RNA preparation, a PCR reaction was set up using primers of any gene. Absence of any amplification indicated a pure RNA sample, devoid of any genomic DNA comtamination.

2.3.8 *cDNA preparation*

3 µg of RNA was taken and cDNA was prepared by Biorad Iscript cDNA synthesis kit as per manufacturer's instructions.

2.3.9 *Transcript level analysis*

1 µl of the prepared cDNA was taken and 2.5 µl each of appropriate forward and reverse primers (0.2 µM) was added alongwith 1.5 µl of nuclease free water. To this reaction mixture, 7.5 µl of SYBR Green was added. The real time PCR reaction was run in Applied Biosystems real time PCR machine and transcript levels were quantified. GAPDH was taken as an internal control in all cases.

2.3.10 *Sterol extraction from Candida albicans*

Sterol extraction was done from *Candida albicans* using the protocol from Arthington-Skaggs *et al.*, 2000 0.1 O.D cells from a 10 ml overnight grown primary culture of *Candidaalbicans* was used to inoculate a 50 ml secondary culture in YEPD, which was

grown for 16 hours. Cells were harvested and pellet weights equalized. 4.0 gm glass beads and 10 ml methanol was added and the cells were lysed by vortexing 10 times for 1 minute each, followed by 1 minute incubation on ice. The cell lysate was transferred to a glass vial, and 20 ml chloroform was added to it. These vials were kept on a rocker for 2 hours in the dark at 37°C. Samples were filtered in a culture tube through Whatman filter paper. The filtrate was collected and to this 0.2 volume of 0.9% saline was added. Any upper layer that formed was moved, and samples were dried under N_2 gas at 50-60°C. To the dried sample, 400 μl of chloroform, 3 ml absolute ethanol, 300 μl of alcoholic KOH (33% w/v) was added and boiled at 65°C for 45 minutes. Finally, 5 ml n-hexane was added for sterol extraction. The samples were brought to room temperature, 1 ml water was added, and vortexed for 5 minutes. The upper organic (hexane) layer was separated. 100 μl of 1 mg/ml of cholesterol was added tothe samples as an internal standard. For derivatization of sterols, 100 μl of BSTFA+TMCS 99:1 (N,O-Bis(trimethylsilyl) trifluoroacetamide with trimethyl-chlorosilane) was added, and samples were incubated at 80°C for 1 hour. Finally, samples were dried under N_2 gas at 50-60°C, and resuspended in 400 μl hexane and analysed by GC-MS. Gas Chromatography-Mass Spectrometry was performed using the Shimadzu QP-2010 Plus in AIRF, JNU. A DB5-MS column (with dimensions of 30 m×0.2 mm with a film thickness of 0.20 μm) was used with an Electrospray Ionization source and Helium as the carrier gas (flow rate of 1.21 ml/min at a pressure of 173.4 kPa). 2 μl of the sample was injected using the splitless mode. The initial column oven temperature was 100°C which was held for 1 min, elevated to 240°C at 20°C/min and the final temperature was 300°C at 3°C/min with a 10 minute hold. Peaks were identified on the basis of the retention time as well as the total mass/charge ratio of thespecies. Measurement of ergosterol levels was done by normalizing the area of the ergosterol peaks in the sample with that of cholesterol.

2.3.11 *Candida albicans spot assays*

Spot assays were performed to monitor the growth of strains under different conditions, like the presence of a drug or cell wall perturbing agent etc as described in (Victoria *et al.*, 2010). Briefly, a primary culture was set up in SD - minimal medium overnight until saturation.Next day, a secondary culture was set up with 2% of the primary innoculum till log phase. The OD_{600nm} was measured and a dilution of 0.1 OD cells was made in 0.9% saline. 5 fold serial dilutions were made in saline and 5 µl of the dilutions were spotted on the appropriate plate and incubated at 30°C. Images were captured at regular intervals in Alpha Fast view in visible light.

2.3.12 *Filamentation assay*

To check for the filamentation pattern of the strains in solid medium, cells were grown to log phase in SD minimal medium. The OD_{600nm} was measured and a dilution of cells corresponding to 0.2/0.4 OD_{600nm} was made in 0.9% saline. 10 µl of these cells were spotted on Spider/YEPD/indicated plates and incubated at appropriate temperatures and images were taken at the indicated time in Nikon SMZ1500 microscope. To check for the filamentation pattern of the strains in liquid medium, a primary overnight culture was set up of the desired strains in SD minimal medium and a secondary culture was set up in 10 ml hyphae inducingSpider medium with cells corresponding to 0.2 OD_{600nm} (Sudbery, 2011). This culture was incubated at 37°C with shaking at 220 rpm and aliquots of 500 µl were taken every 30 minutes. These cells were washed with PBS, and resuspended in 50 µl of 80% glycerol. 10 µl of these cells were placed on a glass slide and covered with a glass slide. The slides were viewed in Nikon eclipse TiE/90i microscope.

2.3.13 *Preparation of plasma membranes from Candida albicans*

Plasma membrane preparations were made from *Candida albicans* cells using the protocol by Shukla *et al*., 2003.A primary culture of the required *Candida albicans* strain was set up in appropriate selective SD- medium at 30°C overnight with shaking at 220 rpm until saturation. Then a secondary culture was set up in 200 mL selective medium using 2% of the primary culture for 16h at 30°C with shaking at 220 rpm. The cells were then harvested and the pellet weight was equalised for all the different strains being used. The pelleted cells were then lysed in buffer containing 50 mM Tris pH 7.5 and 2.5 mM EDTA, protease inhibitor cocktail and 1mM PMSF. Lysis was done by vortexing the cells for 15 rounds (1 minute vortexing followed by 1 minute on ice). The lysate was separated by centrifugation at 1000g to remove the unbroken cells. The supernatant was then ultracentrifuged at 1,00,000 g for 1 h and the crude membranes obtained in the pellet were resuspended in buffer consisting of 10 mM Tris pH 7.5, 0.5 mM EDTA and 10% glycerol. This suspension was then applied to a discontinuous sucrose gradient (53.5% (w/v) sucrose and 43.5% (w/v) sucrose). After centrifugation for 5 h at 100 000 g the purified plasma membranes were recovered at the interface of the two sucrose layers. They were carefully extracted with a syringe and stored at -80°C until further use. Protein estimation was done using BCA kit as per the manufacturer's instructions.

2.3.14 *DPH labeling*

For microscopic studies, late-log phase *Candida albicans* cells were washed with water to remove media and then spheroplasted in lyticase-buffer (3 units/ml of lyticase in lyticase buffer) at room temperature for an hour. After washing, cells were resuspended to an OD_{600nm} of 0.5 in 10 mM PBS containing 2 μM DPH (Sigma Aldrich). Cells were stained in the dark for 20 minutes with gentle shakingand then washed twice to get rid of unbound fluorophore and resuspended in 80% glycerol. The cells were spotted on microscopic slides and

proceeded for microscopy. Microscopic images were captured under DAPI filter.For steady state anisotropy measurements, DPH was added at the same concentration to 50 μg of prepared plasma membranes and kept in dark at 4°C for 10 minutes. Steady state anisotropy measurements were made using an excitation of 348 nm (slit width 5 nm) and an emission of 430 nm (slit width 5 nm).

2.3.15 *Calcein-AM staining*

Calcein-AM staining was done to assess the intracellular viscosity by measuring the steady state anisotropy of Calcein in a particular strain. Log phase cells were taken of 0.5 OD_{600nm} were taken, washed with PBS and resuspended in 100 μM of Calcein-AM and kept for shaking in dark for 20 minutes. The cells were washed twice with PBS and resuspended in 1 mL of PBS and proceeded for steady state anisotropy measurements. An excitation of 495 nm (slit width 5 nm) and an emission of 515 nm (slit width 10 nm) was used.

2.3.16 *Steady state anisotropy measurements*

Anisotropy of DPH and Calcein-AM was measured on a Schimadzu spectrofluorimeter with a manual polarizer attachment. Steady state anisotropy, *r*, was measured as described earlier using equation *(vii).*

2.3.17 *Nile red dynamics*

Late-log phase cells were treated with lyticase (3U/ml) in lyticase-buffer for 1h at 25°C after which the cells were incubated with 0.4 μM of Nile red (Sigma Aldrich), in water for 45 minutes and washed twice prior The cells were then spotted on a microscopic slide and FCS measurements were made.

2.3.18 *mRFP-CaRas1 dynamics*

Late-log phase yeast cells of wild type (WT) strain and the conditional null mutant of *CaGPI19* expressing mRFP-Ras1, were taken and given lyticase-buffer treatment (3U/ml) for 1h at 25°C. The spheroblasted cells were then washed twice and placed on a polylysine coated coverslip and sealed on a glass slide. When required, the spheroplasted cells were incubated with geldanamycin (10 µM), tamoxifen (52 µM) for 1h cytochalasin D (20µM) for 16h, Latrunculin B (12.5 µM) for 1h or Jasplakonilide (1µM) for 2h washed and then samples were prepared for FCS measurements. For FCS measurements of the hyphal cells, 0.2 O.D$_{600nm}$ cells were inoculated in the hyphae inducing medium-Spider (1% mannitol, 1% nutrient broth and 0.2% K$_2$HPO$_4$) for 3 hours till almost all the cells were in the filamentous form. Since the FCS measurements in cells gave us a large spread in the diffusion timescales, we used the average traces of the normalized autocorrelation curves to fit to the model to obtain average diffusion times and diffusion coefficients. The autocorrelation curves were fit with the same equation as that for Nile red.

2.3.19 *Fluorescence correlation spectroscopy measurements*

A home-built fluorescence correlation spectrometer (FCS) set-up was used for this study,having an Olympus IX71 inverted fluorescence microscope with a 60X water-immersion objective (NA 1.2, UPlanSApo, Olympus) The set up was calibrated using Rhodamine-6G (R6G) in water and a 532 nm DPSS laser (Shanghai Dream Laser Technologies) was used throughout this work). The fluorescence signal was passed through a dichroic (Model-XF2016, Omega Optical Inc., USA) and emission filter (Model-607AF75, Omega Optical Inc., USA) then into a fibre patch cord (Model-QMMJ-3S3S-UVVIS-25/125-3-1, Oz Optics, Canada) of diameter 25 µm, which acts as the confocal pinhole. The fluorescence signal was detected using a single photon avalanche photo diode (Perkin Elmer,

SPCM-AQRH-13-FC). The autocorrelation of the fluorescence fluctuations were collected through FLEX correlator card (FLEX990EM-12D, Correlator.com, USA) in LabView software program. The correlation curves for R6G were fitted with 3-D diffusion model to calculate its diffusion time (τ_D) τ_D = 63 μs. From this value and the known diffusion constant of R6G, the axial resolution of the setup was determined to be ~285 nm and the observation volume was calculated to be ~ 1.01 fl. The measured correlation curves of mRFP-Ras1 and Nile Red inside membrane displayed the characteristics of typical two-dimensional diffusion and could be fitted well to two-component diffusion model (2D2C), multiplied with a triplet (flickering) contribution as given by

$$G(\tau) = \left\{ g_{01} \left(1 + \frac{\tau}{\tau_{D1}} \right)^{-1} + g_{02} \left(1 + \frac{\tau}{\tau_{D2}} \right)^{-1} \right\} \left\{ 1 + A_T \exp\left(-\frac{\tau}{\tau_T} \right) \right\} \dots (viii)$$

where the fractions, g_{0i} are related to $1/N_i$ where N_i are the average number of diffusing fluorescent particles in the detection volume), $\tau_{Di(NR)}$ are the diffusion times of mRFP-CaRas1 or Nile red through the detection volume and the subscripts *1* and *2* represent two different components. A_T and τ_T are the contribution and time-constant of triplet conversion/flickering which is explained in Chapter 3.

2.3.20 *Treatment of cells with methyl β-cyclodextrin (βCD) for membrane dynamics*

Spheroplasted cells as described above, were treated with 17.6 mM βCD in buffer for 1h at room temperature. The depletion of ergosterol levels was confirmed by sterol extraction followed by GC-MS.

2.3.21 *Mammalian culture and FCS*

MDA-MB-231 cells were cultured in L15 medium with 10% FBS. *pDsRed-H-Ras* and *pDsRed-H-Ras*^{G12V} were transfected in these cells using lipofectamine from Invitrogen.

DsRed expression was seen after 36h and cells were analyzed for FCS measurements. DsRed is known to exhibit dynamics that can be fitted to a single exponential under low laser power(Schenk *et al.*, 2004) and hence the autocorrelation curves were fitted to the equation given below where the triplet contribution was limited to 8-12 µs (equation *ix*).

$$G(\tau) = \left\{ g_{01} \left(1 + \frac{\tau}{\tau_{D1}} \right)^{-1} \right\} \left\{ 1 + A_T \exp\left(-\frac{\tau}{\tau_T} \right) \right\} \ldots (ix)$$

2.3.22 *Immunofluorescence studies*

A primary culture was set up for the required strains at 30°Covernight followed by a secondary culture for 6h at 30°C with shaking at 220 rpm. The cells were fixed by adding 3.7% formaldehyde in growth medium for 1h at 30°C. Then 1.0 OD of the cells were taken and subjected to lyticase treatment (3U lyticase for 1h at room temperature). The cells were washed twice with 1X PBS and treated with 0.1% triton X-100 for 20 minutes followed bywashing and blocking with 100 µl of BSA (Bovine Serum Albumin, 1 mg/ml) for 20 minutes. The cells were washed and 1° antibody was added (anti-β-actin antibody raised in mouse, Sigma Aldrich Cat# A1978, 1:50 dilution in PBS, or anti-β-actin antibody raised in rabbit, NEB Cat#13E5, 1:50 dilution in PBS, or anti-Ras antibody, 1:400 dilution in PBS, Merck millipore Cat# 05-516) and kept on rocker overnight at 4°C.After washing with PBS, the appropriate secondary antibody (goat anti mouse-FITC, 1:50 dilution in PBS or goat anti rabbit-TRITC 1:20 dilution in PBS)   was added at room temperature for 1h with constant rocking. The cells were washed twice with PBS and resuspended in 50 µL of 80% glycerol and spotted on a slide and covered with a glass slip. The cells were then visualized under Nikon 1X71 confocal microscope or in AIRF, JNU using appropriate FITC (Fluorescein isothiocyanate) and TRITC (Tetramethyl rhodamine) filters.

2.3.23 *Staining of polymerized actin filaments*

The F-actin filaments in the cells were visualized by staining them with phalloidin (Oberholzer *et al*., 2002), which specifically binds to F actin. Rhodamine-phalloidin was used in this study. Briefly, log phase cells were taken, washed with PBS, then resuspended in 3.7% formaldehyde for 30 minutes. Thereafter, the cells were fixed in 3.7% formaldehyde in PK buffer for 1 h at room temperature. Then the cells were washed once with PK buffer and then incubated with 50 mM PK buffer having 0.1% Triton-X 100 for 30 minutes. The cells were finally washed twice with PBS and stained with phalloidin at a dilution of 1:50 in PBS. For CaRas1 and actin co-localization experiments, the anti-Ras antibody (at the same dilution as for immunostaining experiments) was also added along with phalloidin. Images were captured in confocal Nikon 1X71 microscope or in AIRF using appropriate filters.

2.3.24 *Statistical significance*

Student's t test was used to calculate the statistical significance. * denotes p value < 0.001 and ** denotes p value < 0.0001. Sigma Plot 8.0 was used for this analysis.

2.3.25 *Colocalization studies*

Pearson's correlation coefficient was used to calculate the colocalization between CaRas1 and β-actin or between CaRas1 and rhodamine-phalloidin. The analysis was done in Olympus Fluo View Software in AIRF, JNU.

2.3.26 *Immunoblotting*

For immunoblotting, 100 ml culture in late log phase of the required strain grown in SD-minimal medium was harvested, washed with sterile water and lysed using 1 mL lysis buffer. The crude lysate was clarified by centrifugation at 16000g for 15 minutes twice. Protein

estimation was done using BCA kit (Sigma Aldrich) using manufacturer's instructions. Around 500 µg of protein was loaded on a 12% resolving SDS-PAGE. Transfer was set up at 150V for 2 h followed by blocking using 5% skimmed milk for 1 hour. The blot was then probed with primary antibody (1:500 for Phospho p38 MAPK (Thr180/Tyr182 from CST (Cat # 9211S) and 1:2000 for anti-GAPDH (Sigma Aldrich, A9521) overnight followed by washing thrice with PBST (PBS+ 0.05% Tween-20). Secondary antibody was then added at a dilution of 1:5000 for 2 hours after which again washing was done twice with PBST and once with PBS. The blot was developed on an X-ray film using ECL kit (G-biosciences).

2.3.27 *Bacterial Cloning*

To clone any desired DNA fragment or gene of interest into a given vector, the gene (or the DNA fragment) has to amplified from genomic DNA or cDNA with appropriately designed primers. Many a times, if there is limitation of DNA source or to increase the yield of the insert or if primers with suitable restriction sites are not available, then the amplicon is first cloned into a TA vector. These are commercially designed vectors which have a ddT overhang on either ends in them. Many polymerases, like Taq polymerase for e.g., add ddA non-specifically to the amplicon and these can be directly ligated into the TA vector. Direct cloning is also done in which the PCR amplicon has suitable restriction sites which are added at both the 5' and the 3' ends by the primers. This DNA was purified by using 200 mM NaCl and 2.5 volumes of absolute ethanol. This was kept at -20°C for overnight for efficient precipitation and then centrifuged at 12000 rpm for 15 minutes. The precipitated DNA was washed with 70% ethanol and resuspended in sterile nuclease free water. The purified insert DNA and the vector into which the cloning has to be done were both digested with appropriate restriction enzymes overnight. The digestion reactions were then run on an agarose gel and the required bands of interest were cut out with a scalpel. The DNA was

eluted from the gel using Qiagen DNA gel extraction kit by following the manufacturer's instructions. The elutes were quantified using Thermo Scientific NanoDrop® ND-1000 UV-Vis Spectrophotometer. Thereafter,appropriate ligation reactions were set up overnight at 22°C. The ligation mixture was transformed to either *E. coli* DH5α or DH10β competent cells. The colonies were obtained after 16h. These were screened initially by colony PCR and then confirmed by plasmid isolation and restriction digestion of the isolated plasmids.

> ### *Preparation of competent cells.*

Ultra competent bacterial cells were prepared through Rubidium chloride method (Sambrook and Russell, 2006). Briefly, the strain of *E.coli* of which competent cells were to be prepared were streaked overnight on an LB plate and an LB-Ampicillin (Amp) plate and incubated at 37°C for 16h. The cells were streaked on the antibiotic plate to check for any contamination. After ensuring that there was no growth on the LB-Amp plate, the cells from the LB plate were innoculated in 10 ml of LB broth overnight at 37°C with shaking. Next morning, a secondary culture was set up in 100 ml LB (+20 mM $MgSO_4$) broth using 1% of the primary culture and kept at 37°C with shaking till OD_{600nm} reached around 0.5. The culture was transferred into sterile falcons in a laminar hood and harvested at 4500g for 5 minutes at 4°C. The cells were then resuspended in 0.4 volumes (i.e 40 mL) of RFI buffer and kept on ice for 5 minutes after which they were centrifuged at 4500g for 4 minutes at 4°C. The pellet was then gently resuspended in 4 mL of RFII buffer and kept on ice for 15-60 minutes and then aliquoted into microcentrifuge tubes. The prepared competent cells were flash frozen with liquid nitrogen and stored at -80°C until further use.

> ### *Site directed mutagenesis*

To make site directed mutants of a particular gene, the DpnI digestion method was followed (Weiner *et al.*, 1994). Initially the wild type copy of the gene was cloned in the

appropriateplasmid. Then, the whole plasmid was amplified by PCR using overlapping primers, which carried the mismatch in the codon where the mutation was to be introduced. Typically, a 50 µl PCR reaction was set up. This whole PCR product was digested overnight using DpnI enzyme, which specifically digests the parent methylated DNA, leaving the PCR amplified DNA intact. DpnI was inactivated at 65°C for 10 minutes and the product was cooled and used for bacterial transformation. The colonies obtained were screened initially using the colony PCR method with primers specific to the gene. The positive colonies were then given for sequencing and the sequences were aligned with the wild type to confirm the introduction of the mutation.

➤ *Colony PCR*

The colonies obtained after bacterial transformation were streaked on to a master plate (having the appropriate antibiotic) and the tip was resuspended in 10 µl water in a PCR tube. This was treated as the template and a PCR reaction was set up with primers specific to the insert. The PCR product was run on agarose gel electrophoresis and positive colonies wereinoculated in 10 ml LB broth with appropriate antibiotic and then the plasmid was isolated from these cultures.

➤ *Plasmid isolation from bacterial cultures*

A primary culture was set up in 10 ml LB broth with appropriate antibiotic (In this study 100 µg/ml ampicillin or 40 µg/ml kanamycin was used). This was kept at 37°C for 16h at 220 rpm shaking. Next morning, the plasmid was isolated by alkaline lysis method (Sambrookand Russell, 2006). Briefly, the cells were harvested at 5000 rpm for 5 minutes at 4°C. Then 200 µl of solution I was added to the pellet and resuspended and transferred to a 2 mlmicrocentrifuge tube. Then 400 µl of solution II was added followed by gentle inversion of the tube a couple of times. Solution III was added to this and mixed by inverting the

tube.This was centrifuged at 13000 rpm for 15 minutes at 4°C. The supernatant was transferred to a fresh 2 ml microcentrifuge tube and 5 µl of 10mg/ml RNAse was added and ket at 37°C for 30 minutes. Then 800 µl of 1:1 mixture of phenol and chloroform was added and mixed and centrifuged at 10000 rpm for 10 minutes at 4°C. The upper aqueous layer was taken in a fresh tube and another round of extraction was done with chloroform. The upper aqueous layer was taken in a fresh 1.5 ml microcentrifuge tube and isopropanol was added upto the brim of the tube and kept at -20°C for 30 minutes after which the tubes were centrifuges at 12000 rom for 10 minutes at 4°C. A final wash was given with 500 µl ethanol and the tubes were air dried to remove any residual traces of ethanol. The plasmids were dissolved in 30 µl of sterile water and stored at 4°C for short term use and -20°C for long term usage.

➢ *Restriction digestion*

To check the positive clones, the plasmids isolated were subjected to restrictiondigestion. Typically 2 µl plasmid was taken in a microcentrifuge tube and 1 µl of each restriction enzyme was added along with the appropriate buffer and water was added to make up the volume to 20 µl. The reaction was incubated at 37°C overmight. 10 µl of the reaction was checked on agarose gel to check the release of the dropout.

Table I: List of *Candida albicans* strains used in this study.

S.No.	Strain name	Genotype	Source
1.	BWP17 (Wild type)	ura3::imm434/ura3::imm434*iro1/iro1*::imm434 *his1*::hisG/*his1*::hisG*arg4/arg4*	(Wilson *et al*., 1999)
2.	BWP17-*mRFP-CaRas1*	BWP17 with *CaRAS1/mRFP-CaRAS1*	This study
3.	*Cagpi19* heterozygote	BWP17 with *Cagpi19::HIS1/CaGPI19*	(Victoria *et al*., 2010)
4.	*Cagpi19* null	BWP17 with *Cagpi19::HIS1/pMET3-GFP-CaGPI19*	(Victoria *et al*., 2010)
5.	*Cagpi19* null-mRFP-Ras1	*Cagpi19* null with *CaRAS1/mRFP-CaRAS1*	This study
6.	*Cagpi2* heterozygote	BWP17 with *Cagpi2::ARG4/CaGPI2*	(Yadav *et al*., 2014b)
7.	WT-*URA3*	BWP17 with *CaRPS1/Carps1Δ::pACT1-CaGFP::URA3*	(Yadav *et al*., 2014b)
8.	WT-CaRas1 OE	BWP17 with *CaRPS1/Carps1Δ::pADH1-mRFP-CaRAS1::URA3*	This study
9.	WT-CaRas1^{G13V} OE	BWP17 with *CaRPS1/Carps1Δ::pADH1-mRFP-CaRAS1 G13V::URA3*	This study
10.	*Caras1* null	BWP17 with *Caras1::HIS1/ Caras1::ARG4*	Priyanka Jain, 2016
11.	*Caras1* null-CaRas1 OE	*Caras1* null with *CaRPS1/Carps1Δ::pADH1-mRFP-CaRAS1 G13V::URA3*	This study
12.	*Caras1* null-CaRas1^{G13V} OE	*Caras1* null with *CaRPS1/Carps1Δ::pADH1-mRFP-CaRAS1^{G13V}::URA3*	This study
13.	*Cahsp90* null	BWP17-*mRFP-RAS1* with *Cahsp90::HIS1/pMET3-CaGPI19::URA3*	This study

14.	WT-*CaGPI2-RFP*	BWP17 with *CaGPI2/CaGPI2-RFP::ARG4*	This study
15.	SN152 (Wild type)	*arg4_/arg4_ leu2_/leu2_ his1_/his1_ URA3/ura3_::imm434 IRO1/ iro1::imm434*	He´le`ne Tournu, Katholieke Universiteit Leuven
16.	SN152-Prey *CaGPI2*	SN152 with Prey *CaGPI2* between *CaXOG1* and *CaHOL1* loci on chromosome 1	This study
17.	SN152-Bait *CaGPI19*	SN152 with Bait *CaGPI19* between *CaRXT3* and *ORF19.3569* loci on chromosome2	This study
18.	SN152-Prey *CaGPI19*	SN152 with Prey *CaGPI19* between *CaXOG1* and *CaHOL1* on chromosome 1	This study
19.	SN152-Bait *CaGPI2*	SN152 with Bait *CaGPI19* between *CaRXT3* and *CaORF19.3569* on chromosome 2	This study
20.	SN152-Bait *CaGPI2*+Prey *CaGPI19*	SN152 with Bait *CaGPI2* between *CaRXT3* and *ORF19.3569* loci on chromosome 2 and Prey *CaGPI19* between *CaXOG1* and *CaHOL1* loci on chromosome 1	This study
21.	SN152-Bait *CaGPI19*+Prey *CaGPI2*	SN152 with Bait *CaGPI19* between *CaRXT3* and *ORF19.3569* loci on chromosome 2 and Prey *CaGPI2* between *CaXOG1* and *CaHOL1* loci on chromosome 1	This study
22.	WT-*CaGPI2* hz-mRFP-RAS1	*Cagpi2* heterozygote with *CaRAS1/mRFP-CaRAS1*	This study
23.	BWP17-*pACT1-CaGPI2-mRFP-CaRAS1* (also referred to as WT-*pACT1-CaGPI2* in this study)	BWP17-mRFP-Ras1 with *CaRPS1/Carps1Δ::pACT1-CaGPI2::URA3*	This study
24.	BWP17-*pACT1-GFP-mRFP-RAS1*	BWP17-mRFP-Ras1 with *CaRPS1/Carps1Δ::pACT1-CaGFP::URA3*	This study

Table II: List of plasmids used in this study.

S.No.	Plasmid	Source
1.	*mRFPFF-YcpARG4*	This study
2.	*mRFPFF-ARG4-RFPSF*	This study
3.	*pACT1-GFP*	Alistair Brown, Aberdeen
4.	*pMET3-GFP-URA3*	This study
5.	*pMET3-GFP-HIS1*	This study
6.	*pJET-ARG4*	This study
7.	*pJET-RFP-ARG4*	This study
8.	*pEGFP*	Alistair Brown, Aberdeen
9.	*pGFP-ARG4*	This study
10.	*pTZ-HIS1*	(Victoria *et al,* 2010)
11.	*Ycplac111*	Michael Hall, University of Basel
12.	*pRS-ARG4*	(Wilson *et al*., 1999)
13.	*pURA3-MET3-GFP*	(Gerami-Nejad *et al*., 2004)
14.	*CIp10ADH1-mCherry*	(Keppler-Ross *et al*., 2008)
15.	Bait *CaGPI2*	This study
16.	Bait *CaGPI19*	This study
17.	Prey *CaGPI2*	This study
18.	Prey *CaGPI19*	This study
19.	TA-CmCh-*CaGPI2*	This study
20.	TA-CmCh-*CaGPI19*	This study
21.	*pADH1-mRFP-CaRAS1*	This study
22.	*pADH1-mRFP-CaRAS1^{G13V}*	This study
22.	*pJET1.2* blunt	Thermo Scientific Inc.
23.	*pDsRed-Express C1*	Rohini Muthuswami, SLS,JNU
24.	*pDsRed-Express C1-H-Ras*	This study
25.	*pDsRed-Express C1-H-Ras^{G12V}*	This study
26.	*pGEX-HIS1*	Yadav, B., 2013

Table III: List of primers used in this study.

Primer	Sequence (5'-3')
RFPFF FP	GCGCCCGGGATGGTTTCAAAAGGTGAAGAA
RFPFF RP	GCGGGTACCTTCTGATGAAGCTTCCCAACC
RFPSF FP	GCGGAGCTCGATTATTTAAAATTGTCATTT
RFPSF RP	GCGGGCGCCTTATTTATATAATTCATCCAT
RASRFPFP	AAAAAGAAACCCCGGGCAAACACAAATTCATATCCACACA TATACATACCATGGTTTCAAAAGGTGAAGAAGATAATAT
RASRFPRP	GATTACCAACACCACCACCTCCAACAACAACTAATTTATA TTCTCTCAATTTATATAATTCATCCATACCACCAGTTG
RAS1 FP	GCGAAGCTTATGTTGAGAGAATATAAATTA
RAS1 RP	GCGGCTAGCTCAAACAATAACACAACATCC
RFP FP	GCGCTGCAGATGGTTTCAAAAGGTGAAGAA
RFP RP	AAACTGCAGTTTATATAATTCATCCATACC
RPS1 int RP	TTTCTGGTGAATGGGCGAC
HSP90 HISI FP	ATGGCTGACGCAAAAGTTGAAACTCACGAATTCACTGCTGA GATCTCTCAGTTGAACCGGGGATCCTGGAGGATGAG
HSP90 HISI RP	TTAATCAACTTCTTCCATAGCAGATTCTCCAGCTGGTTCGTC AGTTGAGGCAGTAAACGGAATATTTATGAGAAACT
HSP90 FP	GCGAAGCTTATGGCTGACGCAAAAGTTGAA
HSP90 RP	GCGGCTAGCTTAATCAACTTCTTCCATAGC
HSP90 NULL FP	GTAGAAAAAAACATTATAGAATGTTCTTTTTGGTTCTATAG AATTCCATCAGAAATCTAGAAGGACCACCTTTGATTG
HSP90 NULL RP	AAGACATCAACTGAGAGATCTCAGCAGTGAATTCGTGAGTT TCAACTTTTGCGTCAGCCATTTTAATAAACGCGGATCC
HSP90 UPS FP	GTAGAAAAAAACATTATAGAATGTTCTTTT
MET3 RP	CATTTTAATAAACGCGGATCC
HRAS FP	GCGAGATCTATGACGGAATATAAGCTGGTG
HRAS RP	GCGAAGCTTTCAGGAGAGCACACACTT
HRAS G12V FP	AAGCTGGTGGTGGTGGGCGCCGTCGGTGTG
HRAS G12V RP	CAGCGCACTCTTGCCCACACCGACGGCGCC

ARG4 BAMHI FP	GCGGGATCCTACAATCATTTTGATAATCGA
ARG4 NOTI RP	GCGGCGGCCGCTTAACTTAAAATTGATTTTAA
RFP XHOI FP	CCGCTCGAGATGGTTTCAAAAGGTGAAGAA
RFP BAMHI RP	CGCGGATCCTTATTTATATAATTCATCCATACC
GPI2 FP	GCGAAGCTTATGGAAGAAATACATATAAGCTCT
GPI2 RP	GCGGCTAGCTCAGCTTTGTATACTTGACTT
RFP RT FP	GTGGTCCATTACCATTTGCTT
Bait GPI2 FP	GCGCTGCAGGAAGAAATACATATAAGCTCTTCCAT
Bait GPI2 RP	GCGAAGCTTACGCGTTCAGCTTTGTATACTTGACT
Bait GPI19 FP	GCGCTGCAGATATTCCATTTTAACCAAAAAGAGAA
Bait GPI19 RP	GCGAAGCTTACGCGTTCATTCATATAGAACATCAT
Prey GPI2 FP	GCGAGGCCTATGGAAGAAATACATATAAGC
Prey GPI2 RP	GCGGGCGCGCCGCTTTGTATACTTGACTTC
Prey GPI19 FP	GCGAGGCCTATGATATTCCATTTTAACCAA
Prey GPI19 RP	GCGGGCGCGCCTTCATATAGAACATCATTC
CmCh FP	GTGCTTTAAAAGGTGAAATTAAACAAAGAT
NmCh RP	TCTTCTGGATACATTCTTTCTGATGAAGCT
GPI2 RFP FP	ACAAGGACCATGGGATGTGGCGAAACCAAAGTTAATGAAG TCAAGTATACAAAGCATGGTTTCAAAAGGTGAAGAAGAT
GPI2 ARG4 RP	TAGTCTTGGTTTGCTTTAGTGAATAATTTTATATAATAAATT AGATAGTTCACCCTTAACTTAAAATTGATTTTAAATT
GPI19 RFP FP	ACCAAGTGGTGTTTGGGATTTGCCTATTACATTAGTGAATG ATGTTCTATATGAAATGGTTTCAAAAGGTGAAGAAGAT
GPI19 ARG4 RP	ATAGTTTTTTGCTTTTCATTAATATTTGTGCATTTTATTCATT ATCATCAGTTTTTTAACTTAAAATTGATTTTAAATT
ERI1 RFP FP	CATTGTATCATGGAGTGGGTTAAAATTATTCCGTCATTCTA AAGGTATTCAAGGGATGGTTTCAAAAGGTGAAGAAGAT
ERI1 ARG4 RP	AGGTTCAAGAACCTATTCCAAATTAAATAGACTACATTTCG CAACTCTTGGAAATTTAACTTAAAATTGATTTTAAATT
HSP90 RT FP	AAGTGCTGGTGCTGACGTTT
HSP90 RT RP	ACCACCAGCGTTAGATTCCC
GAPDH RT FP	CAGCTATCAAGAAAGCTTCTG
GAPDH RT RP	GATGAGTAGCTTGAACCCAA

2.4 Growth media and Buffers used

2.4.1 *Growth media*

1) Luria Bertani (LB) medium

Components	Grams/100 ml
Luria Bertani powder	2.5
Agar (for solid media)	1.7

2) YEPD (Yeast Extract Peptone Dextrose) (Enriched Media)

Components	Grams/100 ml
Yeast Extract	1
Bacteriological peptone	2
D-glucose	2
Agar (for solid media)	2.5

3) Ura⁻ Met⁻ Cys⁻ medium (Minimal Medium)

Components	Grams/100 ml
Yeast Nitrogen Base (without amino acids)	0.67
Ura- Met- Cys- Drop out mix	0.2
D-glucose	2
Agar (for solid media)	2.5

4) Ura⁺ Met⁻ Cys⁻ medium (Minimal Medium)

Components	Grams/100 ml
Yeast Nitrogen Base (without amino acids)	0.67
Ura- Met- Cys- Drop out mix	0.2
D-glucose	2
Uridine	0.012
Agar (for solid media)	2.5

5) Ura⁻ Met⁻+ Cys+ (5mM)medium (Minimal Medium)

Components	Grams/100 ml
Yeast Nitrogen Base (without amino acids)	0.67
Ura- Met- Cys- Drop out mix	0.2
D-glucose	2
Methionine	0.067
Cysteine	0.074
Agar (for solid media)	2.5

6)Ura⁻ Met⁻ Cys⁻ Drop out Mix

Components	Amount/25 grams
Adenine	50 mg
Arginine	200 mg
L-Alanine	200 mg
Asparagine	200 mg
L-Aspartic acid	200 mg

L-Glutamine	200 mg
Glutamic acid	200 mg
Glycine	200 mg
L-Histidine	200 mg
myo-Inositol	200 mg
L-Isoleucine	200 mg
L-Leucine	1 gm
PABA (Para-aminobenzoic acid)	20 mg
L-Phenylalanine	200 mg
L-Proline	200 mg
L-Serine	200 mg
L-Threonine	200 mg
L-Tryptophan	200 mg
L-Tyrosine	200 mg
L-Valine	200 mg
L-Lysine	200 mg

7) Spider Medium

Components	Grams/100 ml
Mannitol	1 gm
Nutrient Broth	1 gm
K_2HPO_4	0.2 gm
Agar (for solid media)	2.5
pH adjusted to 7.0	

2.4.2 *Buffers and Solutions*

1) 10X TAE (Tris Acetic Acid EDTA) Buffer

Components	Concentration
Tris base	400 mM
Glacial acetic acid	400 mM
EDTA	10 mM

2) Lyticase Buffer

Components	Concentration
Sorbitol	1M
$MgCl_2$	10mM
Tris (pH 7.2)	50mM

3) 10X Phosphate Buffer Saline (PBS)

Components	Concentration
Sodium Chloride	1.37 mM
Potassium Chloride	27 mM
Disodium hydrogen phosphate	100 mM
Potassium dihydrogen phosphate	20 mM
pH was adjusted to 7.4	

4) 10X FCS buffer

Components	Concentration
Potassium Chloride	1.5 M
Dipotassium hydrogen phosphate	100 mM
Potassium dihydrogen phosphate	20 mM
pH was adjusted to 7.4	

5) 6X DNA Gel Loading Dye

Components	Amount/10 ml
Bromophenol blue (0.25% w/v)	25 mg
Sucrose (40% w/v)	4 gm

6) 4X SDS sample buffer

Components	Amount/ 1 ml
1M Tris.Cl pH 6.8	200 µl
SDS (Sodium Dodecyl Sulphate)	0.8 gm
100% glycerol	400 µl
β-mercaptoethanol (β -ME)	50 µl
MQ water	310 µl

7) 1X SDS Running Buffer

Components	Amount /1000 ml
Tris base	3.03 gm
Glycine	18.82 gm
10% SDS	10 ml

8) 30% acrylamide mix

Components	Amount /100 ml
Acrylamide	29.0 gm
N, N'-Methylenebisacrylamide	1.0 gm
Volume made up to 100 ml	

9) 12% SDS-PAGE Resolving Gel

Components	Volume (For 5 ml)
Distilled water	1.6 ml
30% acrylamide mix	2.0 ml
1.5M Tris.Cl pH 8.8	1.3 ml
10% SDS	0.05 ml
10% APS	0.05 ml
TEMED	0.002 ml

10)5% SDS-PAGE stacking gel

Components	Volume (For 5 ml)
Distilled water	3.4 ml
30% acrylamide mix	0.83 ml
1.5M Tris.Cl pH 8.8	0.63 ml
10% SDS	0.05 ml
10% APS	0.05 ml
TEMED	0.005 ml

11) Immunoblotting transfer Buffer

Components	Amount/1000 ml
Tris base	3.03 gm
Glycine	14.42 gm
Methanol	200 ml

12) Lysis buffer for genomic DNA extraction

Components	Concentration
Tris.HCl pH 8.0	100 mM
EDTA pH 8.0	50 mM
SDS	1%
Freshly prepared in autoclaved water	

13) PK buffer for Phalloidin staining of polymerized actin filaments

Components	Volume/1000 ml
1M Dipotassium hydrogen phosphate	19.05 ml
1M Potassium dihydrogen phosphate	30.9 ml
pH was set to 6.6	

14) Lysis buffer for immunoblotting

Components	Concentration
Tris-HCl pH 7.4	25 mM
EDTA	0.5 mM

Sodium chloride	150 mM
Sodium fluoride	10 mM
Triton X-100	0.1%
Glycerol	10%
Protease inhibitor cocktail (1000X)	1X
0.2 M PMSF	0.02 mM

Buffers required for competent cell preparation

RFI buffer

Components	Concentration
Rubidium Chloride	100 mM
Manganese(II) chloride tetrahydrate	50 mM
Potassium acetate	30 mM
Calcium chloride dihydrate	10 mM
Glycerol	15% w/v
pH adjusted to 5.8 with acetic acid	

RFII buffer

Components	Concentration
Rubidium Chloride	10 mM
MOPS buffer	10 mM
Calcium chloride dihydrate	75 mM
Glycerol	15% w/v
pH adjusted to 6.5 with NaOH	

Buffers for plasmidisolation by alkaline lysis method.

Solution I

Components	Concentration
Glucose	50 mM
Tris.Cl pH 8.0	25 mM
EDTA pH 8.0	10 mM
To be autoclaved and stored at 4°C	

Solution II

Components	Concentration
NaOH (Sodium hydroxide)	0.2 N
SDS	1%
Freshly prepared in autoclaved water	

Solution III

Components	Volume/100 ml
Potassium acetate 5M	60 ml
Glacial acetic acid	11.5 ml
Autoclaved water	28.5 ml
Stored at 4°C	

Reaction cocktail for a typical PCR reaction

Components	Volume
DNA template	2.0 µl
PCR XT-20 buffer	2.5 µl
25mM Magnesium chloride	4.0 µl
Forward primer	2.5 µl
Reverse primer	2.5 µl
10mM dNTPs	1.0 µl
XT-20 DNA polymerase	0.3 µl
Sterile nuclease free water	Upto 25 µl

Reaction was set up according to manufacturer's instructions in a PCR thermocycler.

Reaction cocktail for a typical DNA ligation reaction

Components	Volume
Vector	100 ng
Insert	10-30 ng (depending on the ligation ratio required)
10 X T4 DNA Ligase buffer	2.0 µl
T4 DNA Ligase	1.0 µl
Sterile nuclease free water	Upto 20 µl

Reaction was set up in a water bath overnight at 22°C

Reaction cocktail for a typical DNA double digestion reaction

Components	Volume
Plasmid	2.0 μg
Restriction enzyme 1 (NEB)	1.0 μl
Restriction enzyme 2 (NEB)	1.0 μl
10X Cutsmart buffer (NEB)	2.0 μl
Sterile nuclease free water	Upto 20 μl

Reaction was set up in a water bath overnight at 37°C

2.5 Nomenclature

Since this whole text has descriptions from *Candida albicans* as well as *Saccharomyces cerevisiae*, to avoid confusion to the readers, the nomenclature followed throughout this text is given below (Table IV). Unless otherwise stated, the proteins/genes mentioned in the text refer to those in *Candida albicans*.

Table IV: Nomenclature followed in this study

Example	Description
CaGpi19	*Candida albicans* Gpi19 protein
CaGPI19	*Candida albicansGPI19* gene
Cagpi19	*Candida albicansgpi19* gene disrupted/downregulated
ScGpi19	*Saccharomyces cerevisiae* Gpi19 protein
ScGPI19	*Saccharomyces cerevisiaeGPI19* gene
Scgpi19	*Saccharomyces cerevisiaegpi19* gene, disrupted/downregulated
PIG-N, PGAP1	Gene in humans
PIG-N, PGAP1	Protein in humans
pgap1	Gene in humans, disrupted/downregulated

Chapter 3

Ras dynamics in GPI anchor biosynthetic mutants

3.1 *Previous studies on* **Gpi2/PIG-C** *and* **Gpi19/PIG-P**

The GPI-GnT complex, as already explained in the Introduction chapter, catalyzes the first and committed step of the GPI anchor biosynthesis pathway. It consists of six subunits in yeast and fungi, namely, Gpi1(PIG-Q), Gpi2(PIG-C), Gpi3(PIG-A), Gpi15(PIG-H), Gpi19(PIG-P) and Eri1(PIG-Y); their mammalian homologues are mentioned in brackets. Not much is known about how different subunits of this complex interact with each other and with the other cellular pathways in *Candida albicans*. PIG-P, the mammalian homologue of Gpi19 has been shown to associate with PIG-A and hGPI1 in human JY5 cell line by co-immunoprecipitation experiments(Hong *et al*., 1999). In humans, deficiency of this gene product is implicated in Down's syndrome. This is also known as DSCR5 and in case of Down's syndrome, there is a two-fold increase in its expression in fetal brain tissue (Newman *et al*., 2005). PIG-C on the other hand, which is the mammalian homologue of Gpi2, has been shown to form a complex with PIG-Q, which in turn stabilizes the association of PIG-A and PIG-H (Hong *et al*., 1999). It is believed that PIG-C is a scaffolding protein which stabilizes the entire GPI-GnT complex. A study in yeast has also shown physical association of ScGpi2 with ScGpi19 in a large-scale split ubiquitin assay (Miller *et al*., 2005). However, in spite of all this information in humans and yeast, very little is known about GPI anchor biosynthesis pathway and the inter subunit interactions in the GPI-GnT complex in *Candida albicans*. Our lab has been working on GPI anchor biosynthesis in *Candida albicans* and has characterized different subunits of the GPI-GnT complex and also other enzymes responsible for the subsequent and the later steps of the pathway. The first subunit to be successfully characterized in the lab was CaGpi19 (Victoria *et al*., 2010). For this, a *Cagpi19* conditional null mutant was made wherein one allele of *CaGPI19* was disrupted and the second allelewas placed under the control of the regulatable *MET3* promoter and could be repressed by the addition of methionine and cysteine to the growth medium. This was necessary as most of the

proteins involved in the GPI anchor biosynthesis pathway are essential in *Candida albicans* and disrupting both the alleles is lethal to the organism. So, the *Cagpi19* conditional null mutant was generated in the lab and was found to exhibit a hyperfilamentation phenotype with higher CaRas1 activity (Victoria *et al.*, 2010). Also, this mutant has lower *CaERG11* levels which resulted in a decrease in ergosterol levels and sensitivity towards azoles (Victoria *et al.*, 2012). It was shown that *CaGPI19* regulates ergosterol levels in a*CaERG11* dependent manner, both exhibiting a mutual co regulation (Victoria *et al.*, 2012). Interestingly, it was also seen that the *Cagpi19* null mutant has higher *CaGPI2* levels. Simultaneously, it was also seen that the *Cagpi2* null mutant, generated in a similar fashion, has higher levels of *CaGPI19*(Yadav *et al.*, 2014b).The *CaGPI2* mutant was found to have a hypofilamentous phenotype and higher ergosterol levels. We also showed that the hyperfilamentous phenotype of *Cagpi19* null could be reversed by disrupting a single allele of *CaGPI2* in the *Cagpi19* null background; similarly, the azole resistant phenotype of the *CaGPI2* heterozygous mutant could be reversed by disrupting a single allele of *CaGPI19* in the *CaGPI2* heterozygous background. So, to summarize, *CaGPI19* regulates ergosterol biosynthesis via *ERG11* whereas *CaGPI2* controls filamentation through the Ras signaling pathwayand *CaGPI2* and *CaGPI19* negatively regulate each other (which explains hyperfilamentation in *Cagpi19* null mutant and azole resistance in *Cagpi2* null mutant)(Yadav *et al.*, 2014b).

3.2 *Membrane packing studies in Cagpi19 null*

3.2.1 *Steady state anisotropy studies using DPH*

As the *Cagpi19* null mutant has lower ergosterol levels, which is a major component of the fungal membrane, we started off by examining whether the cell membrane in this mutant was also affected (Alvarez *et al.*, 2007; 1996). So we monitored the steady state anisotropy in this

mutant. Plasma membrane preparations were made and these were stained with the membrane selective dye, DPH (1,6-Diphenyl-1,3,5-hexatriene) to monitor steady state anisotropy. DPH has a rotational ellipsoid shape and it only absorbs light that is polarized along its long axis (z axis) (Lakowicz, 1999). If the molecule is perfectly rigid during the course of the measurement, one expects the fluorescence emitted to also be polarized in the same plane and the medium is considered to be highly anisotropic. On the other hand, if the molecule is rapidly rotating one expects the emitted light to be depolarized and the medium has little or no anisotropy. Thus, fluorescence anisotropy is a measure of the rigidity of the environment in which the probe is located. Any changes in the packing of the plasma membrane of the cells would cause a change in the rotational mobility of the membrane bound DPH that would be monitored as a change in fluorescence anisotropy.

DPHhad a reduced steady state fluorescence anisotropy in the *Cagpi19* null (0.131 ± 0.027) as compared to the wild type (0.169 ± 0.011). This can be explained by lower ergosterol levels in the membrane, which lead to a poorer membrane packing. Sterol intermediates like lanosterol that accumulate in the *Cagpi19* null(Victoria *et al*., 2012)are apparently unable to compensate for the loss of ergosterol in the membrane. We also stained these *Candida albicans* strains with DPH to ensure that the dye stains specifically the plasma membrane (Figure 3.1).
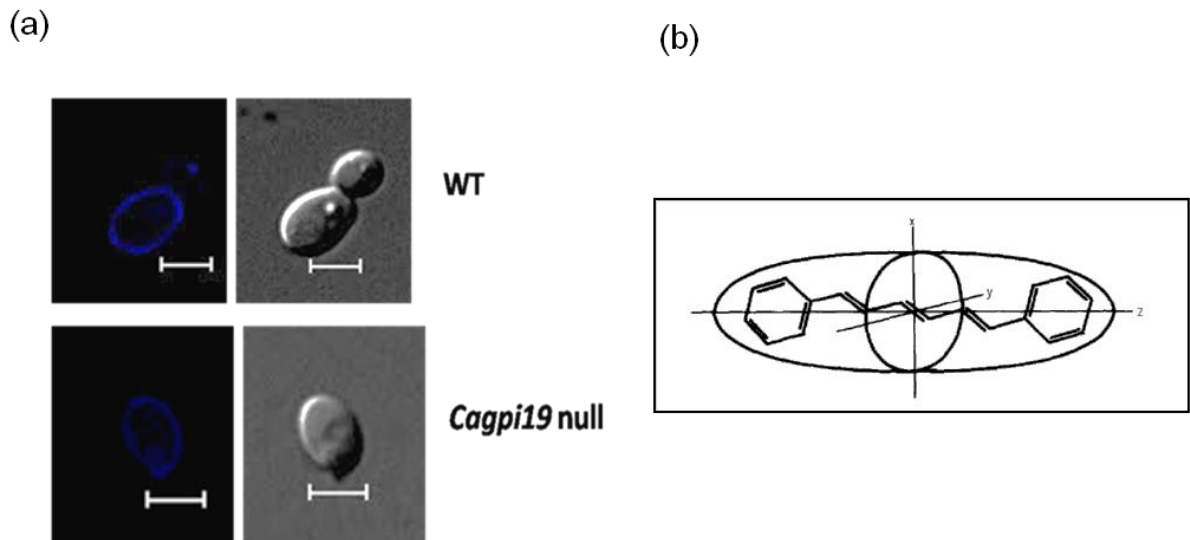
Figure 3.1: DPH staining of *Candida albicans* strains. (a) The indicated *Candida albicans* strains were stained with the membrane selective dye, DPH. DPH stained only the plasma membrane of these cells. The cells were stained with 2µM DPH for 40 minutes at room temperature. The scale bar corresponds to distance of 5 µm. The experiment was done thrice and representative images are shown. **(b)** DPH (1,6-Diphenyl-1,3,5-hexatriene) molecule.

3.2.2 *Study of membrane dynamics using Nile red through FCS*

To further confirm that the plasma membranes of *Cagpi19* null cells were poorly packed, the cells were also stained with another membrane probe, Nile red, and its dynamics in the membrane was studied. The cells were stained with the dye and diffusion was monitored by fluorescence correlation spectroscopy. This method allowed us to study translational diffusion of Nile red. FCS is a fluorescence based biophysical technique in which the diffusion of any fluorescent probe is monitored in a very small confocal volume of about 1 fl. Based on the rate of diffusion of the probe in and out of the confocal volume, we see fluctuations in the fluorescence signal intensity. The sample is diluted enough to ensure that there are few (typically less than 10) molecules in the confocal volume at any given point of time. These fluctuations are then correlated with themselves (described in detail in the Materials and Methods chapter) and plotted as a function of time. Hence, faster is the diffusion of the molecules, more frequent are the fluctuations.

For FCS measurements, the laser (532 nm) was focused in the membrane of the cells to excite Nile Red. The autocorrelation curves were collected for each of the variants. The curves fitted well to a two-component 2-dimensional diffusion (2D2C) model, multiplied with a term for the triplet contribution, as discussed in the Materials and Methods chapter (equation *(viii)*). This particular model was used as Nile red mainly binds to the hydrophobic cell membrane and its diffusion in the cell membrane can be best explained by a 2D diffusion model (Chow *et al.*, 2012). 2 components were used to account for the diffusion of free and bound Nile red. In addition, a triplet component was added which was fixed at 4 μs. The first diffusion time (τ_{D1}) in the case of Nile red was fixed at 55 μs corresponding to the diffusion time of free Nile red (Figure 3.2; equation *(x)*).The second diffusion time (τ_{D2}) was presumed to be arising from diffusion of Nile red in the membrane. Equation*(viii)* was used to fit the correlation curves.

$$G(\tau) = \left[\left(\frac{1}{N_1}\left(1 + \frac{\tau}{\tau_{D1}}\right)^{-1}\right)\right]\left[\left(1 + \left(\frac{\tau}{\tau_{D1\times\kappa2}}\right)\right)^{1/2}\right]^{-1} \dots(x)$$

$$G(\tau) = \left(\frac{1}{N_1}\left(1 + \frac{\tau}{\tau_{D1}}\right)^{-1} + \frac{1}{N_2}\left(1 + \frac{\tau}{\tau_{D2}}\right)^{-1}\right)\left(1 + A_T \exp\left(-\frac{\tau}{\tau_T}\right)\right) \dots(viii) \text{ (as described in Methods)}$$

where N_i are proportional to the average number of diffusing fluorescent particles in thedetection volume, τ_{Di} are the diffusion times of the probe through the detection volume, subscripts *1* and *2* represent the two different components, $A_T = \frac{T}{1-T}$,where T is the number of fluorophores in the triplet state, and τ_T is the triplet time.When the Nile red dye was monitored in the membrane of the wild type and the *Cagpi19* null cells (Figure 3.2), Nile red showed a faster diffusion in the membrane, again suggesting poorer membrane packing in the mutant.
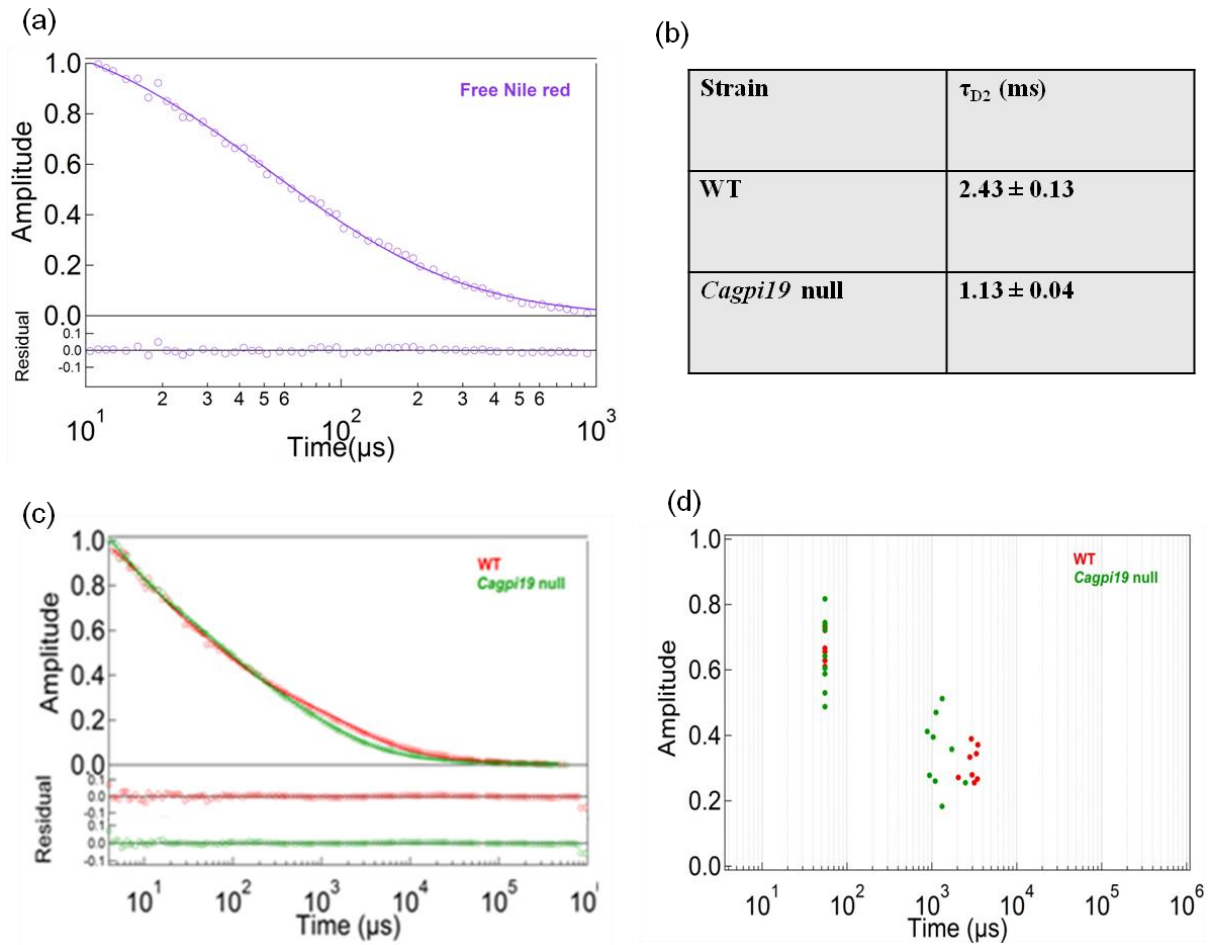
Figure 3.2:(a) FCS measurements showing Nile red dynamics in *Cagpi19* null.(a) Autocorrelation curve of free Nile red in buffer. The trace was fit to a 3D diffusion equation(equation *(iii)*) and a diffusion time of 55 µs was obtained**(b)** Table showing the diffusion time of Nile red in *Candida albicans*after fitting the average FCS trace with the 2D2C component fit as described in the Materials and Methods section.Values are given ± S.D.**(c)** Fluorescence autocorrelation curves $G(\tau)$ showing dynamics of the *Cagpi19* null mutant with respect to the wild type. **(d)** Scatter plot showing amplitude versus diffusion times in each individual cell. Data were collected for more than 10 cells in each case.

Unstained wild type cells were taken as a negative control (Figure 3.3). FCS measurements of these cells did not give any correlation.

Figure 3.3: Unstained wild type cells give no autocorrelation. Wild type cells (BWP17) without any fluorophore were taken for FCS measurements. As seen in the figure, there was no correlation in these cells. Proper correlation was observed, however, in the cells where a fluorescent probe was present (BWP17-mRFP-CaRas1).

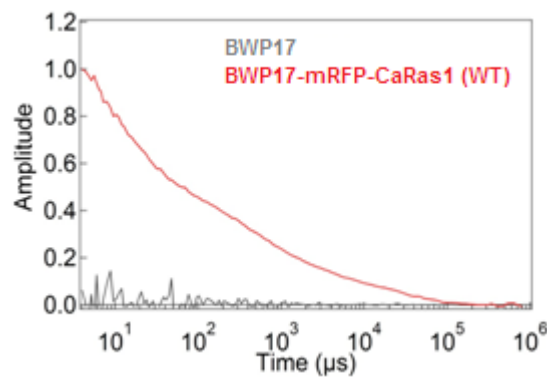Thus, from the above experiments we concluded that the dyes experienced greater translational as well as rotational mobility in the plasma membrane of *Cagpi19* null. It has been previously by shown by Soraya Victoria (Victoria, S., 2010) that DPH also has shorter average fluorescence lifetimes in the mutant cell membranes, indicating that deficiency in ergosterol has a significant effect on the cell membranes of the mutant strain.

3.3 CaRas1 *dynamics in Cagpi19 null*

CaRas1 is a major player in controlling the filamentation process in *Candida albicans*. CaRas1 is attached to the plasma membrane via a prenyl and a farnesyl anchor in its activated form (Piispanen *et al*., 2011). Activation of CaRas1 causes association of GTP with CaRas1, which in turn activates CaCyr1 which forms a sensor apparatus complex comprising of CaCyr1-CaCap1 and G actin (Wang *et al*., 2010). Since the *Cagpi19* null has higher CaRas1 activity (Victoria *et al*., 2010), and has a poorly packed plasma membrane, we were interested in studying whether an alteration in CaRas1 mobility/ dynamics was responsible for the higher CaRas1 signaling. So, we started off by looking at what happens to CaRas1 dynamics in the plasma membrane of *Cagpi19* mutant.

3.3.1 *Construction of mRFP tagging cassette*

To begin with, we tagged CaRas1 at the N terminus with mRFP. For this tagging, we cloned two halves of *mRFP* on either sides of the selection marker, *ARG4* in this case (Figure 3.4). The cassette was amplified with primers specific to the upstream region of *CaRAS1*, and this PCR product was used to transform the wild type (BWP17) and *Cagpi19* null. The two halves were chosen such that there was a small overlapping region of DNA between them which helped in reconstitution of the complete mRFP sequence, by looping out of the *ARG4* sequence via homologous recombination (Gerami-Nejad *et al*., 2009).
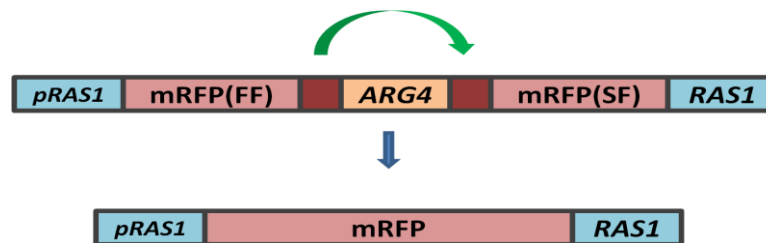
Figure 3.4: Strategy showing the tagging of CaRas1 with mRFP. Two halves of *mRFP* were cloned on either side of the *ARG4* marker with a homologous region in between them for recombination. Amplification of this cassette with appropriate *CaRAS1* flanking primers and subsequent transformation into the required *Candida albicans* strain led to tagging of CaRas1 with mRFP.

The first half of *mRFP* was amplified using primers RFP FF FP and RFP FF RP and cloned upstream of *ARG4* in *YCpARG4* using SmaI and KpnI sites, to get *RFPFF-ARG4* plasmid (Figure 3.5). CIp10ADH1-mCherry was used as a template for amplification of *mRFP* (Keppler-Ross *et al*., 2008).

Then, the second half of *mRFP* was cloned downstream of *ARG4* using sites SacI and SfoI toget the *RFPFF-ARG4-RFPSF* plasmid (Figure 3.5).

Figure 3.5: Cloning of *RFPFF-ARG4-RFPSF* cassette. (a) Cloning of *mRFPFF*. (i) Colony PCR showing amplification of *mRFPFF* from the colonies obtained after transformation. Lane 1: Negative control (no template), lane 2: 1 kb DNA ladder, lane 3-9: PCR amplification of different colonies obtained after bacterial transformation. Only lane 5 shows a positive amplification of the expected size (~450 bp). **(ii)** Restriction digestion showing release of mRFPFF (~450 bp) from *mRFPFF-YcpARG4* after digestion with KpnI and S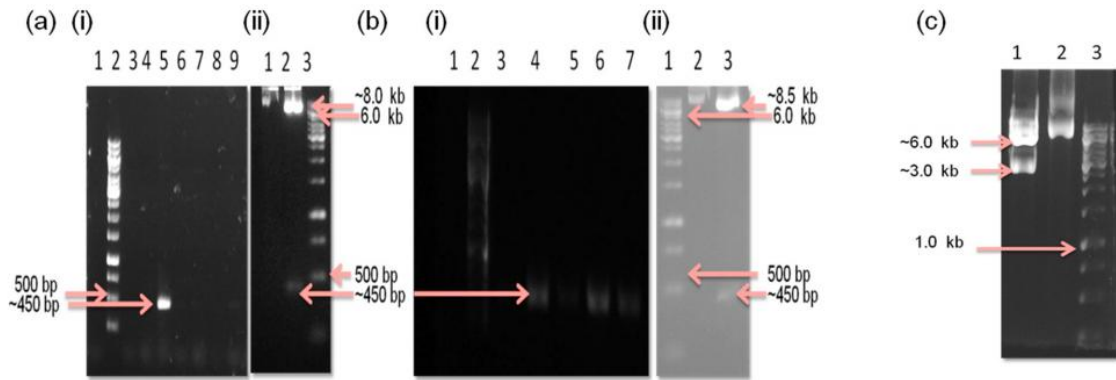maI confirming that *mRFPFF* has been cloned into *YcpARG4*. Lane 1: undigested plasmid, lane 2: plasmid digested with the restriction enzymes KpnI and SmaI showing a release of the expected size of *mRFPFF*, lane 3: 1 kb DNA ladder. **(b)** Cloning of *mRFPSF*. **(i)** Colony PCR showing amplification of *mRFPSF* from the colonies obtained after transformation. Lane 1: Negative control (no template); lane 2: 1 kb DNA ladder; lane 3-7: PCR amplification of different colonies obtained after bacterial transformation. All the colonies showed a positive amplification(~450 bp)**(ii)** Restriction digestion of one colony (C5)showing release of mRFPFF (~450 bp) from*mRFPFF-YcpARG4* after digestion with SacI and SfoI confirming that mRFPSF has been cloned into *mRFPFF-YcpARG4* to get the *mRFPFF-ARG4-mRFPSF* plasmid. **(c)**Release of the complete *mRFPFF-ARG4-mRFPSF* after digestion with SmaI and SfoI. Lane 1: plasmid digested with the restriction enzymes SfoI and SmaI showing a release of the expected size of *mRFPFF-ARG4-mRFPSF*(~3kb) lane 2: undigested plasmid, lane 3: 1 Kb DNA ladder.

3.3.2 *Generation of mRFP-CaRas1 strains*

The*mRFPFF-ARG4-mRFPSF* construct was amplified using *CaRAS1* flanking primers and used to transform wild type BWP17and *Cagpi19* null mutant downstream of the native *CaRAS1* promoter, thereby tagging the CaRas1 with mRFP at the N-terminus. Lithium acetate method was used for transformation and details are given in Materials and Methods chapter. The colonies obtained were grown for four generations on synthetic medium supplemented with arginine, so that the *ARG4* could be removed after reconstitution of mRFP.The colonies were confirmed by observing PCR amplification of the colonies obtained after transformation (Figure 3.6).
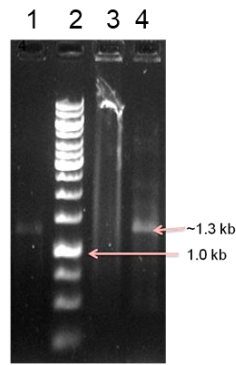
Figure 3.6: Conformation of*mRFP-CaRAS1* strains: Agarose gel electrophoresis showing PCR amplification using genomic DNA of strains obtained after transformation of *mRFPFF-ARG4-mRFPSF* cassette in wild type BWP17 and *Cagpi19* null strains of *Candida albicans*. Lane 1 and 4: PCR amplification using mRFP RTFP and RAS1RTRP in wild type and *Cagpi19* null respectively showing expected size of ~1.3 kb. Lane 2: 1 kb DNA ladder. Lane 3: Negative control.

The positive colonies were screened for fluorescence in a TRITC (Tetramethylrhodamine)using a confocal microscope to check for the expression of mRFP (Figure 3.7).

(a)   (b)

BWP17   *Cagpi19* null
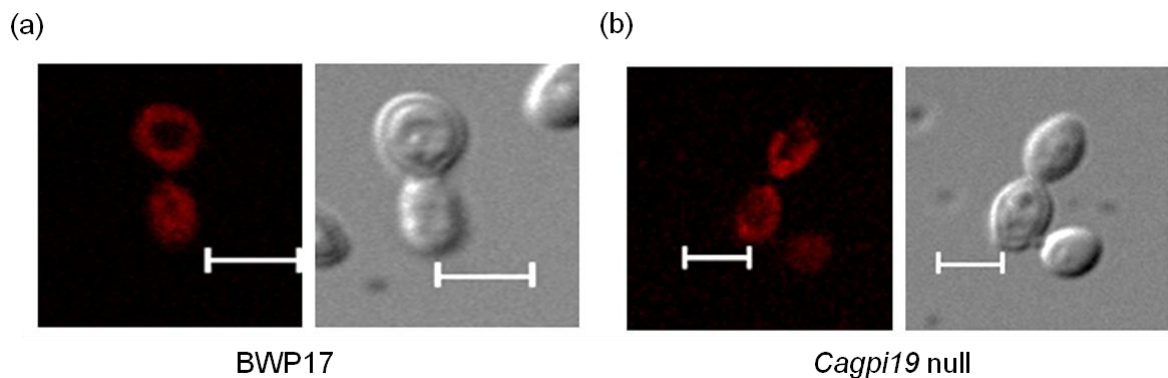
Figure 3.7: Microscopic confirmation of mRFP-CaRas1 expression. The positive colonies obtained after transformation of the mRFPFFARG4-mRFPSF cassette were screened by fluorescence. **(a)** shows the wild type BWP17 cellsexpressing mRFP-CaRas1(WT)and**(b)** shows fluorescence in the *Cagpi19* null cells expressing mRFP-CaRas1. The experiment was done thrice and representative images are shown.

Also, the *Candida albicans* wild type strain BWP17 was transformed with a soluble form of mRFP (Kind gift from Prof. Neta Dean, Stony Brook University). The plasmid was linearized with StuI and integrated at the *RPS1* locus(Yadav *et al*., 2014b)(Figure 3.8). Dynamics of

free mRFP was measured by FCS. The cells expressing free mRFP. i.e. the BWP17-mRFP cells were lysed with detergent and autocorrelation was measured to obtain the diffusion of free mRFP (Figure 3.8) and equation *(xi)* which corresponds to a 2 dimensional 1 component (2D1C) diffusion equation (since all of the mRFP is free) was used and we obtained a diffusion time of 125 µs which was for the unhindered diffusion of mRFP.The triplet time (τ_T) was fixed at65 µs which accounts for the flickering of mRFP (Hendrix *et al*., 2008) Flickering is a process in which the fluorophore tends to go into light induced dark states which can interfere with our measurements, if they lie in the same time scales. mRFP is known to enter into long dark states, of the order of around 63 µs.

$$G(\tau) = \left(\frac{1}{N} \left(1 + \frac{\tau}{\tau_D} \right)^{-1} \right) \left(1 + A_T \exp\left(-\frac{\tau}{\tau_T} \right) \right) \quad .....(xi)$$
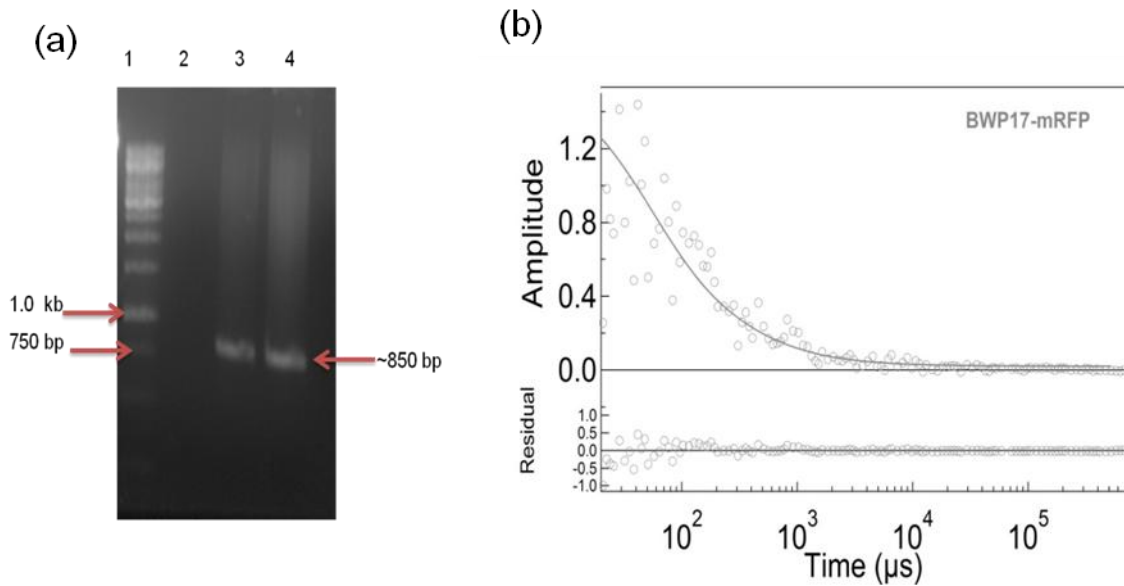
Figure 3.8: Generation of BWP17-mRFP. (a) Agarose gel showing the confirmation of BWP17-mRFP.*CIp10ADH1mRFP* was linearized with StuI enzyme and transformed into wild type *Candida albicans* wild typestrain BWP17. Colonies were obtained after transformation and they were screened by isolating the genomic DNA and subjecting it to PCR amplification. The agarose gel shows the presence of the expected 900 bp band after amplification with mRFP FP and RPS1 internal RP. The lane next to the ladder is the negative control (untransformed cells) which show no amplification. Lane 1: 1 kb DNA ladder, lane 2: Negative control (untransformed wild type cells) lane 3 and 4: Positive colonies showing amplification of the desired size.**(b)**Dynamics of free mRFP**. BWP17-mRFP cells were lysed with detergent (0.1% Triton X-100)and the dynamics of free mRFP was measured by FCS. The correlation curves were fit to a 2D1C diffusion equation and a diffusion time of 125 µs was obtained.

3.3.3 Study of **CaRas1** *dynamics through FCS in the Cagpi19 null*

Hereafter, unless otherwise stated, the BWP17 strain expressing mRFP-CaRas1 will be referred to as WT and *Cagpi19* **null refers to** *Cagpi19* **null expressing mRFP-CaRas1.** The tagging of CaRas1 with mRFP did not appear to affect CaRas1 activity in the wild type and the *Cagpi19* null. The *Cagpi19* null continued to retain its hyperfilamentation phenotype even after tagging with mRFP (Figure 3.9). The filamentation assay was done by a labmate, Snehlata Singh. The diffusion of CaRas1 in the plasma membrane of the wild type and the *Cagpi19* null mutant was studied using fluorescence correlation spectroscopy (FCS) as described in Materials and Methods chapter. The autocorrelation curves were collected for each of the strains. The curves were fitted to a two-component 2-dimensional diffusion model, multiplied with a term for triplet contribution.The 2 dimensional 2 component (2D2C) diffusion, the same as that used for Nile red, equation *(viii)* was used as we were interested in monitoring the lateral diffusion of CaRas1 in the membrane, which could be best explained by a 2D diffusion model. The first diffusion time (τ_{D1}) was fixed at 125 µs which was for the unhindered diffusion of mRFP, as shown in Figure 3.8. Diffusion of mRFP-Ras1 in the membrane corresponded toτ_{D2}. As explained above, in case of mRFP-Ras1 also, the triplet time (τ_T) was fixed at65 µs which accounts for the flickering of mRFP (Hendrix *et al*., 2008) The residuals obtained suggest a good fit in all cases.
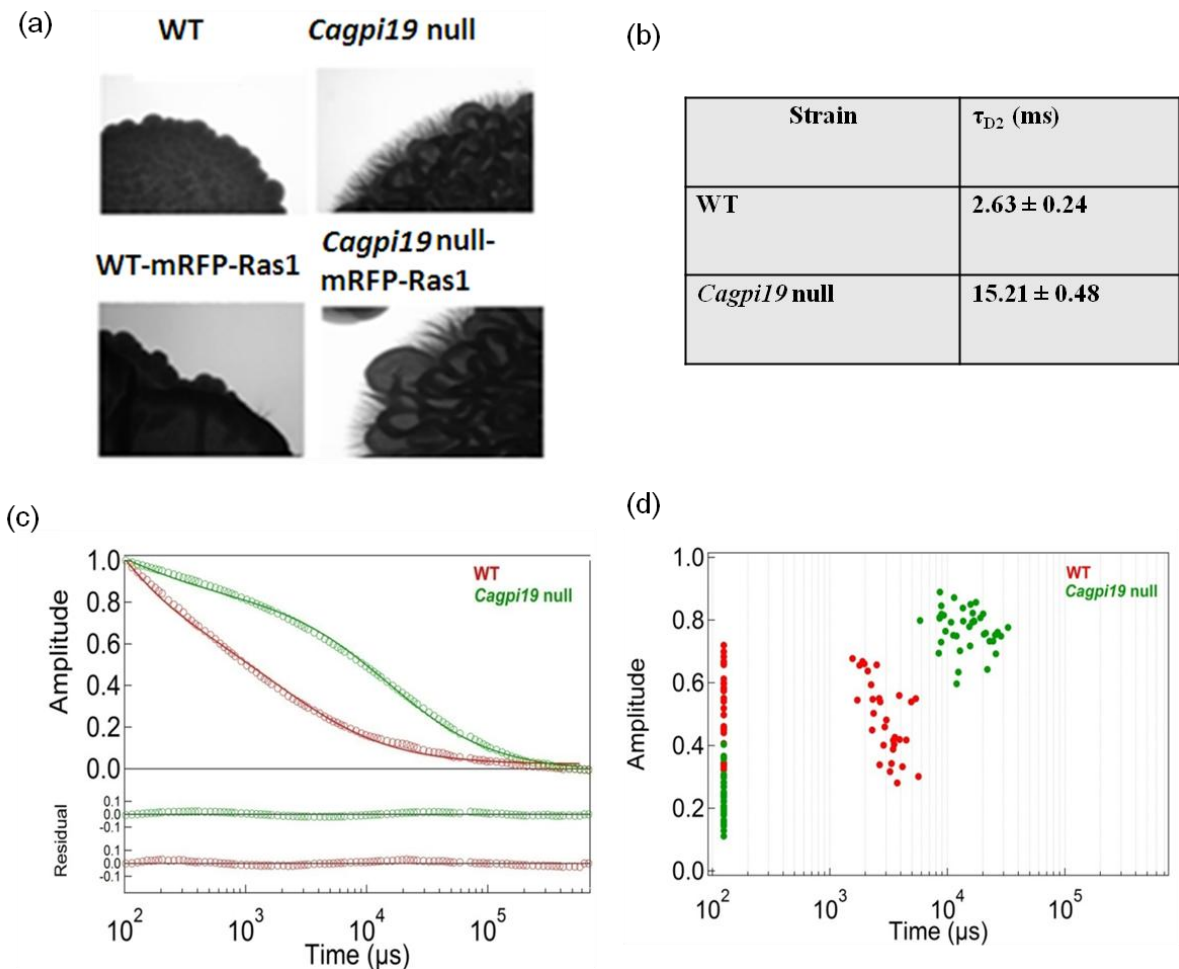
Figure 3.9: CaRas1 dynamics in *Cagpi19* null mutant. (a) Filamentation pattern in the wild type (WT) and *Cagpi19* null. Strains were spotted on spider medium and kept at 37°C. Images were captured after 4 days. The *Cagpi19* null continues to be hyperfilamentous even after tagging CaRas1 with mRFP, thus showing that tagging CaRas1 doesn't alter its function. The experiment was repeated thrice and representative images are shown.**(b)** Table showing diffusion times of CaRas1 in the wild type (WT) and *Cagpi19* null. Values are given ± S.D.**(c)** Plot of autocorrelation curves $G(\tau)$ versus time, which shows the diffusion pattern of CaRas1 in the wild type (WT) and *Cagpi19* null and **(d)** scatter plots with amplitude versus diffusion times showing the dynamics of each individual cell. Data were collected for more than 25 cells in each case.

CaRas1dynamics in the *Cagpi19* null was much slower than the wild type, giving a difference of more than five-fold (Figure 3.9). What explains the remarkable slowing down of CaRas1 in this mutant even though steady state anisotropy values of DPH suggest that the membrane is more fluid and CaRas1 is expected to have better mobility? Is this because of any changes in the CaRas1 signaling pathway in the *Cagpi19*null?

3.4 CaRas1 *dynamics after treatment with sodium vanadate*

To test whether CaRas1 remains in its activated state, we treated the wild type cells with sodium vanadate. Sodium vanadate, like AlF_4^-, is a phosphate mimetic and is used to trap the transition state of ATPases/ GTPases (Huyer *et al.*, 1997). This is because it can mimic the γ phosphate which results in blocking of GDP in the active site of the enzyme in its transition state immediately after the γ phosphate has been cleaved. Thus, the enzyme remains associated with its effector proteins, thereby mimicking a complex that would be formed under conditions when CaRas1 signaling pathway is turned on (Figure 3.10).

(c)

Strain	τ_{D2} (ms)
WT	2.63 ± 0.24
WT+ vanadate	21.02 ± 1.88
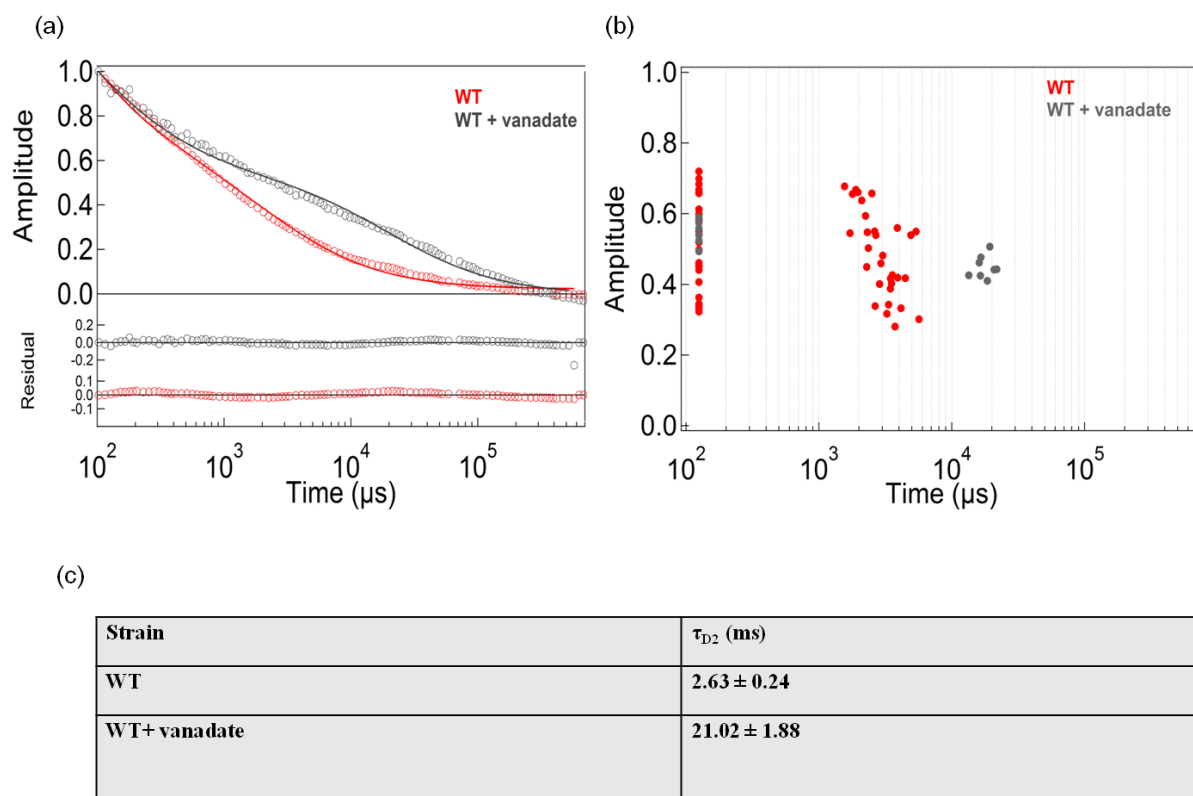
Figure 3.10: CaRas1 dynamics of WT treated with vanadate.(a) Plot of autocorrelation curves $G(\tau)$ versus time, which shows the diffusion pattern of CaRas1 in the wild type (WT) after treatment with sodium vanadate. **(b)** Scatter plots with amplitude versus diffusion times showing the dynamics of each individual cell. Data was collected for more than 10 cells in each case. **(c)** Table showing diffusion times of CaRas1 in the wild type (WT) after treatment with sodium vanadate. Values are given ± S.D.

Wild type cells treatedwith vanadate gave extremely slow CaRas1 dynamics, similar to the *Cagpi19* null. This led us to hypothesize that heightened CaRas1 signaling could be responsible for slower CaRas1 dynamics.

3.5 *Study of* CaRas1 *dynamics in* CaRas1 *overexpression strains*

3.5.1 *Generation of* CaRas1 *overexpression strains*

To confirm the hypothesis that heightened CaRas1 signaling could indeed be responsible for slower CaRas1 dynamics, we generated two mutants. The first one was wherein wild type CaRas1 was overexpressed in wild type (WT) and in the second one, the constitutively active form of CaRas1, i.e. CaRas1^{G13V} was overexpressed. To generate these mutants, *pEGFP* vector was taken as the parent plasmid and *CaRAS1* and *CaRAS1^{G13V}* were cloned in this vector in HindIII and NheI sites to obtain *pADH1-CaRAS1* and *pADH1-CaRAS1^{G13V}*, respectively (Figure 3.11). The plasmids *pEA-GFP-CaRAS1* and *pEA-GFP-CaRAS1^{G13V}* (kind gift from Prof. Deborah Hogan, (Piispanen *et al.*, 2011)) were taken as the templates.
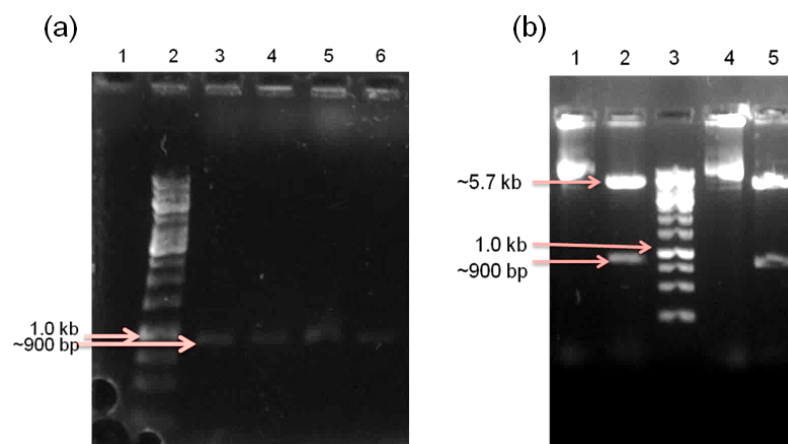
Figure 3.11: Cloning of *pADH1 -CaRAS1* AND *pADH-CaRAS1^{G13V}*.(a)Colony PCR of *CaRAS1* and *CaRAS1^{G13V}*. (i) Colony PCR showing amplification of *CaRAS1* and *CaRAS1*^{G13V}from the colonies obtained after transformation using RAS1 FP and RAS1 RP. Lane 1: Negative control (no template), lane 2: 1 kb DNA ladder; lane 3-4: PCR amplification of different colonies obtained after bacterial transformation of the ligation product of *CaRAS1* into *pEGFP* vector (~900 bp), lane 5-6: PCR amplification of different colonies obtained after bacterial transformation of the ligation product of *CaRAS1^{G13V}*into *pEGFP* vector (~900 bp). **(b)**Restriction digestion showing the release of *CaRAS1* and *CaRAS1^{G13V}*. Lane 1: undigested plasmid, lane 2: plasmid digested with the restriction enzymes HindIIIand NheIshowing a release of the expected size of *CaRAS1* (~900 bp), lane 3: 1 kb DNA ladder, lane 4: uncut plasmid and lane 5: plasmid digested with the restriction enzymes HindIII and NheIshowing a release of the expected size of *CaRAS1^{G13V}*(~900 bp).

Once *CaRAS1* and *CaRAS1*^{G13V}were cloned in *pEGFP* vector, *CaRAS1* needed to be tagged with mRFP so that FCS measurements could be done using the 532 nm laser. For that, mRFP was cloned in PstI site upstream of *CaRAS1/CaRAS1*^{G13V} using primers RFP PSTI FP and RFPPSTI RP into both*pEGFP-CaRAS1* and the *pEGFP-CaRAS1*^{G13V}. Proper orientation of mRFP was confirmed by PCR amplification using RFPPSTI FP and RPS1 int RP (Figure 3.12).
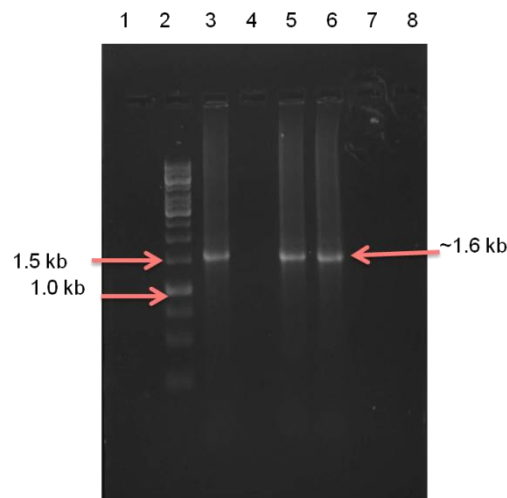
Figure 3.12:Cloning of *mRFP* in *pADH1-CaRAS1* and *pADH1-CaRAS1*^{G13V} vectors.Agarose gel electrophoresis showing the amplification of *mRFP-CaRAS1* using RFP FP and RAS1 RP confirming the integration of mRFP in the correct orientation in the vectors. Lane1: negative control, lane 2: 1 kb DNA ladder, lane3: amplification of *mRFP-RAS1* showing a band at the expected size of 1.6 kb, lane 4: negative colony, lane 5 and 6: amplification of *mRFP-CaRAS1*^{G13V} showing a band at the expected size of 1.6 kb, lane 7 and 8: negative colonies.

Now, the *pEGFP-mRFP-CaRAS1* and the *pEGFP-mRFP-CaRAS1*^{G13V}plasmids were digested with StuI and linearized. StuI cuts the plasmids at the *RPSI* locus present in them. The digested plasmid was then transformed into wild type BWP17 and transformant colonies were obtained on U⁻M⁻C⁻ plates. These colonies were streaked on another similar plate and their genomic DNA was isolated. Positive transformant colonies were confirmed by PCR amplification using Ras1 FP and RPS1 int RP (Figure 3.13) and checked for fluorescence. Now these strains were ready for FCS measurements.

Figure 3.13: Generation of WT-CaRas1 OE and WT-CaRas1^{G13V} OE strains: (a) Integration of *pADH1-mRFP-CaRAS1* and *pADH1-mRFP-CaRAS1^{G13V}*into BWP17 strain of*Candida albicans*.Agarose gel electrophoresis showing the PCR amplification from genomic DNA of the colonies obtained after linearizing *pADH1-mRFP-CaRAS1* and *pADH1-mRFP-CaRAS1^{G13V}* plasmids by digestion with StuI and transforming them into BWP17 strain of *Candida albicans.* Lane1: negati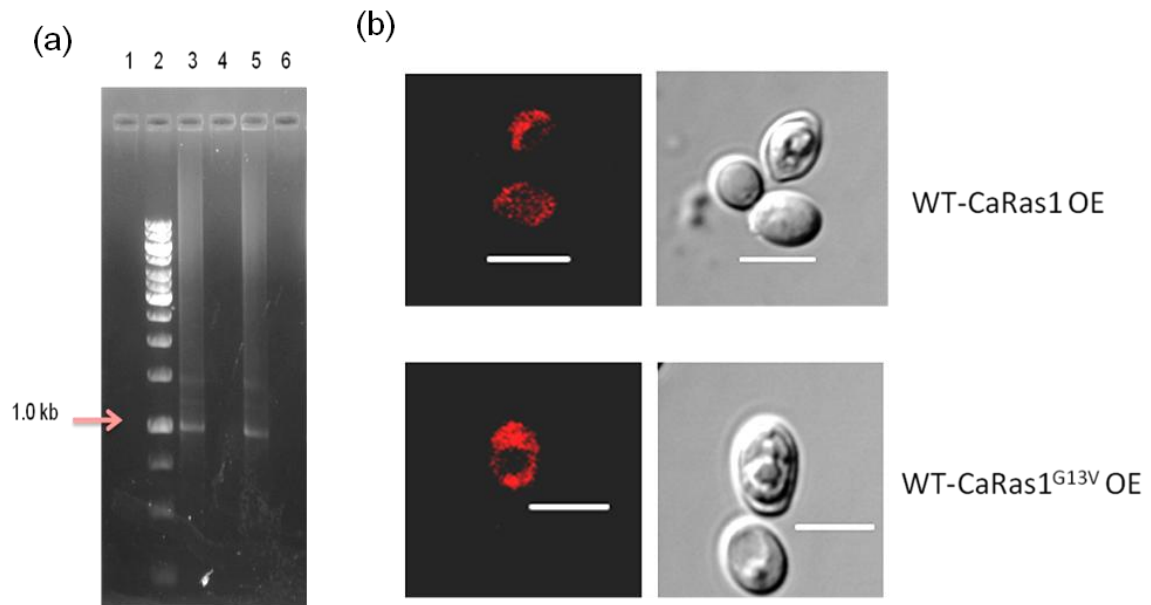ve control, lane 2: 1 kb DNA ladder, lane 3: amplification of *CaRAS1-RPS1* using RAS1 RP and RPS1 int RP (~1.0 kb) confirming the integration of *pADH1-mRFP-CaRAS1* at the *RPS1* locus of BWP17. lane 4: negative colony, lane 5: amplification of *CaRAS1-RPS1^{G13V}* using RAS1 RP and RPS1 int RP confirming the integration of *pADH1-mRFP-CaRAS1^{G13V}* at the *RPS1* locus of BWP17, lane 6: negative colonies.**(b)**Fluorescence microscopy to check the expression of mRFP-CaRas1 and mRFP-CaRas1^{G13V}**.** Microscopic images showing the expression of mRFP-CaRas1 and mRFP-CaRas1^{G13V} in the positive colonies obtained after transformation. The experiment was done thrice and representative images are shown. Scale bar corresponds to a distance of 5 μm.

Hereafter these strains have been referred to as WT-CaRas1 OE and WT-CaRas1^{G13V} OE. CaRas1 dynamics in these overexpression strains were measured as described in the Materials and Methods section (Figure 3.14).

3.5.2 *Study of* CaRas1 *dynamics in* CaRas1 OE *and* CaRas1^{G13V}OE *strains*

The filamentation pattern of WT-Ras1 OE and WT-CaRas1^{G13V} OE was studied and hyperfilamentation in these strains ensured that CaRas1 was overexpressed (Figure 3.14). Interestingly, the constitutively active form of CaRas1, i.e. CaRas1^{G13V}, when overexpressed in WT, gave a much slower dynamics than its wild type counterpart whereas

overexpressionof the wild type form of CaRas1 had dynamics similar to that of the wild type strain (Figure 3.14). This suggests that slowing down of CaRas1 dynamics is because of CaRas1 hyperactivation; both in the WT-CaRas1^{G13V} and the *Cagpi19* null.

(a)

(b)

Strain	τ_{D2} (ms)
WT	2.63 ± 0.24
WT-CaRas1 OE	3.97 ± 0.40
WT-CaRas1^{G13V} OE	12.48 ± 1.68

Figure 3.14: CaRas1 dynamics upon CaRas1 hyperactivation.(a) Filamentation pattern showing the increase in filament formation upon CaRas1 overexpression (WT-Ras1 OE and WT-CaRas1^{G13V} OE; indicating that indeed CaRas1 is overexpressed. Cells were spotted on Spider medium and kept at 37°C. Images were taken after 4 days. The experiment was done thrice and representative images are shown. **(b)** Table showing the diffusion time of CaRas1 in WT-CaRas1 OE and WT-CaRas1^{G13V} OE as measured by FCS. Values are given ± S.D.**(c)** Average FCS traces represented by fluorescence autocorrelation curves $G(\tau)$ and showing the dynamics of CaRas1 in WT-CaRas1OE relative to the wild type (WT) and **(d)** scatter plots with amplitude versus diffusion times showing the dynamics of each individual cell.**(e)**Average FCS traces represented byfluorescence autocorrelation curves $G(\tau)$ showing the dynamics of CaRas1 in WT-CaRas1^{G13V}OE relative to the wild type (WT) and **(f)** scatter plots with amplitude versus diffusion times showing the dynamics of each individual cell.Data were collected for more than 25 cells in each case.

We also confirmed this in a strain where no endogenous *CaRAS1* was present. We transformed the *pEGFP-mRFP-CaRAS1* and the *pEGFP-mRFP- CaRAS1^{G13V}* plasmids in the *Caras1* null strain and studied CaRas1 dynamics (Figure 3.15). *Caras1* null was previously made in the lab in Priyanka Jain (Jain. P, 2016) As expected, filamentation was restored in the *Caras1* null when CaRas1 or the CaRas1^{G13V} was overexpressed.
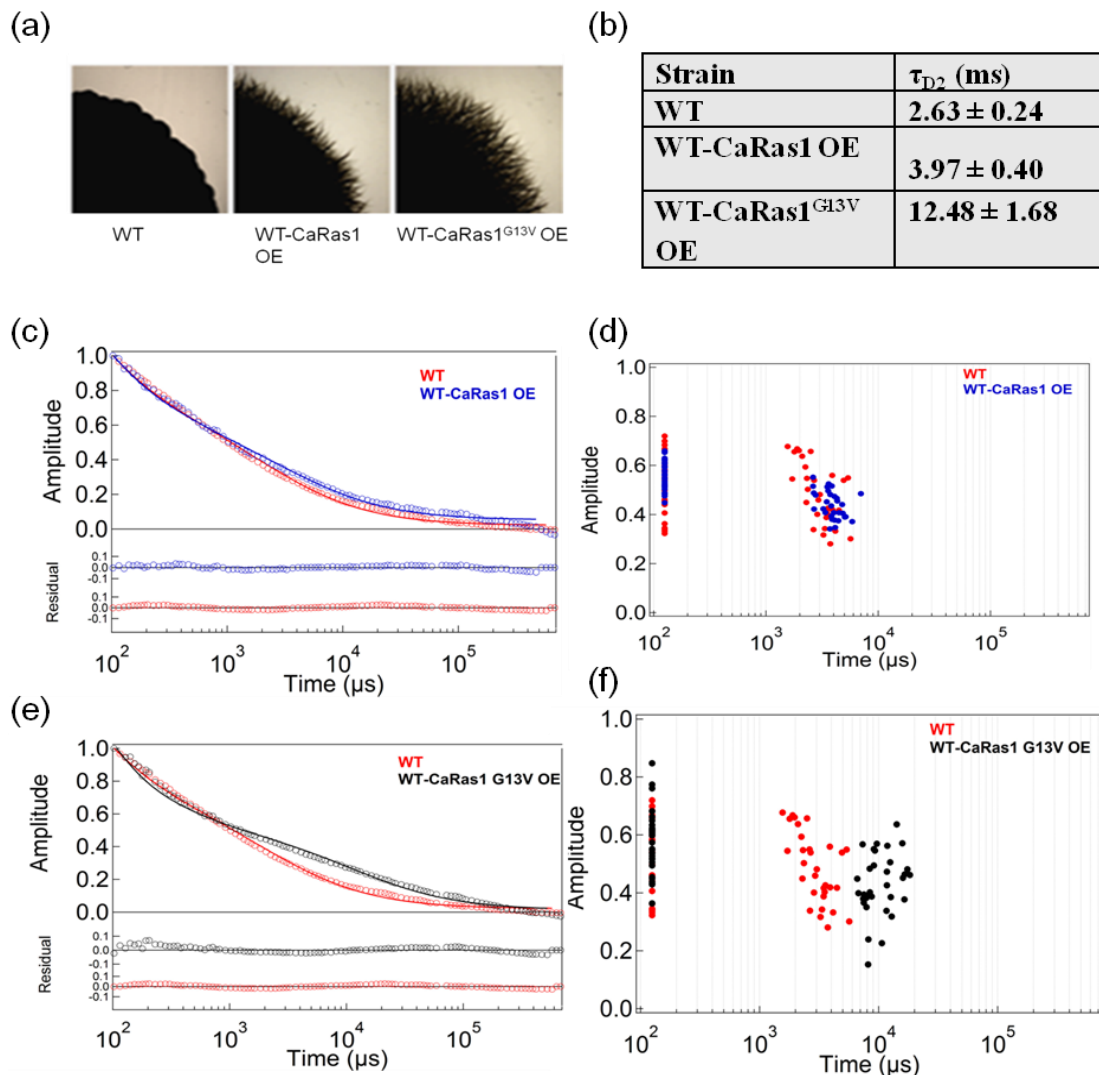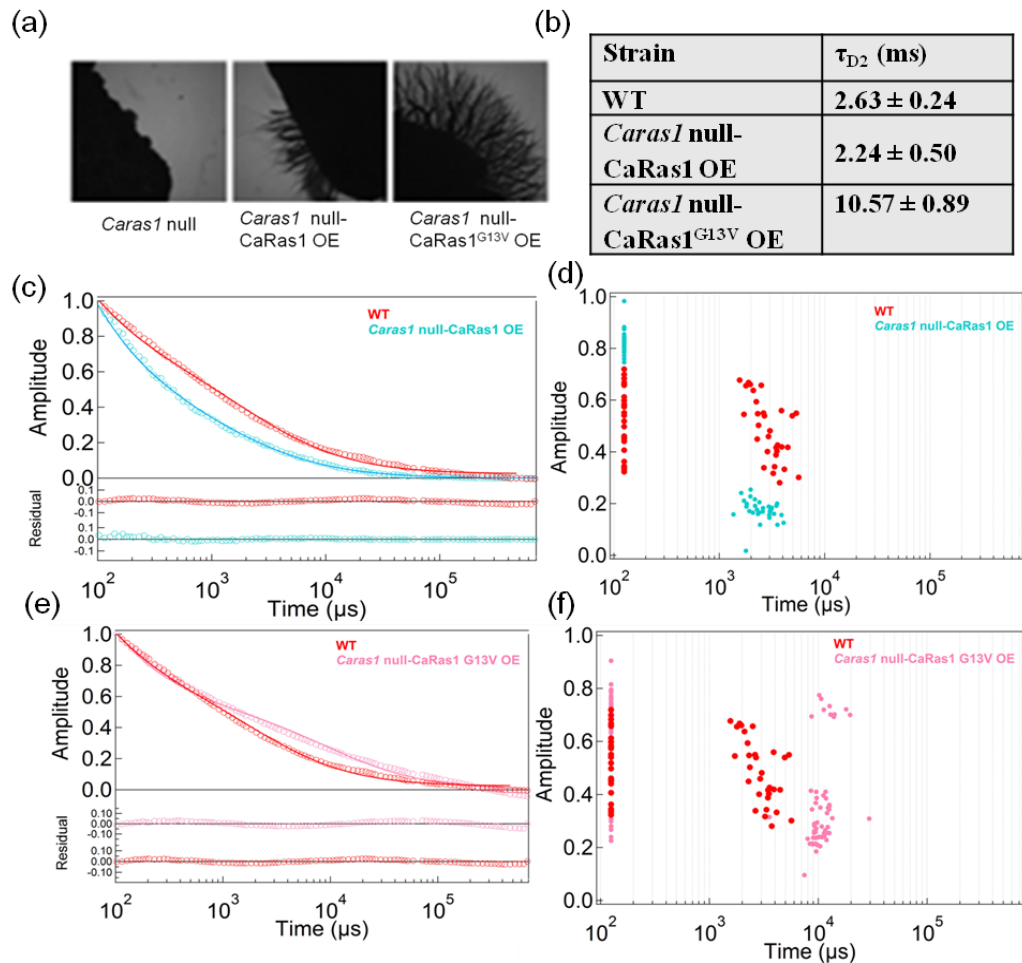

Figure 3.15: CaRas1 dynamics upon CaRas1 hyperactivation in *Caras1* null.(a) Filamentation pattern showing the increase in filament formation upon CaRas1 overexpression (CaRas1 OE CaRas1^{G13V} OE) in*Caras1* null strain; indicating that indeed CaRas1 is overexpressed. Cells were spotted on Spider medium and kept at 37°C. Images were taken after 7 days. The experiment was done thrice and representative images are shown.**(b)** Table showing the diffusion time of CaRas1 in *Caras1*null-CaRas1 OE and in *Caras1*null-CaRas1^{G13V} OE as measured by FCS. Values are given ± S.D.**(c)** Average FCS traces represented by fluorescence autocorrelation curves *G*(τ)showing the dynamics of CaRas1 in *Caras1* null-Ras1OE relative to the wild type (WT) and **(d)** scatter plots with amplitude versus diffusion times showing the dynamics of each individual cell. **(e)** Average FCS traces represented by fluorescence autocorrelation curves *G*(τ)showing the dynamics of CaRas1 in *Caras1* null-Ras1^{G13V} OE relative to the wild type (WT) and **(f)** scatter plots with amplitude versus diffusion times showing the dynamics of each individual cell.Data were collected for more than 25 cells in all cases.

In this case also, we obtained the same results. When wild type CaRas1 was overexpressed in the *Caras1* null, dynamics was similar to the wild type. On the other hand, when CaRas1^{G13V} was overexpressed, CaRas1 dynamics slowed down significantly, as was observed in the *Cagpi19* null (Figure 3.15). This further strengthened our hypothesis that constitutively active CaRas1 signaling leads to slower CaRas1 dynamics.

3.6 *Study of* **H-Ras** *dynamics in mammalian cell lines*

We also validated this hypothesis in the mammalian systems. Human *H-RAS* was cloned in *pDsRed-Express C1* vector in HindIII and BglII sites (Figure 3.16) and the constitutively active G12V mutation was introduced by site directed mutagenesis using DpnI method as described in the Materials and Methods chapter to generate *pDsRed-Express C1-H-Ras* and *pDsRed-Express C1-H-Ras^{G12V}* (Weiner *et al*., 1994). MDA-MB-231 cell line grown in L15 medium (Invitrogen) supplemented with 10% FBS were used for this study (Figure 3.16).

Figure 3.16: Cloning of human H-Ras. **(a)** Agarose gel showing the release of human *H-RAS* from pDsRed Express C1 vector. Lane 1: 1 kb DNA ladder; lane 2 undigested plasmid of colony 1, lane 3: Release of human *H-RAS* from pDsRed Express C1 vector (~570 bp) after digestion with HindIII and BglII, lane 4: undigested plasmid of colony 1, lane 5: Release of human *H-RAS* from *pDsRed Express C1* vector (~570 bp) after digestion with HindIII and BglII. **(b)** Vector map of pDsRed used for tagging human *H-RAS* with DsRed. **(c)** Sequence alignment using NCBI BLAST showing the introduction of the G12V mutation in *H-RAS* (subject) when aligned with wild type *H-RAS* (Query). The mutation is highlighted in green.

Transient transfection of both these plasmids was done in this cell line and expression of DsRed-H-Ras and DsRed-H-Ras^{G12V} was seen in the microscope (Figure 3.17). Hras dynamics in these cell lines was studied by FCS. As discussed in the Materials and Methods chapter, equation *(ix)* was used to fir the autocorrelation traces.

$$G(\tau) = \left\{ g_{01} \left(1 + \frac{\tau}{\tau_{D1}} \right)^{-1} \right\} \left\{ 1 + A_T \exp \left(-\frac{\tau}{\tau_T} \right) \right\} \dots (ix)$$
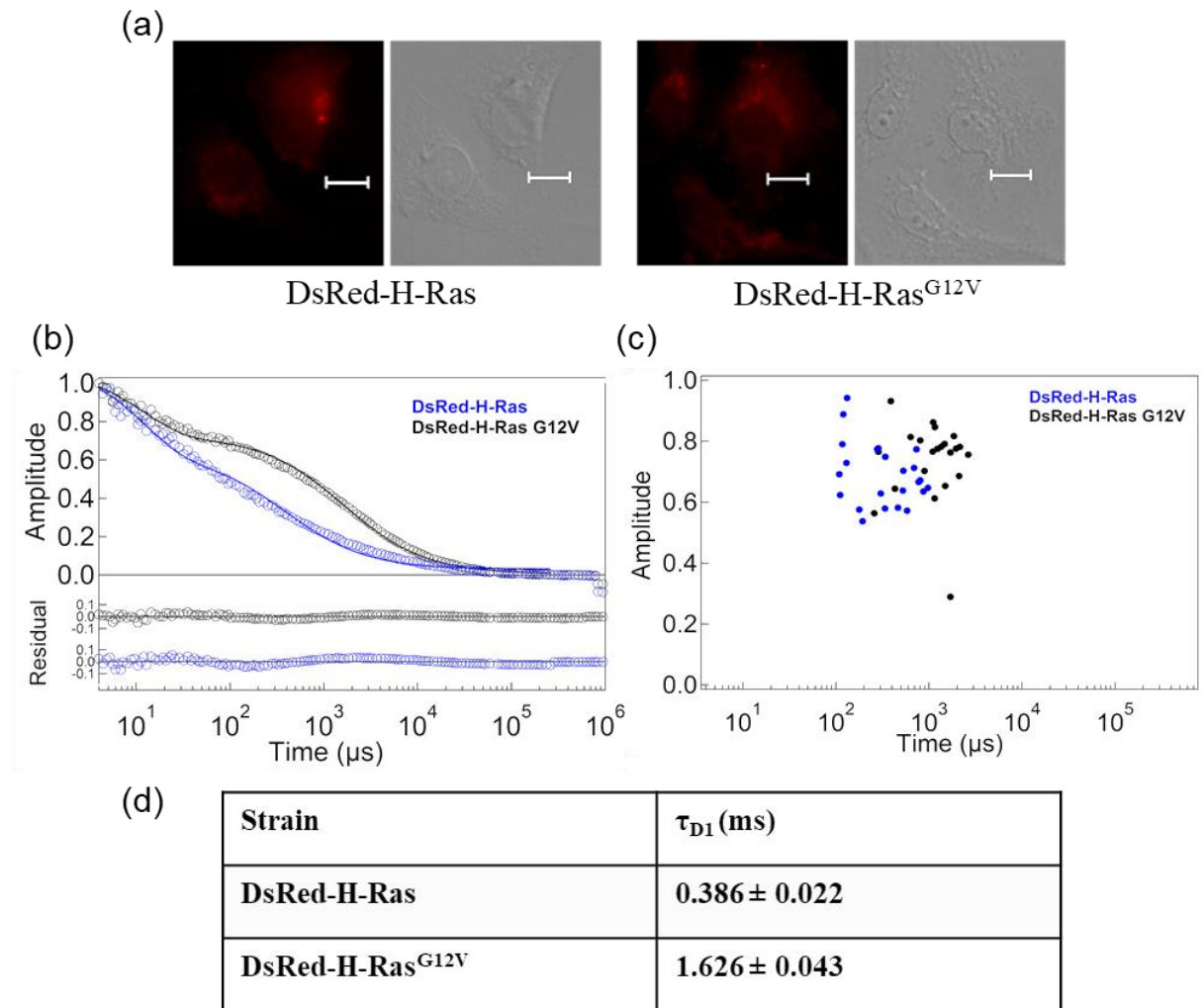
Figure 3.17: H-Ras dynamics in mammalian cells. (a) Microscopic images showing the expression of DsRed –H-Ras and DsRed-H-Ras^{G12V}. Transient transfection of the plasmids expressing DsRed-H-Ras and DsRed-H-Ras ^{G12V} was done in MDA-MB-231 cell line and images were taken after 36h. The experiment was done twice and representative images are shown. **(b)** Average FCS traces represented by Fluorescence autocorrelation curves $G(\tau)$ and showing the dynamics of DsRed–H-Ras and DsRed–H-Ras^{G12V} and **(c)** scatter plots with amplitude versus diffusion times showing the dynamics of each individual cell. **(d)** Table showing the diffusion time of H-Ras and H-Ras^{G12V} as measured by FCS. Values are given ± S.D.

Even in mammalian systems, we could see a slowing down in case of H-Ras[G12V] relative to the wild type (Figure 3.17). This further validates our point that Ras hyperactivation leads to slowing down of its membrane dynamics in the cell.

We also observed that FCS measurements of untransfected MDA-MB-231 cells did not give any significant correlation in the time scales that we were monitoring (Figure 3.18).
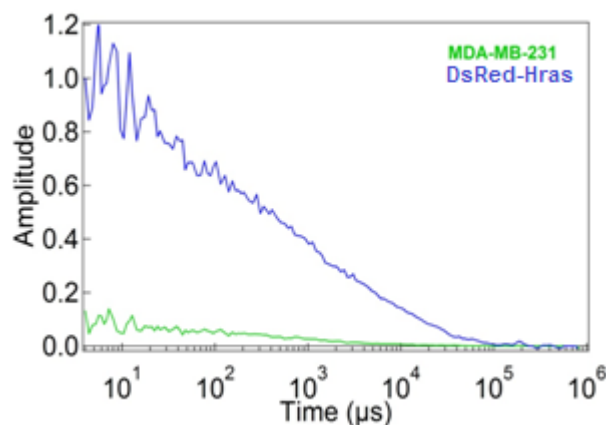

Figure 3.18: **FCS measurements of MDA-MB-231 cells.** FCS measurement of untransfected MDA-MB-231 cells was done to check for any background correlation that might interfere with the DsRed signal. However, the counts were very less (around 3-4) and no significant autocorrelation was observed in the time scales of DsRed-Hras that could cause any interference in our measurements.

3.7 *Study of* **CaRas1** *dynamics in CaGPI2 overexpression mutant*

Now, having seen that CaRas1 hyperactivation can cause slowing down of CaRas1 dynamics in *Candida albicans*, we also wanted to explore what happens to CaRas1 dynamics in a *CaGPI2* overexpression mutant. As already explained, *CaGPI2* is shown to be responsible for cross-talk of the GPI-GnT complex with CaRas1 signaling (Yadav *et al.*, 2014b). Also, *Cagpi19* null mutant has high levels of *CaGPI2* that in turn triggers higher CaRas1 signaling and produces its hyperfilamentous phenotype. So, we expected that if we overexpressed *CaGPI2*, we should get similar CaRas1 dynamics as observed in the *Cagpi19* null. This led us to study CaRas1 dynamics in the *CaGPI2* overexpression mutant. A single copy of *CaGPI2* was over expressed from the *RPSI* locus by transforming WT cells where CaRas1

was already tagged with mRFP with *pACT1-CaGPI2* plasmid (Yadav *et al*., 2014b) after digestion with StuI (Figure 3.19). As previously reported in (Yadav *et al*., 2014b), this strain displayed a hyperfilamentous phenotype.
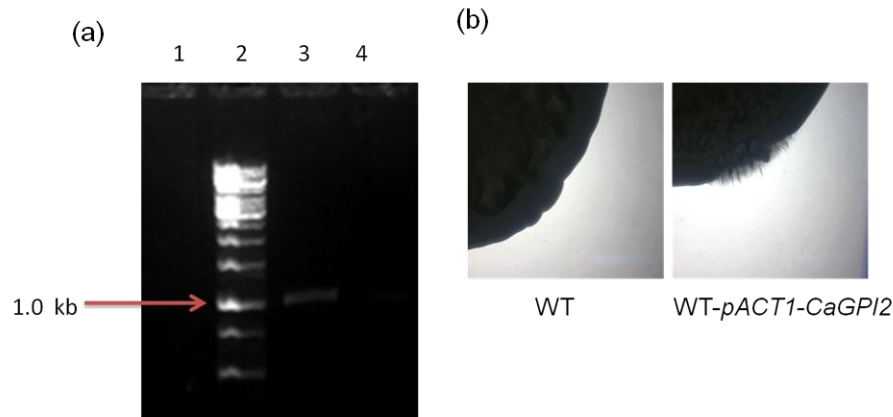

Figure 3.19: Generation of WT-*pACT1-CaGPI2*::*mRFP-CaRAS1*. (a) Confirmation of *pACT1-CaGPI2* transformation into WT. (a) Agarose gel showing the confirmation of WT-*pACT1-CaGPI2.pACT1-CaGPI2* was linearized with StuI enzyme and transformed into*Candida albicans* strain WT. Colonies were obtained after transformation and they were screened by isolating the genomic DNA and subjecting it to PCR amplification. The agarose gel shows the presence of the expected 1000 bp band after amplification with *CaGPI2* FP and RPS1 int RP. Lane 1: Negative control (untransformed wild type cells), lane 2: 1 kb DNA ladder lane 3 and 4: Positive colonies showing amplification of the desired size (~1.0 kb). **(b)**Filamentation study of WT-*pACT1-CaGPI2*. Microscopic images showing the hyperfilamentous phenotype of WT- *pACT1-CaGPI2* strain relative to the wild type. Cells were grown in hyphae inducing Spider medium and images were captured after 8 days. The experiment was done thrice and representative images are shown.

CaRas1 dynamics was studied in this *CaGPI2* overexpression strain and indeed, overexpression of *CaGPI2* in this strain caused a significant slowing down of CaRas1 dynamics, as expected, similar to that observed in the *Cagpi19* null (Figure 3.20).
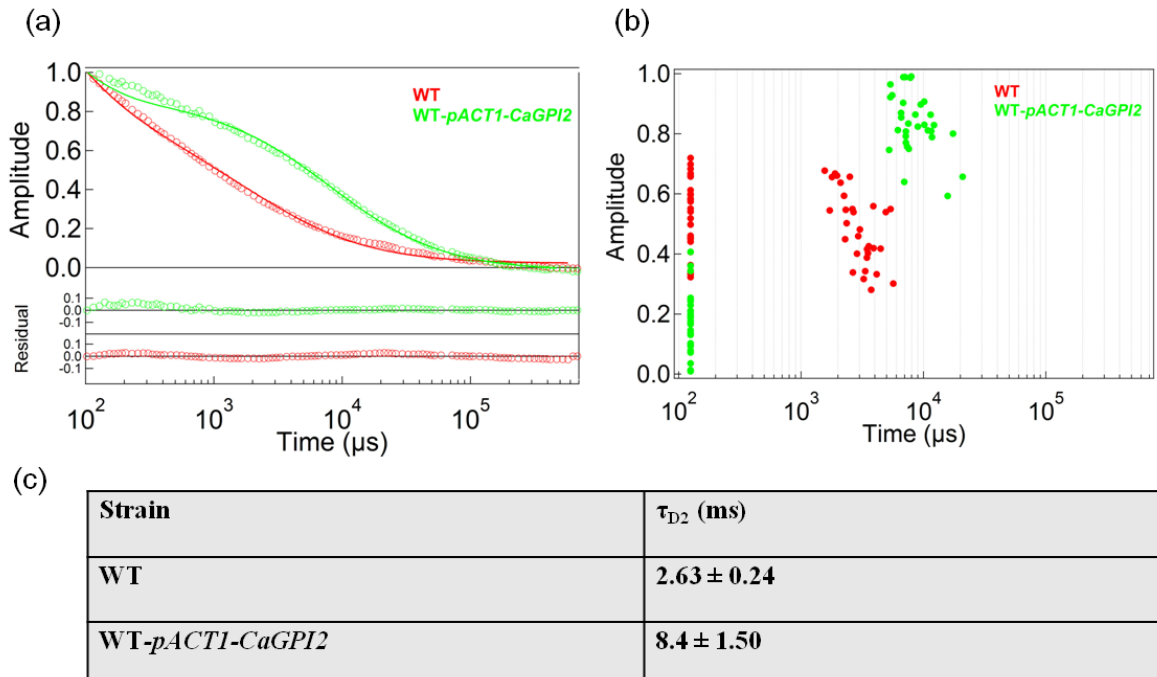
(c)

Strain	τ_{D2} (ms)
WT	2.63 ± 0.24
WT-*pACT1-CaGPI2*	8.4 ± 1.50

Figure 3.20:CaRas1 dynamics in *CaGPI2* overexpression mutant. (a)Average FCS traces represented by fluorescence autocorrelation curves $G(\tau)$showing the dynamics of CaRas1 in the WT-*pACT1-CaGPI2* overexpression mutant relative to the wild type (WT) and **(b)** scatter plots with amplitude versus diffusion times showing the dynamics of each individual cell. Data were collected for more than 25 cells in each case. **(c)**Table showing the diffusion time of Ras in the *CaGPI2* overexpression mutant as measured by FCS. Values are given ± S.D.

3.8*Study of* **CaRas1** *dynamics in hyphal cells*

We also went on to study the CaRas1 dynamics in the hyphal form of *Cagpi19* null relative to the wild type (Figure 3.21). The hyphal form was induced by using Spider medium (Sudbery, 2011). The induction was done for three hours at 37°C to ensure that all of the yeast cells were converted to their hyphal form. FCS measurements were performed in a similar manner as in the yeast cells.
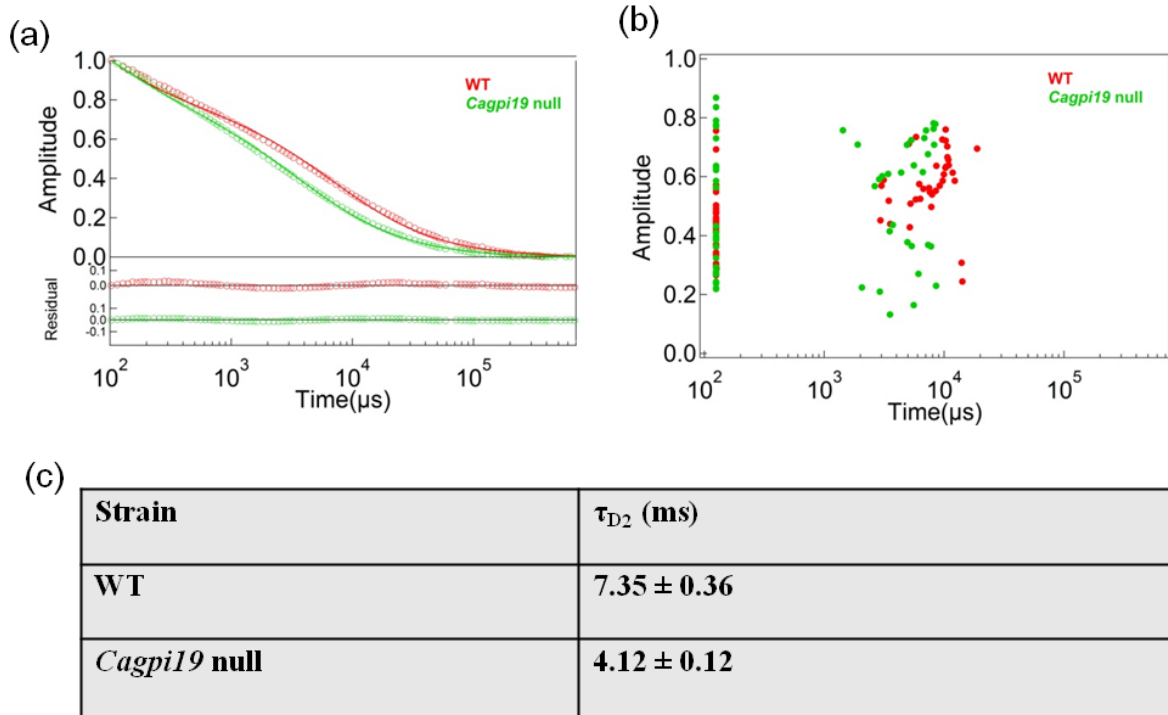
Figure 3.21: CaRas1 dynamics in the hyphal form of *Cagpi19* null. (a) Plot of autocorrelation curves $G(\tau)$ versus time, which shows the diffusion pattern of CaRas1 in the hyphal form of wild type (WT) and *Cagpi19* null and **(b)** scatter plots with amplitude versus diffusion times showing the dynamics of each individual cell. The data were collected for more than 25 cells in each case. **(c)** Table showing diffusion times of CaRas1 in the wild type (WT) and *Cagpi19* null. Values are given ± S.D.

We observed a couple of interesting features of CaRas1 dynamics here:

1) CaRas1 in the wild type and mutant cells had comparable dynamics.

2) CaRas1 dynamics in the hyphal form of the *Cagpi19* null was faster than in its yeast form.

It must be pointed out that hyphal induction at elevated temperatures results in lifting of the inhibitory effect of Hsp90 on the Ras signaling pathway in the wild type as well as the mutant (Shapiro *et al*, 2009). This would result in comparable CaRas1 dynamics. Further, a significant degree of membrane reorganization and cytoskeletal changes occur during hyphal transition. These changes are required for the maintenance of the hyphal form (Braun and Calderone, 1978; Lenardon *et al*., 2010). It must also be pointed out that CaRas1 dependent

cAMP-PKA activity has been shown to be higher in yeast cells than in hyphal cells (Zhu *et al*., 2009). It is possible that once hyphae are induced, the levels of active CaRas1 in the cell drop and maintenance of hyphae require lower levels of active CaRas1. Thus, FCS profiles show a shift to faster dynamics in hyphal cells as compared to yeast cells of the mutant.

3.9 *Chapter summary*

In this chapter, we have shown that even though *Cagpi19* null mutant has a poorer membrane packing, as was evident from the steady state anisotropy values of DPH and faster Nile red dynamics in the cell membrane relative to the wild type; yet the mutant shows a much slower dynamics of CaRas1 as compared to the wild type. On probing this further, we showed that a similar slowing down of CaRas1 dynamics is seen in the constitutively active CaRas1[G13V]OE mutant (which always remains GTP bound and so keeps the signaling pathway activated throughout); both in the wild type as well as *Caras1* null background, as well as in a mutant where *CaGPI2* was over expressed (wherein we know that there is a higher CaRas1 signaling and hyperfilamentation, Yadav *et al*, 2014). Moreover, we also showed that this slowing down of CaRas1 dynamics at the cell membrane is not restricted only to *Candida albicans*. A similar slowing down of Hras was observed in the human Hras[G12V] mutant also. From this, we can say that CaRas1 hyperactivation, either due to *CaGPI19* downregulation, or *CaGPI2* overexpression, or due to expression of a constitutively active CaRas1[G13V] variant, causes a slowing down of CaRas1 dynamics at the membrane. How exactly does this hyperactivation cause slowing down of CaRas1 is discussed in the next chapter.

Chapter 4

Study of CaRas1hyperactivation in Cagpi19 null

4.1 CaRas1 *signaling inCandida albicans*

In this chapter, the mechanism behind the slowing down of CaRas1 dynamics upon its hyperactivation is studied. As described in the Introduction, CaRas1 controls filamentation in *Candida albicans* through the MAPK pathway or the cAMP-Protein Kinase A (PKA) pathway.The major pathway, is however the cAMP-PKA pathway, which controls filamentation in response to a variety of stimuli, like temperature, serum, CO_2 and other agents(Inglis and Sherlock, 2013). In the cAMP-PKA signaling pathway, upon receiving a stimulus, CaRas1 binds to GTP, to form CaRas1-GTP. CaRas1-GTP interacts with the regulatory subunits of the adenylyl cyclase (CaCyr1) and causes their dissociation; which in turn activates the catalytic subunits of CaCyr1. Activation of CaCyr1 increases the levels of cAMP in the cell, which leads to activation of PKA, which in turn activates the transcription factor, CaEfg1, and initiates the formation of hyphae. This signaling pathway is regulated at a number of check points by some regulatory proteins. One of them is CaHsp90, the well known heat shock protein. Under normal temperature conditions, it interacts with the cAMP-PKA signaling pathway and keeps filamentation under check (Shapiro *et al.*, 2009). It is important to note that, in addition to its role in the protein folding machinery, it also interacts with and participates in many biological signaling pathways in response to various stimuli. The CaHsp90 molecule in *Candida albicans* functions as a dimer, and has three distinct domains, the N-terminal ATP binding domain, the middle domain that interacts with the various client proteins and the C-terminal domain which is responsible for dimerization of the protein. CaHsp90 has an intrinsic ATPase activity, albeit weak, in the absence of any client proteins. The transcription of CaHsp90 is triggered by a specific transcription factor, CaHsf1and up regulation of CaHsp90 transcript levels, in turn, repressCaHsf1, thereby maintaining an autoregulatory loop between them so as to have fixed levels of CaHsp90 levels in the cell (Leach *et al.*, 2012). Under normal circumstances, the heat shock protein

CaHsp90 blocks the interaction of CaRas1-GTP with its effectors in the CaRas1-cAMP-PKA pathway, thereby maintaining the yeast form of *Candida albicans*. This inhibition is independent of the negative regulators of the pathway, like CaIra2, CaPde1, and CaPde2 (Shapiro *et al*., 2009). CaHsp90 interacts with this CaRas1-PKA pathway via its co-chaperone CaSgt1, which is essential for its activity in *Candida albicans*(Shapiro *et al*., 2012). However, under conditions of elevated temperatures, the CaHsp90 mediated inhibition is relieved. Ras1-GTP now can freely interact with its effectors and initiate the signaling pathway, giving rise to filamentation (Figure 4.1). It has also been reported that downregulation of CaHsp90, or treating *Candidaalbicans* with an Hsp90 inhibitor, like geldanamycin, makes them undergo filamentation without the need for elevated temperature (Shapiro *et al*., 2009). Thus, compromising CaHsp90 levels bypasses the requirement of higher temperatures for filamentation by activating the CaRas1-PKA pathway.
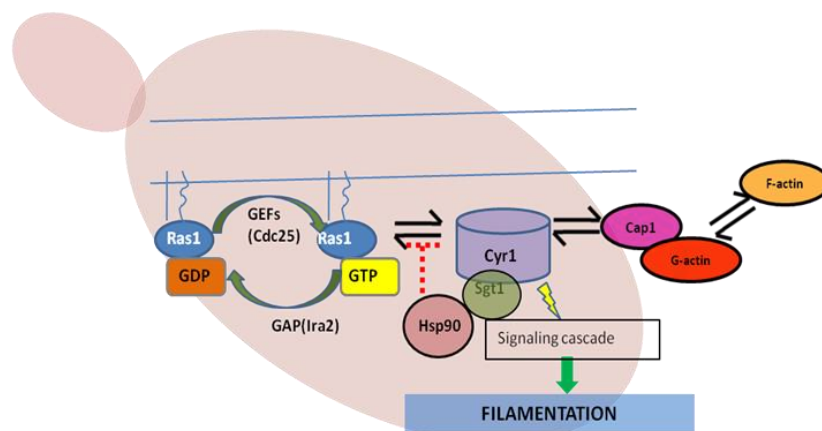
Figure 4.1: Inhibition of CaRas1 signaling pathway by CaHsp90. Figure showing the inhibition of CaRas1 signaling pathway through interaction with its co-chaperone, CaSgt1. CaSgt1 interacts with CaCyr1 and blocks the downstream signaling pathway, thereby inhibiting filamentation.

4.2 CaHsp90 *deficiency could be responsible for slower* CaRas1 *dynamics in Cagpi19 null*

Also, it has been previously reported that *Candida albicans* strains expressing hyperactive Ras phenotypes have lower levels of CaHsp90 activity (Shapiro *et al*., 2009). Looking at the phenotypes of the *Cagpi19* null more closely, we see that it filaments at room temperature,

has higher chitin levels as estimated by Calcofluor White (CFW) staining, has higher CaRas1 activity, as seen by higher activity of PKA and is also heat shock sensitive (Victoria *et al.*, 2010, 2012). All of these are characteristics of CaRas1 hyperactivation due to CaHsp90 deficiency (Shapiro *et al.*, 2009). So, is it possible that in *Cagpi19* null, lower CaHsp90 levels, are responsible for slower CaRas1 dynamics?

Indeed, we found that the *Cagpi19* null has around 40% lower transcript levels of *CaHSP90* than the wild type. We also checked for the activity of CaHsp90 in this mutant by assaying for the phosphorylation levels of one of the well known client proteins of *Candida albicans* CaHsp90, the CaHog1 protein (Shapiro *et al.*, 2009). This protein is phosphorylated at its threonine180 and tyrosine182 residue upon its activation. Immunoblotting showed that indeed the level of phosphorylated Hog1 is much lower in the mutant than the wild type (Figure 4.2). This experiment was done alongwith a lanmate, Subhash Chandra Sethi.
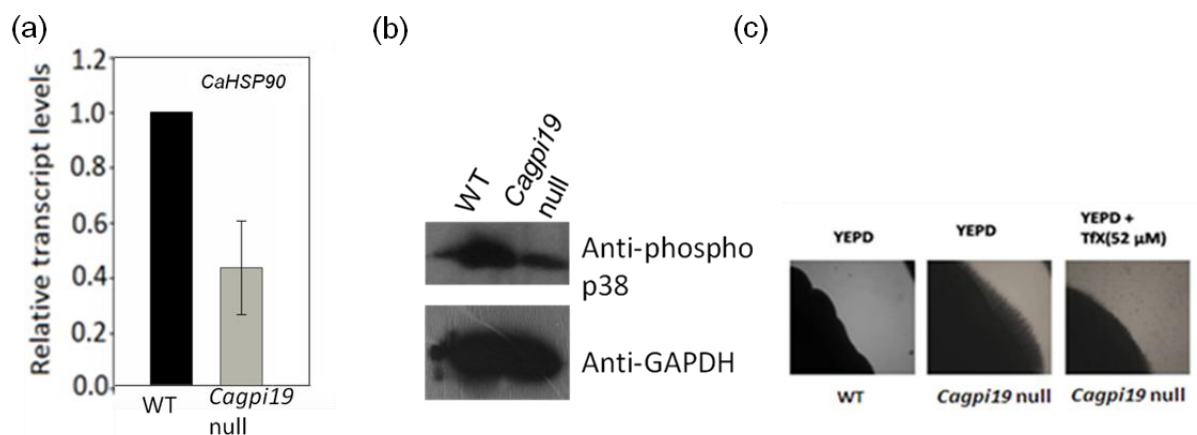

Figure 4.2:CaHsp90 deficiency in *Cagpi19* null. (a) Quantification of the transcript levels of *CaHSP90* in the *Cagpi19* null strain by quantitative real time PCR method. The experiment was done thrice in duplicates and representative values are shown. GAPDH was taken as the internal control. Wild type with the *URA3* marker was taken as the vector control for the *Cagpi19* null since the *URA3* gene is known to affect the transcript levels of many genes involved in hyphal formation(Cheng *et al.*, 2003) **(b)** Western blot showing a decrease in the levels of phosphorylated CaHog1, which is a well known CaHsp90 client protein, inthe *Cagpi19* null relative to the wild type. 5 seconds exposure was given to the X-ray film. GAPDH was taken as the internal control. The experiment was done thrice and representative images are shown. **(c)** Hyperfilamentation phenotype of the *Cagpi19* null mutant at 30 $^{\circ}$C relative to WT strain is reversed upon addition of tamoxifen(TfX), which is a CaHsp90 activator. Images were taken after 14 days. The experiment was done thrice and representative images are shown.

We also found that the filamentation at room temperature could be reversed by growing the cells with tamoxifen (Figure 4.3). Tamoxifen is actually an anti-cancer drug but is known to increase the activity of CaHsp90 in *Candida albicans* (Zhao *et al.*, 2010). We went on to further study CaRas1 dynamics in these cells. Upon treatment with tamoxifen, CaRas1 dynamics in the *Cagpi19* null became much faster, almost as fast as that in the wild type strain (Figure 4.3). Hence, from this, we can say that CaHsp90 downregulation is responsible for the slower dynamics of CaRas1 in the *Cagpi19* null.
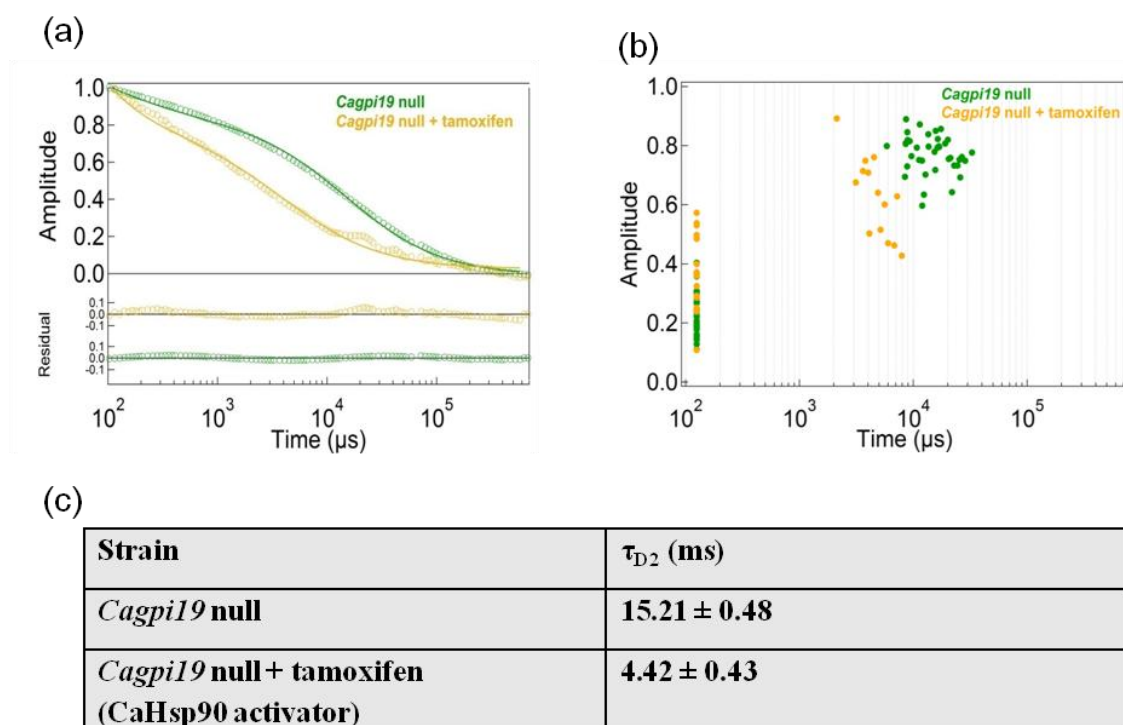

Strain	τ_{D2} (ms)
Cagpi19 null	15.21 ± 0.48
Cagpi19 null + tamoxifen (CaHsp90 activator)	4.42 ± 0.43

Figure 4.3: CaRas1 dynamics in *Cagpi19* null after CaHsp90 activation. (a) Average fluorescence autocorrelation G(τ)curves and **(b)** plots of amplitude versus diffusion times in individual cells before and after treating the *Cagpi19* null with tamoxifen, a CaHsp90 activator. The data were collected for more than 25 cells in each case. **(c)** Table showing the diffusion times of the indicated strains as obtained after fitting the FCS traces to the 2D2C model. Values are given $\pm$ S.D.

4.3 CaHsp90 *inhibition/downregulation in wild type gives slower CaRas1 dynamics*

4.3.1 CaRas1 *dynamics after treatment of wild type with geldanamycin*

We also further validated this by inhibiting CaHsp90 activity in the wild type strain with a CaHsp90 inhibitor, geldanamycin (GdA). It binds to the ATP binding pocket of CaHsp90 in

the N-terminal domain, thereby preventing the binding of any other nucleotides (Roe *et al.*, 1999). The wild type cells showed increased filamentation in the presence of geldanamycin, indicating a reduction in the activity of CaHsp90. For studying CaRas1 dynamics, cells were treated with 10 μM geldanamycin for 1 hour after lyticase treatment and CaRas1 dynamics was measured through FCS. The cells gave a much slower dynamics, as compared to those without the treatment (Figure 4.4).
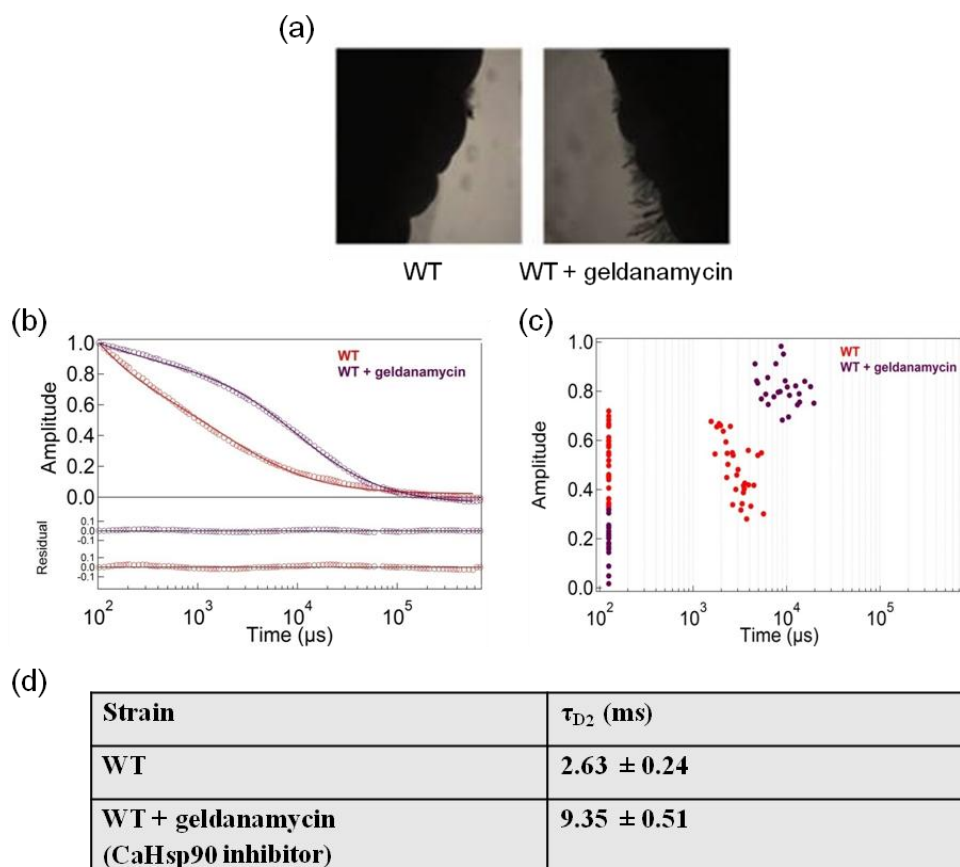

Strain	τ_{D2} (ms)
WT	2.63 ± 0.24
WT + geldanamycin (CaHsp90 inhibitor)	9.35 ± 0.51

Figure 4.4:CaRas1 dynamics after inhibition of CaHsp90. (a) Filamentation pattern of wild type (WT) cells treated with geldanamycin. The WT cells were grown in the presence of CaHsp90 inhibitor, geldanamycin (10 μM) and grown at 30°C. Images were captured after 14 days. The geldanamycin treated cells show increased filamentation.The experiment was repeated thrice and representative images are shown.**(b)** Average fluorescence autocorrelation $G(\tau)$ curves after treatment of wild type (WT) cells with an CaHsp90 inhibitor (geldanamycin). **(c)** Plot of amplitude versus diffusion times for the same FCS data obtained for individual cells. The data were collected for more than 25 cells in each case. **(d)** Table showing the diffusion times of the indicated strains as obtained after fitting the FCS traces to the 2D2C model. Values are given ± S.D.

4.3.2 *Generation of Cahsp90 null*

Further, we made a *Cahsp90* conditional null mutant in the *Candida albicans* wild type background, as *CaHSP90* is an essential gene and disruption of both the alleles is lethal to theorganism. To make this mutant strain one allele of *CaHSP90* was disrupted with the *HIS1* marker and the other allele was placed under the regulatable *MET3* promoter (Gerami-Nejad *et al*., 2004). Methionine-cysteine (5mM) was used to repress the *CaHSP90* allele (Figure 4.5).
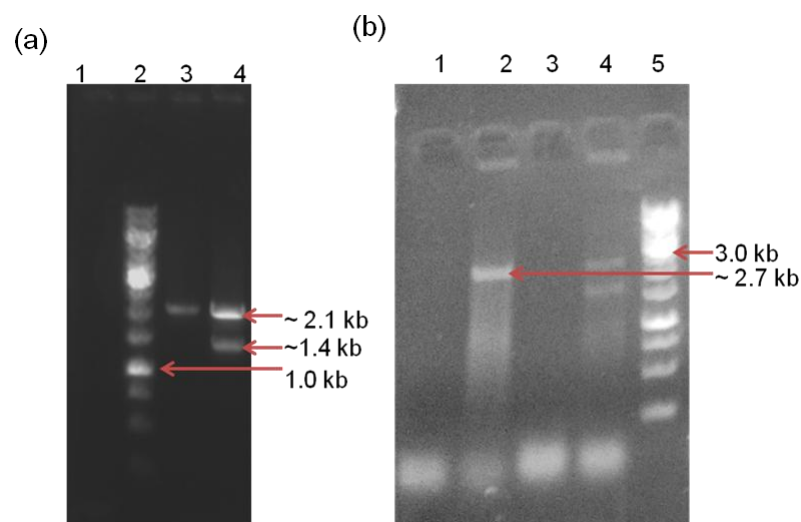

Figure4.5: Generation of *Cahsp90* conditional null mutant in *Candida albicans.* (a)Agarose gel electrophoresis showing generation of *Cahsp90* heterozygous mutant. Lane 1: Negative control, lane2: 1 kb DNA ladder, lane 3: Wild type, lane4: *Cahsp90* heterozygous mutant showing the disrupted (1.4 kb) allele and the wild type *CaHSP90* (2.1 kb) allele upon PCR amplification with HSP90 FP and HSP90 RP. **(b)** Agarose gel electrophoresis showing generation of *Cahsp90* conditional null mutant. Lane 1: Negative control, lane 2: positive colony showing amplification of 2.7 kb using HSP90 UPS FP and MET3 RP, lane 3 and 4: negative colonies, lane 4: 1 kb DNA ladder.

4.3.3 CaRas1 *dynamics in Cahsp90 null*

As expected, the strain showed a hyperfilamentation phenotype at room temperature, indicating that Ras is hyperactivated in this mutant (Figure 4.6). CaRas1 dynamics was studied in this mutant and found to be significantly slower than in the wild type. The timescales obtained for CaRas1 diffusion in the *Cahsp90* conditional null closely matched

that for the WT-Ras1^{G13V} OE hyperactive strain and the *Cagpi19* null (Figure 4.5). This confirmed our hypothesis that CaHsp90 downregulation can cause slowing down of CaRas1 dynamics upon its hyperactivation.
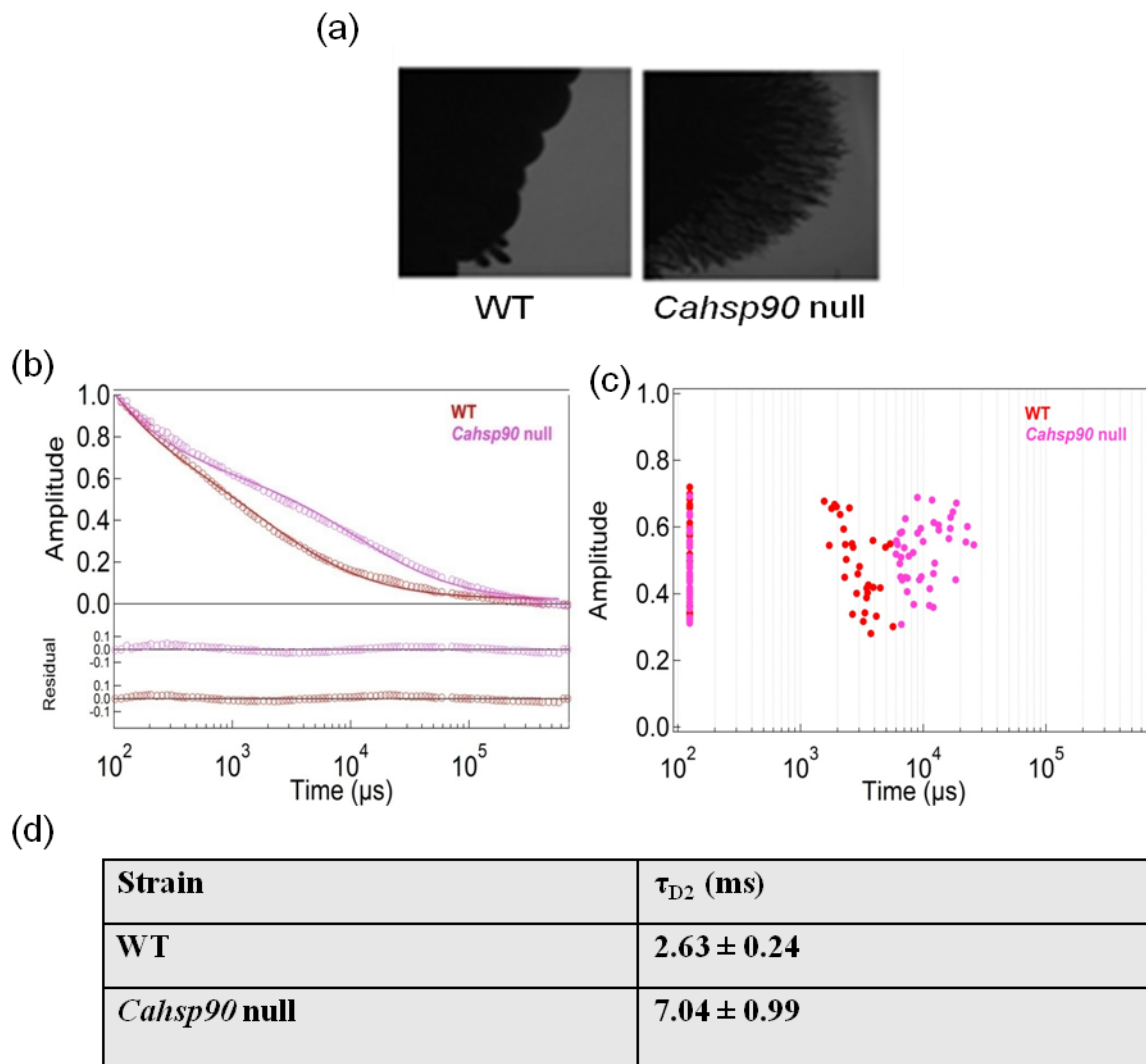
Figure 4.6: **CaRas1 dynamics in*Cahsp90* null.** **(a)** Filamentation pattern of *Cahsp90* null mutant with respect to the wild type. The cells were spotted on YEPD medium and grown at 30°C. The experiment was repeated thrice and representative images are shown. **(b)** Average fluorescence autocorrelation G(τ) curves and **(c)** plots of amplitude versus diffusion times in individual cells of *Cahsp90* null mutant. The data were collected for more than 25 cells in each case. **(d)** Table showing the diffusion times of the indicated strains as obtained after fitting the FCS traces to the 2D2C model. Values are given ± S.D.

4.4 *Study of the role of altered actin polymerization in* **CaRas1** *dynamics*

A recent study reported that Saccharomyces cerevisiae treated with geldanamycin (Hsp90 inhibitor) showed formation of polymerized actin filaments (Senn *et al*, 2012). Studies in *Saccharomyces cerevisiae* have also shown that stabilization of F-actin filaments is required for ScRas hyperactivation. Unlike in the wild type cells, in mutants where there is increased actin polymerization, the adenylyl cyclase ScCyr1 and the cyclase associated protein, ScSrv2, associate with actin aggregates (Gourlay and Ayscough, 2006). Is hyperactivation of CaRas1 in the *Candida albicansCagpi19* null mutant likely to induce actin polymerization? There are reports which show that actin dynamics may control cAMP levels and that CaCyr1-CaCap1-G actin form a kind of sensor apparatus (Shima *et al*., 2000). CaCyr1 when activated by interaction with CaRas1-GTP, interacts with a cyclase associated protein, CaCap1 though its C terminus. On the other hand, CaCap1 also interacts with monomeric G-actin via its proline rich domains to control the actin polymerization in the cell (Zou *et al*., 2009). Interaction of G actin with CaCap1 maintains an equilibrium between the monomeric and polymeric actin inside the cell, the critical concentration of monomeric G-actin being 0.1 µM. Hence, we wanted to study if this complex regulates the dynamics of CaRas1.

4.4.1*β-actin staining in Candida albicans*

The total β-actin of the cell was stained using a β-actin antibody. A FITC (Fluorescein isothiocyanate) labelled secondary anti- mouse antibody was used to observe the β-actin under the microscope (Figure 4.7).
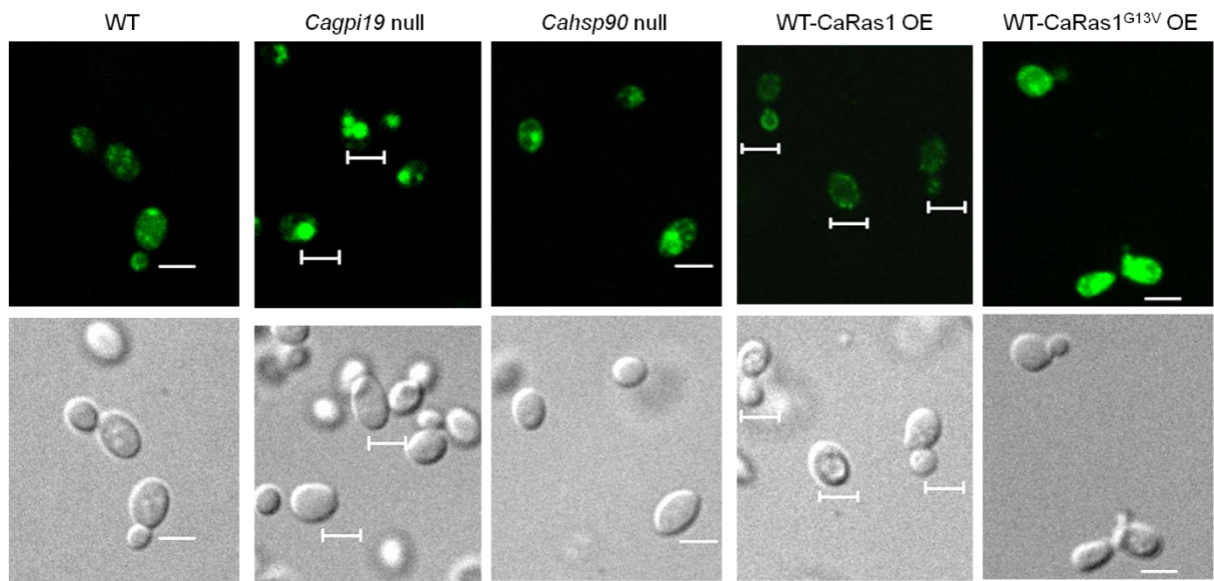
Figure 4.7: β-**actin staining in** *Candida albicans.*Immunostaining of total β-actin in the indicated strains. The punctate staining observed in WT or WT-CaRas1 OE strain is lost upon CaRas1 hyperactivation. Scale bar corresponds to a distance of 5 μm. The experiment was repeated thrice and representative images are shown.

From the β-actin staining, we can see that there is a punctate pattern of actin in the wild type or the WT-CaRas1 OE strain, mostly on the rim of the cell, which is, however, lost in the cells where CaRas1 is hyperactive, like the WT-CaRas1^{G13V} OE or the *Cagpi19* null or the *Cahsp90* null. In these cells, actin is more clustered inside the cell which could mean more of polymerized actin in these cells. Could this contribute to slower CaRas1 dynamics?

4.4.2 *Effect of alteration of actin polymerization on* CaRas1 *dynamics*

To study this, we treated the strains having more clustered actin with a cell permeable inhibitor of actin polymerization, cytochalasin D (Cyto D), which binds to the F-actin filaments and prevents binding of actin monomers, hence depolymerizing the actin filaments (Gabriel et al., 1998) and the wild type strain with Jasplakinolide (JasP), a macrocyclic peptide which promotes actin filament nucleation, thereby inducing actin polymerization (Holzinger, 2009) and then monitored CaRas1 dynamics in them (Figure 4.8).

(i)
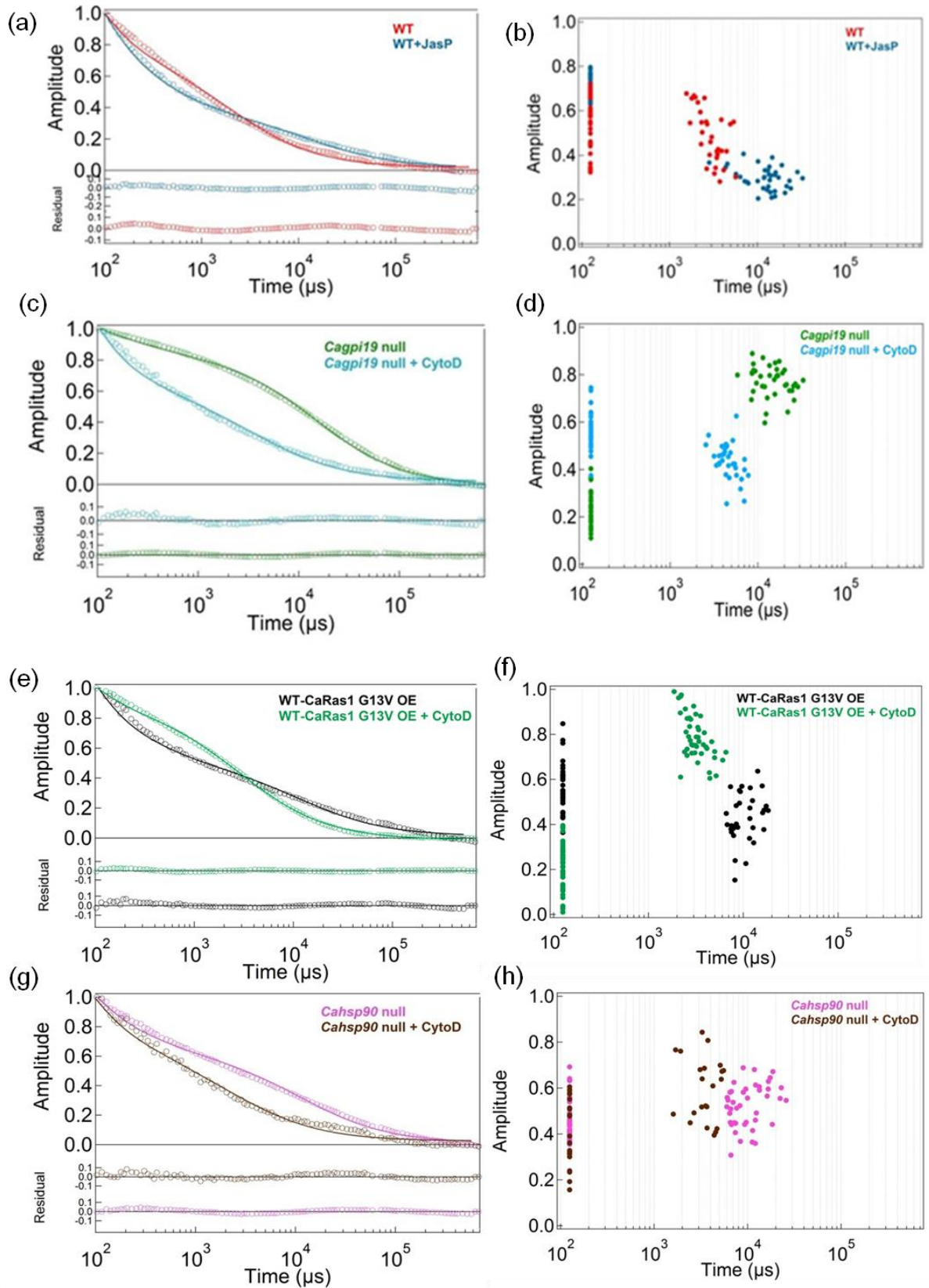
Strain	τ_{D2} (ms)
WT	2.63 ± 0.24
WT + JasP (Actin polymerization inducer)	14.53 ± 2.02
Cagpi19 null	15.21 ± 0.48
Cagpi19 null + Cyto D (Actin polymerization inhibitor)	4.35 ± 0.68
Cahsp90 null	12.03 ± 0.94
Cahsp90 null + Cyto D (Actin polymerization inhibitor)	2.77 ± 0.79
WT-CaRas1^{G13V} OE	12.48 ± 1.68
WT-CaRas1^{G13V} OE + Cyto D (Actin polymerization inhibitor)	3.1 ± 0.19

Figure 4.8: Altered actin polymerization can cause changes in CaRas1 dynamics. (a) Average fluorescence autocorrelation $G(\tau)$ curves after treatment of wild type (WT) cells with an inducer of actin polymerization, jasplakonilide (JasP). **(b)** Plot of amplitude versus diffusion times for the same FCS data obtained for individual cells. The data were collected for more than 25 cells in each case. **(c-d)** Fluorescence autocorrelation curves $G(\tau)$ and a plot of amplitude versus diffusion time of *Cagpi19* null strain before and after treatment with Cyto D. The data were collected for more than 25 cells in each case. **(e-f)** Average fluorescence autocorrelation curves $G(\tau)$ and plot of amplitude versus diffusion time in individual cells of WT-CaRas1^{G13V} OE, before and after treatment with Cyto D. **(g-h)** Fluorescence autocorrelation curves $G(\tau)$ and a plot of amplitude versus diffusion time of *Cahsp90* null strain before and after treatment with Cyto D. The data were collected for more than 25 cells in each case. **(i)** Table showing the diffusion times of the indicated strains as obtained after fitting the FCS traces to the 2D2C model. Values are given $\pm$ S.D.

4.4.3 *Study of changes in intracellular viscosity in Cagpi19 null*

The immediate question that comes up is, does an alteration in actin polymerization in the *Cagpi19* null also change the intracellular viscosity which slows down the dynamics of CaRas1? For this, we stained the cells with an intracellular cytosolic fluorescent probe, Calcein-AM (Spangler *et al.*, 2016). This dye is non-fluorescent as such but when it enters the cytosol, intracellular esterases cleave the acetoxymethyl (AM) and Calcein fluoresces. The steady state anisotropy of this Calcein was measured, which would tell us about the ease of rotation of this probe in the mutant versus the wild type and this was used to get an ideaabout the intracellular viscosity. A higher intracellular viscosity would cause hindered rotation of the fluorescent probe, which would translate into a higher steady state anisotropy.

The staining was done as per the protocol given in Materials and Methods. Anisotropy was measured by recording the fluorescence intensity in the horizontal and vertical direction with the help of a polarizer. Excitation was set at 495 nm and emission at 515 nm. Even though there is a two-fold increase in the steady state anisotropy of Calcein in the mutant (Figure 4.9), this is not enough to explain the huge slowing down of CaRas1. If all the interacting molecules affecting CaRas1 dynamics are assumed to be spherical and taking into account the two-fold increase in the viscosity, then by Stokes-Einstein equation, it would roughly translate into an increase of about 3-15 fold in the molecular weight of the complex.

Strain	Steady state anisotropy (r)
WT	0.072 ± 0.002
Cagpi19 null	0.255 ± 0.002
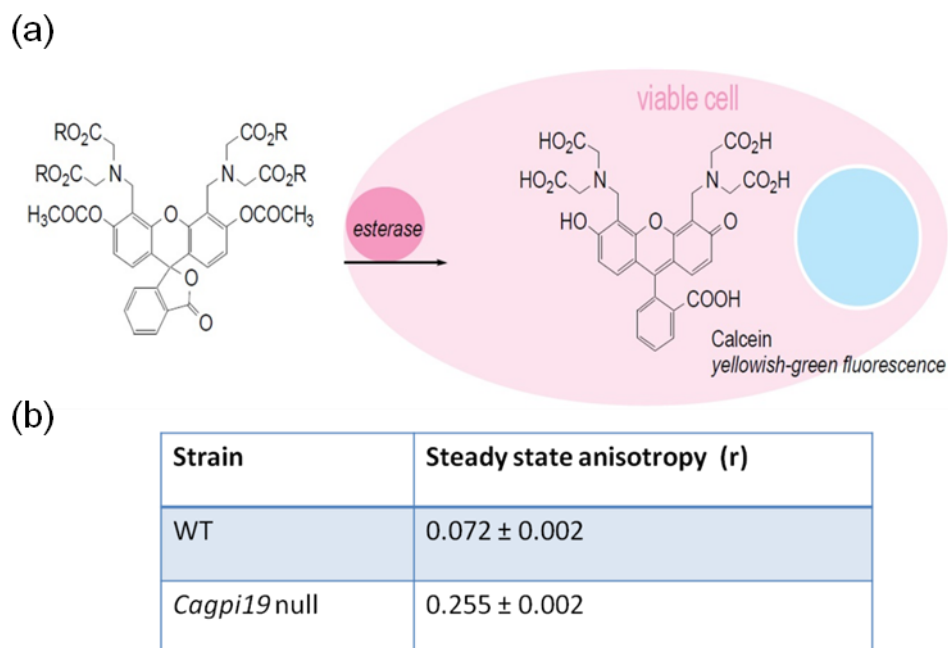
Figure 4.9: Increased viscosity in the *Cagpi19* null. (a) Cartoon showing the action of the fluorescent probe Calcein-AM in the cell. The intracellular esterases cleave the probe and release the fluorescent Calcein inside the cellular cytoplasm. **(b)** Steady state anisotropy of Calcein-AM after staining the wild type and the *Cagpi19* cells. *Cagpi19* null shows a higher anisotropy of Calcein indicating a hindered rotation. The experiment was done thrice and average values $\pm$ S.D are shown.

4.4.4 *Quantification of polymerized actin in Cagpi19 null*

To further validate our results, we checked the level of polymerized actin in the cell by staining the cells with rhodamine-phalloidin, a bicyclic peptide which specifically binds to

polymerized actin filaments, and not to monomeric actin. The peptide is conjugated to the fluorescent molecule TRITC (Tetramethylrhodamine) which helps in observing actin filaments under a fluorescent microscope. There was two-fold higher staining in the *Cagpi19* null as compared to the wild type, indicating more of polymerized actin in the former (Figure 4.10).
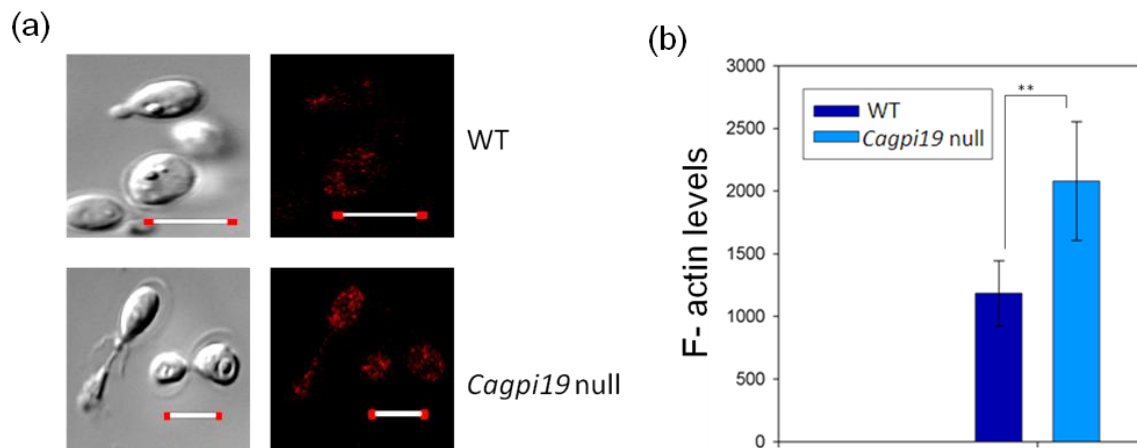

Figure 4.10:Increased actin polymerization in *Cagpi19* null.(a) F-actin levels in the *Cagpi19* null mutant were studied with respect to the wild type. Rhodamine-phalloidin was used to selectively stain the F-actin filaments. WT and *Cagpi19* null without the mRFP-CaRas1 tagging were taken for these studies to avoid interference with the red fluorescence. The experiment was done thrice and representative images are shown. **(b)** Quantification of F-actin levels in the *Cagpi9* null by quantification of staining of Rhodamine-phalloidin. Quantification was done for more than 20 cells in each case. Error bars represent S.D.

4.4.5 *Co-localization studies of* CaRas1 *with polymerized actin and total β-actin*

We also did colocalization studies of CaRas1 and polymerized actin filaments in the *Cagpi19* null using rhodamine-phalloidin and between CaRas1 and total β-actin using an antibody against β-actin (Figure 4.11 and Figure 4.12). We calculated the extent of colocalization bythe Pearson's correlation coefficient and found that there was low colocalization between CaRas1 and polymerized actin in the wild type as well as the *Cagpi19* null (Figure 4.11).
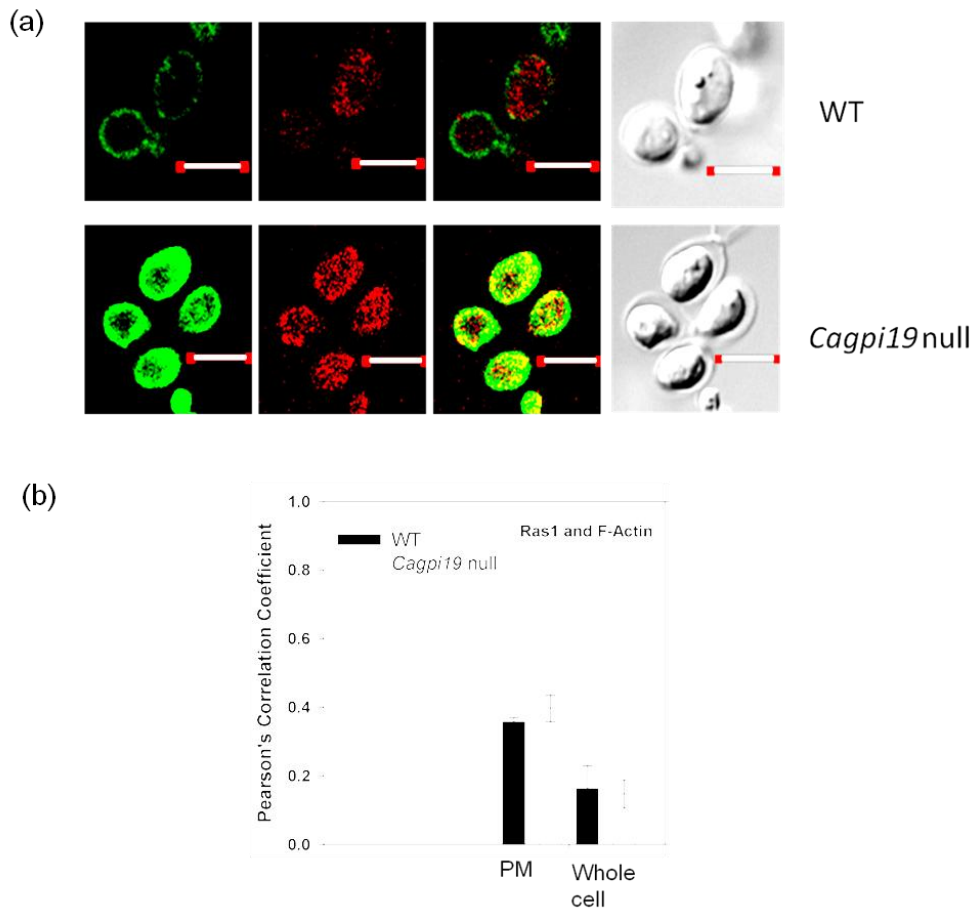
(a)

(b)

Figure 4.11:Colocalization between CaRas1 and F-actin.(a) Colocalization of CaRas1 with the polymerized F-actin in the *Cagpi19* null and the wild type using anti-CaRas1 antibody and rhodamine-phalloidin. The experiment was done thrice and representative images are shown. WT and *Cagpi19* null without the mRFP-CaRas1 tagging were taken for these studies to avoid interference with the red fluorescence. **(b)** Quantification of the extent of colocalization of CaRas1 with F-actin at the plasma membrane and the whole cell using the Pearson's correlation coefficient. Quantification was done for more than 20 cells in each case.Error bars represent S.D.

On the other hand, we did see significantly higher colocalization between CaRas1 and β-actin when we used anti-β-actin antibody that did not distinguish between polymerized and monomeric form of β-actin in the *Cagpi19 null* as compared to the wild type. This was particularly the case when we examined co-localization of the two at the plasma membrane of the cell rather than when we considered the whole cell for the analysis (Figure 4.12).
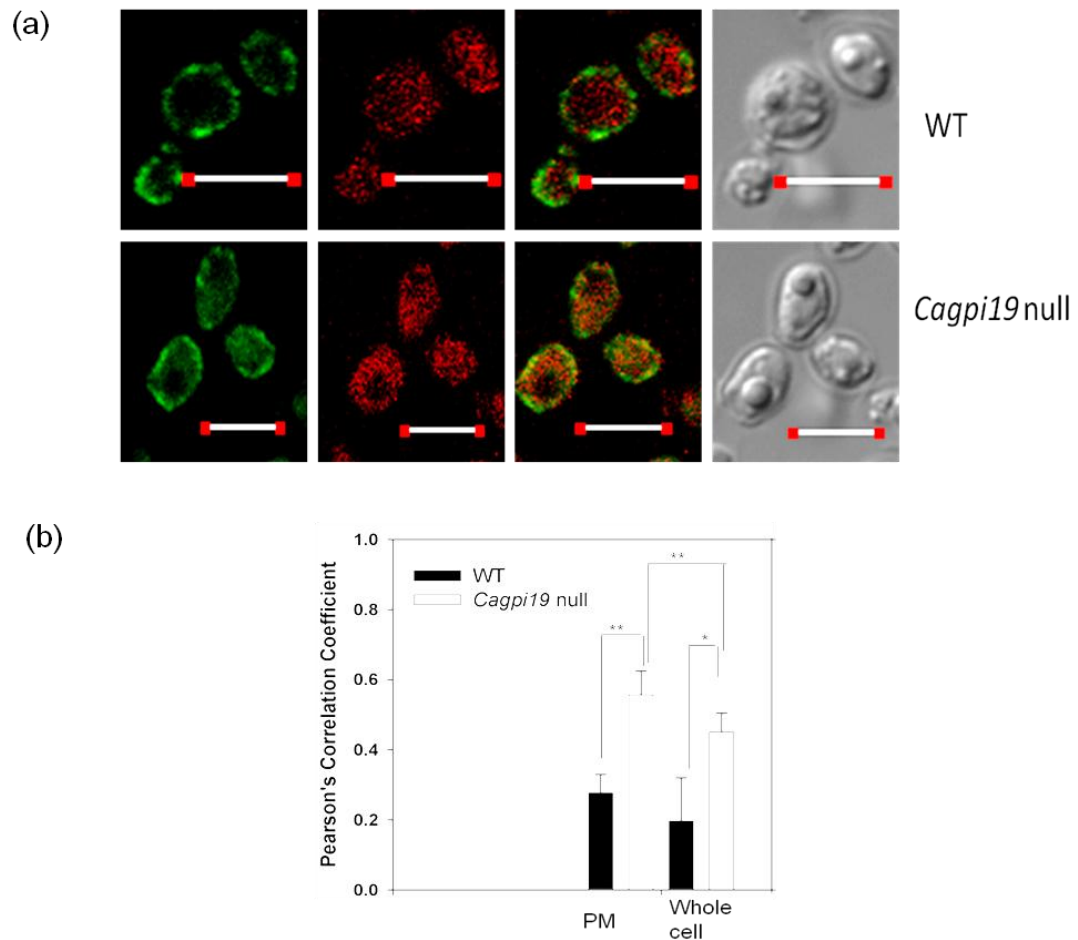
(a)

(b)

Figure 4.12: Colocalization studies between CaRas1 and F-actin and CaRas1 and β-actin.(a) Colocalization between CaRas1 and total β-actin through immunostaining with anti CaRas1 antibody and anti β-actin antibodies respectively. The experiment was done thrice and representative images are shown. WT and *Cagpi19* null without the mRFP-CaRas1 tagging were taken for these studies to avoid interference with the red fluorescence. **(b)** Quantification of the colocalization calculated through the Pearson's Correlation Coefficient. Quantification was done for more than 20 cells in each case. Error bars represent S.D.

This could indicate that CaRas1 specifically colocalizes with monomeric G-actin and not the polymerized F-actin filaments at the plasma membrane. It is known that ScCyr1-ScCap1-G-actin complex is involved in Ras hyperactivation in yeast (Gourlay and Ayscough, 2006). In the yeast, *Saccharomyces cerevisiae*, ScRas hyperactivation requires the binding of the CaCap1 homolog, ScSrv2 with ScCyr1 to cause an increase in the cAMP levels. In human cell lines, the H-Ras^{G12V} mutant is known to have increased actin polymerization (Tanaka *et al*., 1999). In *Candida albicans*, however, to the best of our knowledge, no one has till date

managed to purify CaRas1 along with the CaCyr1-CaCap1-G-actin complex. This could be because of the transient interaction of CaRas1 with this complex (Zou *et al*., 2009). Whereas in the hyperactive *Cagpi19* null strain, CaRas1 could interact with CaCyr1-CaCap1-G actin complex for longer periods of time and hence could be detected in FCS as a slower moving complex and in confocal microscopy as being colocalized with β-actin. Higher interaction of CaRas1 with the CaCyr1-CaCap1 complex also increases cAMP levels, thereby causing hyperactivation of CaRas1. The longer engagement of CaRas1 with this complex could be the reason for slower CaRas1 dynamics in this mutant. We hypothesize that longer engagement of CaRas1 with the CaCyr1-CaCap1-G-actin complex shifts the equilibrium between G-actin and F-actin towards F-actin formation. As mentioned earlier a mechanism whereby G-actin interaction with ScCyr1-ScSrv2 regulates actin polymerization and causes ScRas activation has been proposed in *Saccharomyces cerevisiae* (Gourlay and Ayscough, 2006), however, this model does not explain how ScRas may be hyperactivated. We suggest a mechanism where CaRas1 and G-actin simultaneously interact with the CaCyr1-CaCap1 complex in the absence of CaHsp90. The interaction of G-actin with the CaCyr1-CaCap1 complex would not only stimulate F-actin production but also result in higher cAMP levels. Simultaneously, the association of CaRas1 with CaCyr1-CaCap1 would turn on a CaRas1-dependent cAMP stimulation as well. The combined effect of the two would be sustained high levels of cAMPlevels in the cell causing hyperfilamentation. This model would also explain why there is increased actin filamentation in the mutants where CaRas1 is hyperactive, viz., *Cahsp90* null and the WT-CaRas1[G13V] OE strains. This also explains why there is increased actin filamentation in the *Cagpi19* null (Figure 4.13).
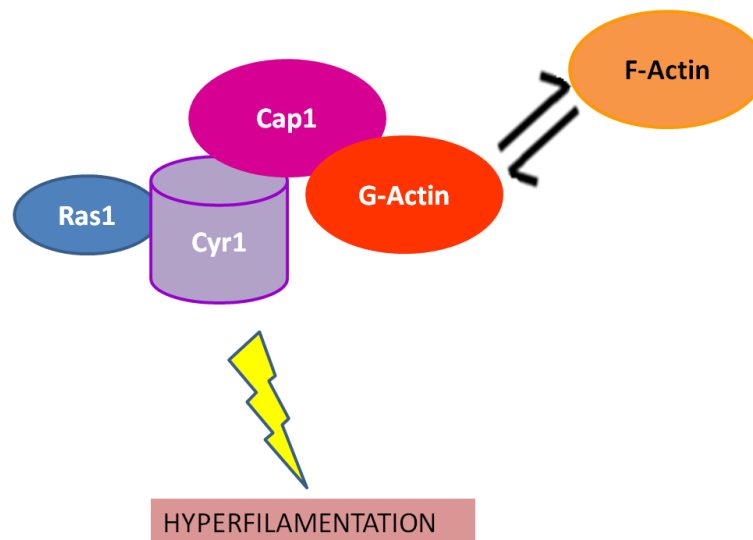
Figure 4.13:Possible existence of CaRas1-CaCyr1-CaCap1-G-Actin complex in *Cagpi19* **null.** We hypothesize that higher engagement of CaRas1 with the CaCyr1-CaCap1-G-actin complex in *Cagpi19* null leads to CaRas1 hyperactivation and increased actin polymerization.

4.5 *Lower ergosterol in the Cagpi19 null does not affect* **CaRas1** *dynamics*

Another phenotype of *Cagpi19* null is that it has lower ergosterol levels (Figure 4.14). The ergosterol level in the mutant is about 60% that of the wild type. This is the reason that Nile red dynamics is faster in this mutant as compared to the wild type (as described in Chapter 3). However, we observed that the lower ergosterol levels did not affect CaRas1 dynamics. For this we treated the wild type cells with βCD (β-cyclodextrin) which sequesters ergosterol from the cell (Christian *et al.*, 1997). We performed GC-MS to confirm that the ergosterol levels were actually reduced after treatment with βCD. We were able to extract out about 50% of the ergosterol in this manner (Figure 4.14). These cells were then monitored for theirCaRas1 dynamics through FCS. We found that there was no significant change in CaRas1 dynamics after a reduction in the ergosterol levels in the wild type cells. This led us to conclude that lower ergosterol levels does not play a significant role in the dynamics of CaRas1 and should have negligible effect on the dynamics of CaRas1 in the *Cagpi19* null (Figure 4.14).
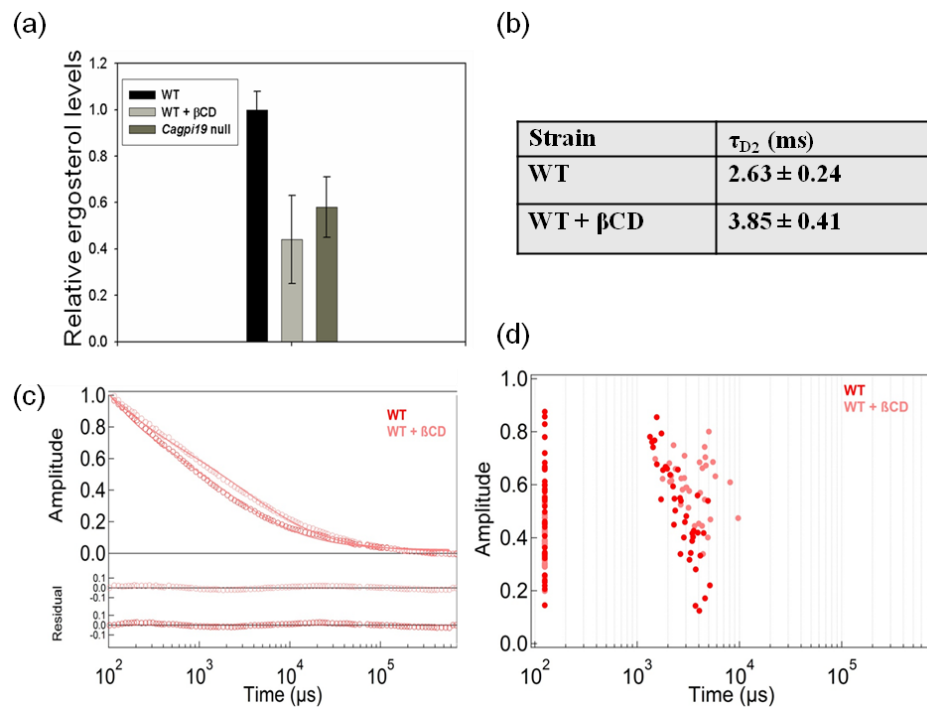
(a)

(b)

Strain	τ_{D_2} (ms)
WT	**2.63 ± 0.24**
WT + βCD	**3.85 ± 0.41**

(c)

(d)

Figure 4.14: Sterol deficiency is not responsible for slower CaRas1 dynamics in *Cagpi19*null. (a) Sterol estimation by GC-MS of the indicated *C.albicans* strains. Wild type (WT) cells treated with βCD and the *Cagpi19* null mutant show lower ergosterol levels compared to the untreated wild type as estimated by GC-MS. The experiment was repeated thrice and representative images are shown.**(b)** Table showing the diffusion times of the indicated strains as obtained after fitting the FCS traces to the 2D2C model.**(c)**Fluorescence autocorrelation curves $G(\tau)$ and **(d)** plot of amplitude versus diffusion times after treatment of wild type (WT) cells with βCD. The data were collected for more than 25 cells in each case.Values are given ± S.D.

4.6 *Chapter summary*

This chapter explores the mechanism behind the slowing down of CaRas1 upon its hyperactivation in *Candida albicans*. We found that *Cagpi19* null had phenotypes typical of an *Cahsp90* mutant strain. We discovered that lower levels of CaHsp90 can cause slowing down of CaRas1 when it is hyperactivated. This could be seen from the fact that treating *Cagpi19* null, with tamoxifen, an activator of CaHsp90 in *Candida albicans* reverses the slow dynamics that was observed in the mutant whereas treating the wild type strain with geldanamycin, an CaHsp90 inhibitor, causes slowing down of CaRas1. We also made a genetic conditional null mutant of *Cahsp90* and showed that it also exhibits slower dynamics. This indicates that a drop in CaHsp90 levels leads to CaRas1 hyperactivation which causes

slowing down of CaRas1 dynamics. It has been shown in *Saccharomyces cerevisiae* that polymerized actin filaments required for hyphal formation are found when the clls are treated with the Hsp90 inhibitor, geldanamycin. Following it up in *Candida albicans*, we also showed that a change in the levels of polymerized actin might be responsible for the slowing down of CaRas1 in the hyperfilamentous *Cagpi19* null. β-Actin staining revealed that actin in the strains where CaRas1 is hyperactive was more polymerized, probably indicating a higher degree of polymerization, than in the wild type strain. Treating these strains with an actin polymerization inhibitor, cytochalasin D, made CaRas1 dynamics much faster, almost close to that seen in the wild type. Also, treating the wild type with an actin polymerization inducer, jasplakinolide, gave slower CaRas1 dynamics. This showed us that increased actin polymerization does slow down CaRas1 dynamics. To check whether this slowing down of CaRas1 is caused by an increase in intracellular viscosity that could also occur when actin polymerizes, we measured the steady state anisotropy of Calcein-AM, a well known fluorescent cytosolic probe. This revealed that even though there is an increase inthe anisotropy of the dye in *Cagpi19* null, suggesting hindered rotational diffusion of the dye due to higher intracellular viscosity, this change by itself is not enough to account for the huge slowing down of CaRas1 in the mutant.

Reports in *Saccharomyces cerevisiae* show that ScRas hyperactivation occurs upon actin polymerization and it requires the binding of the CaCap1 homolog, ScSrv2 with ScCyr1 to cause an increase in the cAMP levels (Gourlay and Ayscough, 2006). A study in yeast also shows that mutants which are deficient in ScSrv2 or mutants where the G-actin binding site of ScSrv2 is truncated fail to increase cAMP levels upon receiving a hyphal stimulus and are consequently, hypofilamentous (Zou *et al*., 2009). In *Candida albicans* pharmacological inhibition of CaHsp90 with geldanamycin results in actin polyerization as seen upon hyphal induction (Senn *et al*., 2012). This led us to examine whether the polymerization status of

actin had been altered in the *Cagpi19* null. Phalloidin staining helped prove that there is higher F-actin (polymerized actin) in the *Cagpi19* null. We also found greater colocalization of CaRas1 with β-actin monomers at the plasma membrane of the *Cagpi19* null. There was very little colocalization of CaRas1 with filamentous actin. We propose that interaction of CaRas1 with the CaCyr1-CaCap1-G-actin complex leads to hyperactivation of CaRas1 signaling which leads to hyperfilamentation and actin polymerization in the *Cagpi19* null. Since CaRas1 engages with this larger signaling complex, it results in slower CaRas1 dynamics when monitored by FCS.

Summary and future perspectives

Summary

This study deals with the GPI anchor biosynthetic pathway in *Candida albicans*. As described in the Introduction section, GPI anchor biosynthesis is a complex pathway, which takes place in the ER of the cell, consisting of more than twenty steps. To our knowledge, no one has shown interaction of the GPI anchor biosynthetic pathway with any other pathway in *Candida albicans*. Our lab previously showed that there is a mutual co-regulation between *CaGPI19*, a subunit of the GPI-GnT complex (which catalyzes the first step of the pathway) and *CaERG11*, a key enzyme involved in the ergosterol biosynthesis pathway in *Candida albicans*and the target of azole antifungal drugs. Downregulation of *CaGPI19* causes downregulation of*CaERG11* and vice-versa (Victoria *et al.*, 2012). We also reported that there is positive regulation between the *CaGPI2*, another essential subunit of the GPI-GnT complex, and the CaRas1 signaling pathway in *Candida albicans*. Downregulation of *CaGPI2* negatively affects cAMP-dependent PKA signaling controlled by CaRas1 resulting in hypofilamentation while overexpression of it activates the CaRas1 signaling pathway causing hyperfilamentation. Also, *CaGPI2* and *CaGPI19* negatively regulate each other (Yadav i., 2014b). This explains why *Cagpi2* mutants are hypofilamentous and are azole resistant while *Cagpi19* mutants are hyperfilamentous and azole sensitive (Victoria *et al.*, 2010, 2012; Yadav *et al.*, 2014b).

CaRas1 is the most important player for hyphal formation in *Candidaalbican*s (Inglis and Sherlock, 2013). Hyphae are in turn involved in a variety of important functions like adhesion to the host cell , aggregation, invasion to the human host etc. and most of the GPI anchored proteins are virulence factors and expressed exclusively in the hyphal form (Plaine *et al.*, 2008). Hence, we wanted to further explore the cross talk between GPI biosynthesis and CaRas1 signaling, focusing particularly on what happens to CaRas1 signaling *per se* when one or more of the subunits of the GPI-GnT complex is downregulated.

We also used the project to establish a new technique for the study of membrane proteins in *Candida albicans* namely, Florescence Correlation Spectroscopic (FCS). FCS is a (near) single molecular technique which enables monitoring the diffusional dynamics of a fluorescent probe molecule at very low concentrations and in a very small confocal volume. This suited our purpose since we wanted to look at endogenous proteins *in vivo* without using overexpression systems. Nobody to the best of our knowledge has used FCS to monitor dynamics of a membrane protein in *Candida albicans* till now. This FCS approach helped us to understand the subtle changes that happen in the Ras signaling when it is hyperactivated versus its overexpression state, which are difficult to study by conventional biochemical/ molecular biology techniques. The following is a summary of our studies:

> *Faster membrane dynamics of Nile red in the Cagpi19 null*

Membrane dynamics of the hydrophobic dye, Nile red when measured by FCS was much faster in the *Cagpi19* null than in the wild type. This was expected as we have already reported from our lab that the *Cagpi19* null has lower ergosterol levels in its membrane. Also*Cagpi19* null has a poorer membrane packing as seen by faster lifetimes of another membrane probe, DPH (1,6-Diphenyl-1,3,5-hexatriene) (Victoria, S., 2010).

> **CaRas1** *dynamics, however, is slower in the Cagpi19 null*

Despite having a less rigid membrane, the *Cagpi19* null mutant showed roughly 5-6 fold slower CaRas1 dynamics than the wild type.

> *Hyperactivation of*CaRas1 *causes slower*CaRas1 *dynamics across species*

We treated the wild type cells with sodium vanadate, which mimics the γ phosphate of GTP and binds to the GDP bound Ras, thereby locking it bound to GAPs. This gave a

much slower diffusion time of CaRas1, indicating that higher engagement of CaRas1 with its downstream effectors, could cause slower dynamics. To confirm this, we generated a series of CaRas1 overexpression mutants wherein we over expressed the wild type CaRas1 and the constitutively active CaRas1^{G13V} (which is always bound to GTP) in the wild type background. We discovered that CaRas1 dynamics was comparable in wild type strain and in the strain which overexpressed CaRas1. But the dynamics was much slower, and comparable to that seen in the *Cagpi19* null when wild type cells overexpressed CaRas1^{G13V}. We also confirmed this in the *Caras1* null background, where no endogenous CaRas1 was present, and got the same results. We also confirmed this in a human breast cancer cell line (MDA-MB-231) in which the diffusion of the constitutively activated H-Ras^{G12V} was much slower than the wild type H-Ras, indicating that the slower dynamics of hyperactivated Ras is seen across species, from *Candida albicans* to human cell lines.

➢ *CaHsp90 deficiency causes* **CaRas1** *hyperactivation in the Cagpi19 null*

We showed that a deficiency of the heat shock protein *Ca*Hsp90, causes CaRas1hyperactivation in the *Cagpi19* null. *Cagpi19* null too had lower *CaHSP90* transcript levels and showed lower phosphorylation of CaHog1, a well known client protein of CaHsp90 (Shapiro *et al*., 2009). Treating the *Cagpi19* null with tamoxifen, an activator of CaHsp90 (Zhao *et al*., 2010), made the dynamics of CaRas1 much faster and comparable to that seen for wild type CaRas1. This trend of slower CaRas1 dynamics upon CaHsp90 downregulation could be seen in the wild type also when it was treated with geldanamycin, a CaHsp90 inhibitor (Roe *et al*., 1999). Treating the wild type with an inhibitor of CaHsp90, made the CaRas1 dynamics much slower, similar to that seen in the *Cagpi19* null. We further confirmed these results by

generating a *Cahsp90* conditional null and observing that CaRas1 dynamics was indeed slower in this strain. This confirmed our hypothesis that CaHsp90 deficiency causes CaRas1 hyperactivation which causes slower CaRas1 dynamics in the *Cagpi19* null.

➢ *Higher actin polymerization in the Cagpi19 null is also responsible for slower* **CaRas1** *dynamics*

Actin polymerization has been linked to hyperactive Ras signaling in *Saccharomyces cerevisiae* and in human cell lines also (Gourlay and Ayscough, 2006). We found that strains expressing hyperactive CaRas1 show actin bundling rather than being uniformly present in the cytosol as seen in the wild type strain. This could indicate higher actin polymerization in these strains.We found that disrupting actin polymerization by Cytochalasin D (Gabriel et al., 1998) made CaRas1 dynamics faster in these strains. Similarly inducing actin polymerization by Jasplakonilide (Holzinger, 2009) in the wild type gave us slower CaRas1 dynamics. We also found out that there is indeed higher actin polymerization in the *Cagpi19* null which could cause slower CaRas1 dynamics.

➢ *Higher actin polymerization leads to increased colocalization of* **CaRas1***with G-actin*

Slower CaRas1 dynamics in *Cagpi19* null upon increased actin polymerization could be because of increased viscosity or due to changes in the CaRas1 signaling *perse*. We found out that the approximate 2-3 fold increase in the viscosity (as measured by changes in the steady state anisotropy of the fluorescent cytosolic probe Calcein-AM) in the *Cagpi19* null could not alone account for the 5-6 fold slower dynamics of CaRas1. Other things being equal (and taking into consideration viscosity changes),

diffusional dynamics of a molecule is largely dependent on its size. This would suggest that CaRas1 is slowing down due to its interaction with a larger signaling platform when it is hyperactivated. We did colocalization studies and found out there is significantly higher colocalization of CaRas1 with total actin rather than with F-actin in the *Cagpi19* null. This indicates that more of CaRas1 is present in regions that also contain G-actin at the plasma membrane. This lead us to hypothesize the existence of CaRas1-CaCyr1-CaCap1-G-actin complex in *Cagpi19* null. In wild type yeast cellsunder normal condition, the cAMP/PKA pathway can be independently triggered by CaRas1-CaCyr1 complex or the CaCyr1-CaCap1-G-actin complex when they receive appropriate cues (Zou *et al*., 2009). Upon CaRas1 hyperactivation we propose that CaRas1 is recruited to the CaCyr1-CaCap1-G-actin complex due to the absence of CaHsp90 that acts as the normal inhibitor of this association. This leads to constitutively activated cAMP/PKA signaling and increased actin polymerization.

➢ *Dynamics of* **CaRas1** *in the CaGPI2 overexpression strain*

We also studied CaRas1 dynamics in the *CaGPI2* overexpression background. This strain is previously reported in our lab to have a hyperfilamentous phenotype (Yadav *et al*., 2014b) indicating a higher level of activation of the CaRas1 signaling pathway. As expected, CaRas1 dynamics in this strain was found to be significantly slower, similar to that obtained in the *Cagpi19* null. We also did preliminary studies which show that as in the *Cagpi19* null, the hyperfilamentation of this strain at room temperature was decreased in the presence of tamoxifen, a CaHsp90 activator and increased in the presence of geldanamycin, an Hsp90 inhibitor; indicating that in this case also, inhibition of CaHsp90 activity could be responsible for slower CaRas1 dynamics (details are mentioned in Appendix).

➢ *Ergosterol deficiency does not affect* **CaRas1** *dynamics in Candida albicans*

We showed that lower ergosterol levels in the *Cagpi19* null are not responsible for altered CaRas1 dynamics. We sequestered ergosterol from the wild type by treating the cells with methyl β-cyclodextrin and saw that there was no significant change in CaRas1 dynamics. This indicates that ergosterol deficiency does not affect CaRas1dynamics in *Candida albicans*. This result is important since it suggests that dynamics of CaRas1 are not likely to depend on ergosterol levels and is unlikely to take place from sterol-rich microdomains unlike what has been observed for mammalian H-Ras (Hancock, 2003; Prior and Hancock, 2012; Roy *et al.*, 1999).

➢ **CaRas1** *dynamics in hyphae*

We also studied CaRas1 dynamics in the hyphal forms of the wild type and the *Cagpi19* null mutant and observed that *Cagpi19* null showed significantly faster CaRas1 dynamics than in its yeast form. This could probably be due to changes in the cell wall and membrane organization that happen during hyphal morphogenesis. These need to be studied further in detail (Braun and Calderone, 1978; Lenardon *et al.*, 2010).

We also wanted to study if there is any physical association between CaGpi2 and CaGpi19. A physical association has been reported in their *Saccharomyces cerevisiae* orthologues (Miller *et al.*, 2005; Newman *et al.*, 2005). We used a bimolecular fluorescence complementation approach (Fan *et al.*, 2008; Ohad and Yalovsky, 2010; Stynen *et al.*, 2010) to study this problem. We cloned *CaGPI2* and *CaGPI19* in the bait and the prey vectors respectively and could not detect any fluorescence after transformation of these in the wild type *Candida albicans* strain. This could be either

because the two proteins do not interact or the site of interaction is blocked by tagging these genes with the fluorescent probe. To check this, we cloned *CaGPI2* in the prey vector and *CaGPI19* in the bait vector. Despite multiple attempts, these plasmids unfortunately could not be successfully transformed into *Candida albicans*during the course of this study.

We also attempted to study the dynamics of the GPI-GnT complex by tagging different subunits with mRFP. This was done with an intention to get an idea about the approximate size of the GPI-GnT complex in *Candida albicans*, which has not been reported so far. We tagged *CaGPI2* with mRFP and got a diffusion time of 5.62 ms. Similar timescales were obtained when another subunit, *Ca GPI15*, was tagged confirming that tagging any subunit does not alter the dynamics of the complex (Subhash Chandra Sethi, unpublished data). This also needs to be done in the *CaGPI19* conditional null background to see the effect of downregulation of one of the subunits of the complex on its dynamics. This would tell us the size and also give us an idea about the stoichiometry of different subunits in the GPI-GnT complex.

Future Perspectives

This study gives an insight into the effects on CaRas1 signaling upon downregulation of *CaGPI19*, a key subunit of the GPI-GnT complex. It shows that CaRas1 hyperactivation due to CaHsp90 deficiency as well as increased actin polymerization causes slower dynamics of CaRas1 at the plasma membrane in the *Cagpi19* null. We postulate the existence of CaRas1-CaCyr1-CaCap1-G-actin at the plasma membrane of the *Cagpi19* null mutant. Studying and characterizing this complex in *Candida albicans* will provide the exact molecular mechanism between CaRas1 signaling and actin polymerization, which is missing till now. This can be exploited further to study virulence factors and cytoskeletal networks and their interaction

through the CaRas1 signaling pathway. How affecting GPI anchor biosynthesis via disruption of *CaGPI19* affects the cytoskeletal organization in *Candida albicans* has beenshown for the first time. Studying the effect of disruption of other subunits of the GPI-GnT complex on cytoskeletal organization needs to be also explored. As *CaGPI2* and *CaGPI19* negatively regulate each other, studying what happens to actin polymerization and colocalization of CaRas1 with monomeric and polymeric actin in the hypofilamentous *CaGPI2* heterozygous mutant is also a problem worth studying. Could the CaRas1-CaCyr1-CaCap1-G-actin complex exist in other species also? Do they also have a similar levels of interaction? These questions need to be answered. If a similar mechanism operates in humans, then the many types of cancers that are caused due to hyperactive Ras signaling (Fernandez-Medarde and Santos, 2011; Prior *et al*., 2012) could be controlled by selectively targeting the actin cytoskeletal network in malignant cells instead and this could open gates to a new line of treatment that could be used in a combinatorial approach in conjugation with the existing drugs.

With respect to studies of physical associations between membrane proteins, BiFC is a useful tool which is being extensively used in plants and human cell lines. We generated the vectors for this and we have initiated these studies in *Candida albicans*. We hope to study interaction between other proteins of the GPI-GnT complex in *Candida albicans* with the help of this technique so that the inter-subunit interactions within the complex are mapped. Studying dynamics of the entire GPI-GnT complex is also a tiny step in this direction. This would tell us the size of the GPI-GnT complex, something which has not been reported anywhere so far. Dynamics of the complex in various heterozygous and conditional null backgrounds of the GPI-GnT complex can also give us an idea of the number of units of each subunit that are there in a functional GPI-GnT complex.

Appendix

A.1 *Physical interaction between subunits of the* **GPI-GnT** *complex*

As described in detail in the Introduction section, not much is known about the physical interaction between different subunits of the GPI-GnT complex in *Candida albicans*. Some studies have been done, however regarding the interaction between different subunits of this complex in yeast and humans. In *Saccharomyces cerevisiae*, a large scale split ubiquitin assay showed a physical interaction between ScGpi2 and ScGpi19 (Miller *et al*., 2005)which was also validated by another group which also showed a physical association betweenScGpi19-HA and FLAG-ScGpi2(Newman *et al*., 2005).Co-immunoprecipitation studies in human cell linesalso show that human PIG-Y (Eri1) binds to PIG-A (Gpi3), but to no other component of the GPI-GnT complex. This could suggest that the interaction of yeastScEri1 with ScGpi2, which is already reported in *Saccharomyces cerevisiae*(Sobering *et al*., 2003) may also be mediated by ScGpi3. It has also been shown that human hGPI1 (PIG-Q) links PIG-A (Gpi3)/PIG-H (Gpi15) to PIG-C (Gpi2) and stabilizes the association of PIG-H with PIG-C (Hong *et al*., 1999). PIG-P (Gpi19) has also been studied in humans and it has been seen that it is required for the formation and activity of the GPI-GnT complex (Newman et al., 2005). It has been shown to interact with PIG-A and a weak interaction has been reported with hGPI1 also (Watanabe *et al*., 2000). ScEri1 was shown to interact with Ras2 in a GTP dependent manner in *Saccharomyces cerevisiae,* with *Sceri* mutants displaying a hypefilamentous and an invasive growth phenotype (Sobering *et al*., 2003). However, there is a difference in the phenotypes of GPI biosynthetic deletion mutants in *Saccharomyces cerevisiae and Candida albicans.* Downregulation of *ScGPI2* leads to hyperfilamentation in *Saccharomyces cerevisiae*, whereas *Cagpi2* mutants show defective filamentation in *Candida albicans* (Sobering *et al.*, 2004; Yadav *et al*., 2014b). This might be because of differences inthe interaction amongst different subunits of the GPI-GnT complex and with the Ras signaling pathway in the two organisms. This makes it necessary to study the inter subunit

interactions in *Candida albicans*. Till date,no reports of any physical interaction amongst the subunits of the GPI-GnT complex have been published. We have recently reported from our lab that *CaGPI19* and *CaGPI2* negatively regulate each other at the genetic level. Downregulation of *CaGPI19* causes an increase in the transcript levels of *CaGPI2* and vice-versa (Yadav *et al*., 2014b).

Since it is known that ScGpi2 and ScGpi19 associate with each other in yeast, we wanted to explore whether this is the case in *Candida albicans*also. For that we started off with a fluorescence based approach known as Bimolecular Fluorescence Complementation. This recent technique is commonly used to study physical association between proteins in plants and humans (Cao *et al*., 2015; Ohad and Yalovsky, 2010; Wang *et al*., 2015; Wojtera-Kwiczor *et al*., 2013). The basis behind this technique is that a fluorescent protein is split into two halves such that they do not spontaneously interact (Figure A.1.1). These halves are then cloned each with a protein for which the interaction is to be studied. These cloned plasmids, typically called the bait and prey plasmids, are then transformed/transfected into the plant/human cell line. If the bait and the prey proteins interact physically, then the two halves of the fluorescent protein come closer and as a result, associate to give fluorescence. This fluorescence can be easily observed under a confocal microscope. For using the same approach in *Candida albicans*, we took vectors optimized for yeast two hybrid in *Candida albicans*(Stynen *et al*., 2010) and cloned the two halves of the red fluorescent probe, mRFP, in the bait and the prey vectors, respectively. The two halves were chosen according to a report by the Zhang group which showed that mRFP when split at a specific location could not spontaneously reassociate but did so when two interacting proteins brought the two halves of mRFP together (Fan *et al*., 2008). We preferred mRFP for its stable fluorescence which would be easy to monitor *in vivo*.
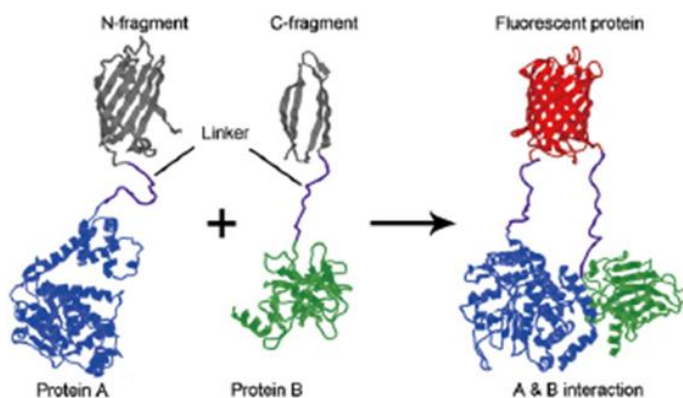
Figure A1.1: Bimolecular Fluorescence Complementation. Cartoon showing the approach towardsBimolecular Fluorescence Complementation (BiFC) technique (Fan *et al.,* 2008).

The two halves of *mRFP*, i.e the N and the C terminal halves were cloned in *Candidaalbicans* expression plasmids by a labmate, Snehlata Singh and then we cloned *CaGPI2* and *CaGPI19* in both the bait and the prey vectors (Figure A1.2). In the prey vector, the gene was cloned such that the fusion protein contained the N-terminal half of mRFP at the C-terminal end of the candidate gene. Similarly, in the bait vector, the fusion protein contained the C-terminal half of mRFP at the N-terminal end of the candidate gene.
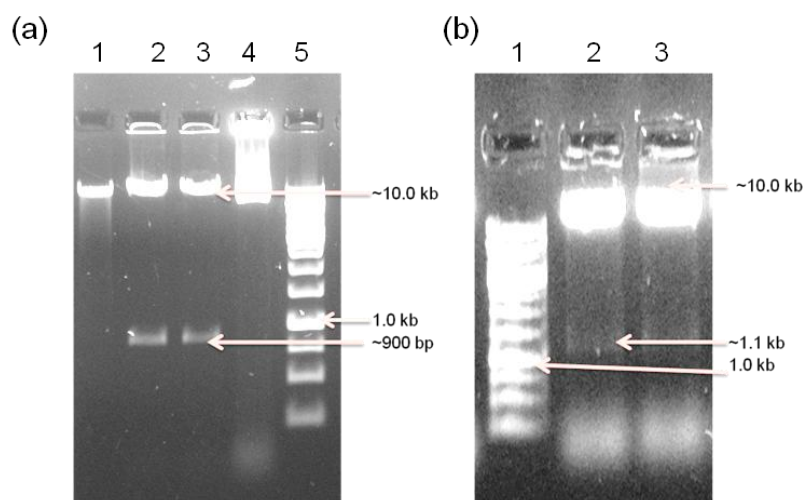

Figure A1.2: Construction of Prey *CaGPI19* and Bait *CaGPI2* (a) Construction of Prey *CaGPI19* Lanes 1 and 4: Uncut plasmid, lane 2 and 3: Positive colonies showing release of *GPI2* (900 bp) with AscI and StuI, lane 5: 1 kbDNA ladder. **(b**) Construction of Bait *CaGPI2.* Lanes 1: 1 kb DNA ladder, lane 2 and 3: Positive colonies showing release of CmRFP-bait *GPI2* (1.1 kb) with NheI and MluI.

The plasmids were linearized by digestion with NotI restriction enzyme and transformed into the wild type SN152 strain of *Candida albicans*as described in(Stynen *et al.,* 2010). The positive colonies were confirmed by PCR amplification from the genomic DNA pf the colonies(Figure A1.3).
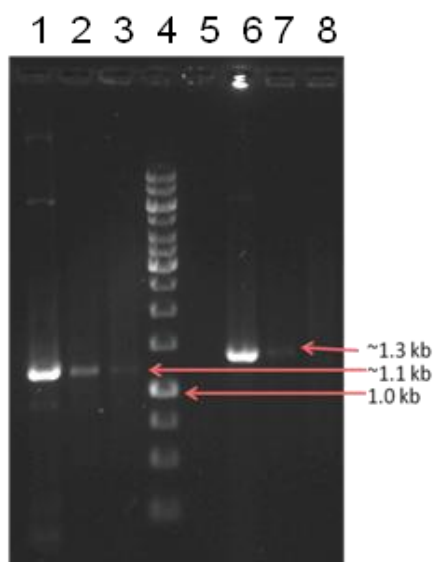

Figure A1.3:Confirmation of positive colonies after co-transformation of Bait *CaGPI2* and Prey *CaGPI19*.Agarose gel electrophoresis showing PCR amplification after genomic DNA extraction of thecolonies obtained after transformation.Lane1-3: PCR amplification of colonies C1, C2 and C3 using CmRFP FP and GPI2 RP showing expected amplicon of 1.1 kb confirming the integration of Bait *CaGPI2* plasmid, lane4: 1 kb DNA ladder, lane 5: negative control (untransformed wil type cells), lane 6-7: PCR amplification of colonies C1, C2 and C3 using GPI19 FP and NmCh RP. Colonies C1 and C2 show the expected amplicon of 1.3 kb confirming the integration of Prey *CaGPI19* plasmid, lane8: negative control.

The positive colonies C1 and C2 in which both the Bait *CaGPI2* and Prey *CaGPI19* were integrated were then checked for fluorescence under a fluorescence microscope (Figure A1.4)
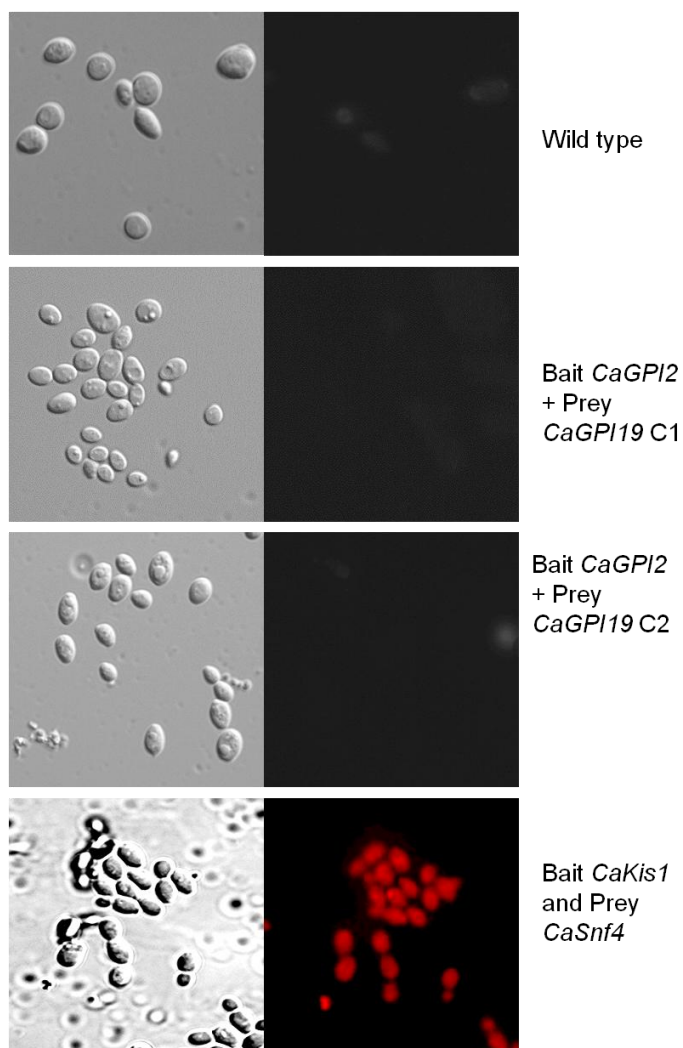
Figure A1.4:Fluorescence expression after co-transformation of Bait *CaGPI2* and Prey *CaGPI19*.The upper panal shows the untransformed *Candida albicans* wild type cells, showing no fluorscence. The middle and the bottom panels show the colonies obtained after transformation of Bait *CaGPI2* and Prey *CaGPI19* plasmids. No fluorescence was seen in these colonies. Fluorescence was seen in the positive control when two interacting proteins Kis1 and Snf4 were transformed into *Candida albicans* (Stynen et al., 2010). The positive control was developed by a labmate, Snehlata Singh.

We could not observe any fluorescence in the positive colonies. One possible explanation could be that the two proteins do not physically interact with each other in *Candida albicans* and do so only at the genetic level. An alternative explanation could also be that the interacting sites are blocked due to the tagging with mRFP.

To check for this latter possibility, we cloned *CaGPI2* in the prey vector and *CaGPI19* in the bait vector (Figure A1.5).
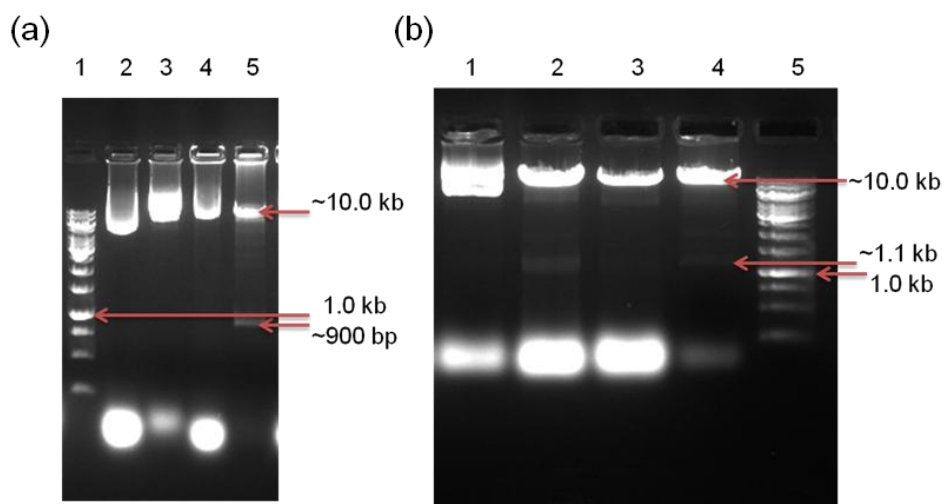
Figure A1.4: Construction of Prey *CaGPI2* and Bait *CaGPI19* (a) Construction of Prey *CaGPI2*. Lane1: 1 kb DNA ladder, lane 2 and 4: Uncut plasmids, lane 3: Negative colony, lane 5: Positive colony showing release of *GPI2* (~900 bp) with AscI and StuI. **(b)**Construction of Bait *CaGPI19*. Lanes 1, 3 and 5: Positive colonies showing release of CmRFP-bait *GPI19* (~1.1 kb) with NheI and MluI, lanes 2 and 4: Uncut plasmid, lane 6:1 kb DNA ladder.

We attempted to use these plasmids to transform the wild type strain of *Candida albicans*but have been unsuccessful in doing so even after repeated attempts.

A2. *Filamentation studies of CaGPI2 overexpression mutants*

Previous and more recent studies from the lab have shown that hyphal morphogenesis and interaction with Ras signalling is primarily dictated by Cagpi2 and involves a physical interaction between CaGpi2 and CaRas1 (Yadav *et al*., 2014b). In *Cagpi19* heterozygous and nullmutant too CaGpi2 levels are significantly upregulated and it has been previously shown that depleting CaGpi2levels can reverse its hyperfilamentous phenotype (Yadav *et al*., 2014b).

Having established in the previous chapters that a decrease in the activity of CaHsp90 causes slowing down of CaRas1 dynamics in the *Cagpi19* null, we wanted to study if the same mechanism also explains the hyperfilamentation of the *CaGPI2* overexpression mutant (Yadav *et al*., 2014b). For this, we treated the WT-*pACT1-CaGPI2* strain with CaHsp90 inhibitor and activator and monitored its filamentation pattern (Figure A2.1).
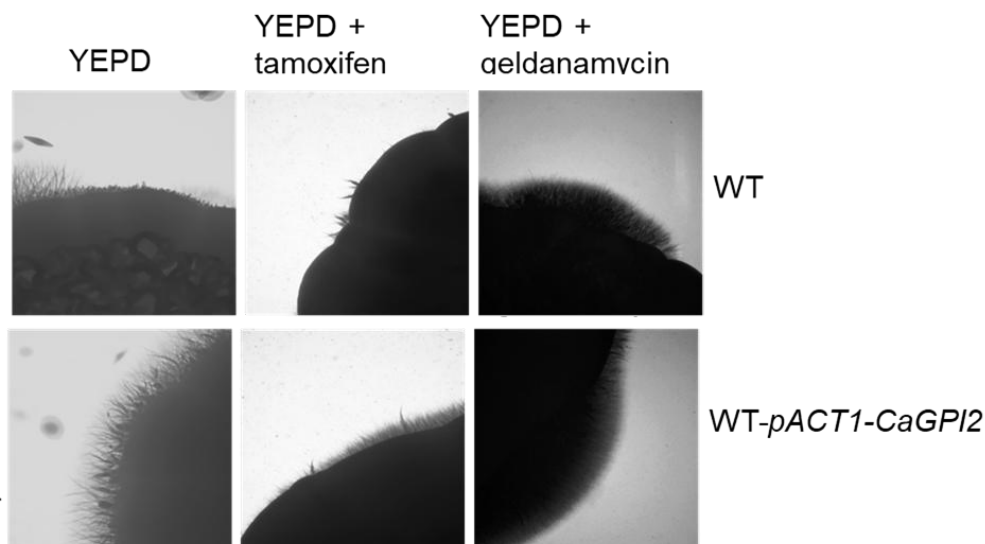
Figure A2.1 Filamentation study of WT-*pACT1-CaGPI2*: Microscopic images showing the filamentation phenotype of WT-*pACT1-CaGPI2* relative to the wild type (WT).The cells were grown in the presence of a CaHsp90 activator, tamoxifen (52µM) and a CaHsp90 inhibitor, geldanamycin (10µM) and kept at 37°C. Images were captured after 10 days. The experiment was done thrice and representative images are shown.

We observed that as in the *Cagpi19* null, the hyperfilamentation of this strain at room temperature was decreased in the presence of tamoxifen, a CaHsp90 activator and increased in the presence of geldanamycin, an Hsp90 inhibitor; indicating that in this case also, inhibition of CaHsp90 activity could be responsible for slower CaRas1 dynamics (Roe *et al.*, 1999; Shapiro *et al.*, 2009; Zhao *et al.*, 2010).

A3. *Study of dynamics of the GPI-GnT complex*

Although there is some information about interaction between different subunits of the GPI-GnT complex in yeast and humans as described above, there is almost no information about the stoichiometry of this complex. How this complex forms inside the cells, how many units of each subunit are required to form a functional GPI-GnT complex, are questions that still remain unanswered.

We were interested in studying this problem. Hence we again decided to use fluorescence correlation spectroscopy to study the GPI-GnT complex. The approach that we used for this

study was to tag each subunit of the GPI-GnT complex with the fluorescent tag, mRFP, starting off with *CaGPI2* and *CaGPI19* and to study their dynamics through FCS. This would give us an idea about the size of the GPI-GnT complex in *Candida albicans*, which is not reported anywhere so far. Also, monitoring the dynamics of this complex in backgrounds where one subunit of the complex is missing, would tell us how the absence of that subunit affects the dynamics of the complex and that can be used to calculate how many units of that particular subunit are involved in a functional GPI-GnT complex.

We tagged *CaGPI2* in the wild type strain BWP17 and the *Cagpi19* conditional null mutant with *mRFP*. For generation of these strains, *mRFP-ARG4* cassette was made in the lab. The *pJET 1.2* blunt vector was taken as the parent vector and *ARG4* marker was cloned in BamH1 and Not1 sites (Figure A3.1).
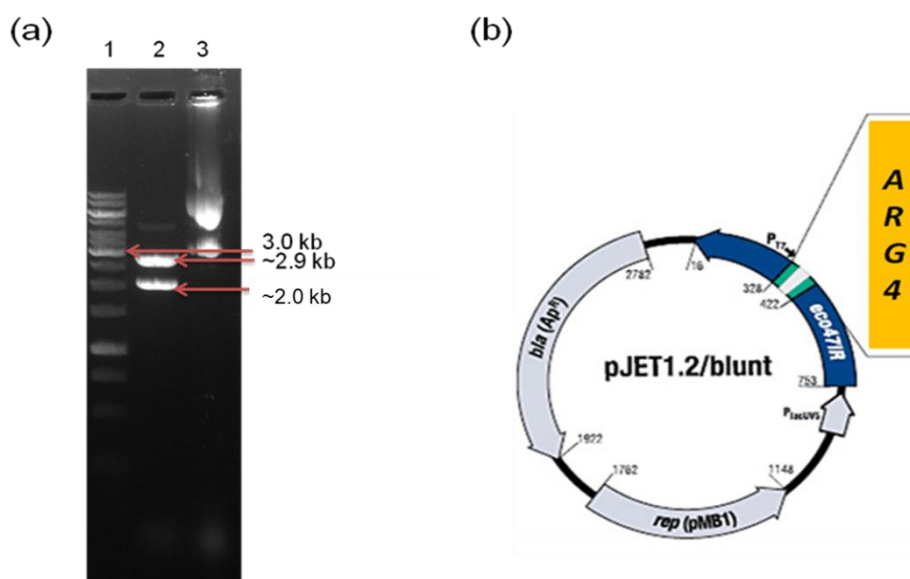

Figure A3.1: Construction of *pJET-ARG4* vector.(a) Restriction digestion showing the cloning of *ARG4*in*pJET 1.2* blunt vector. Lane 1: 1 kb DNA ladder, lane 2: Positive colony showing release of *ARG4* (~2.0 kb) upon digestion with BamH1 and Not1; lane 3: Uncut plasmid. **(b)** Vector map showing the construction of*pJET-ARG4*(modified from Thermo Scientific Inc.).

Then mRFP was cloned upstream of *ARG4* using BamHI and XhoI sites (Figure A3.2). This

gave us the *mRFP-ARG4* cassette that could be used to tag any gene with mRFP at the C
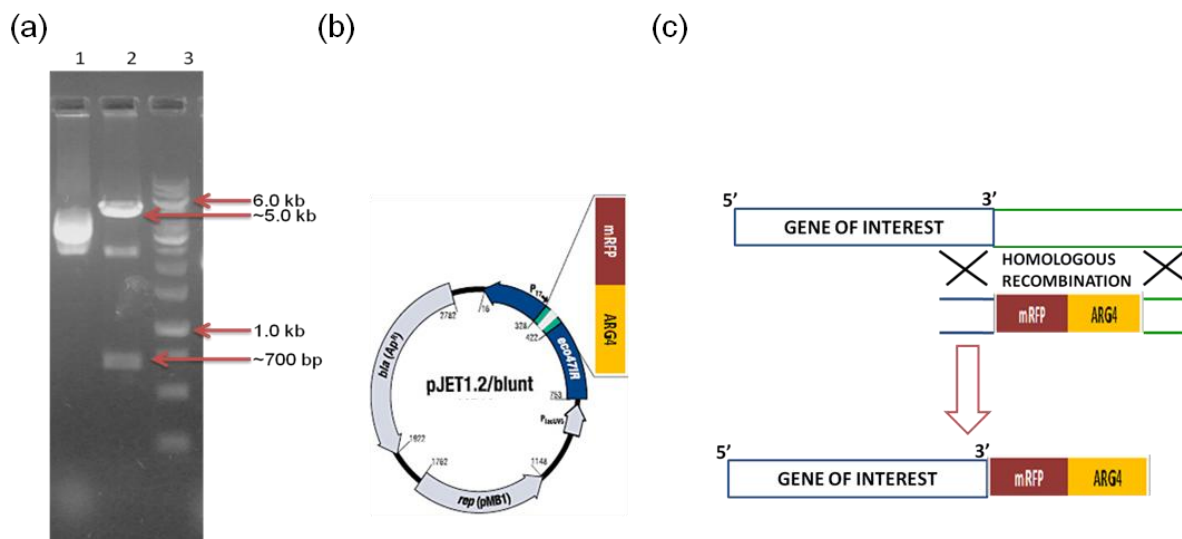
terminus (Figure A3.2).

Figure A3.2: Construction of *mRFP-ARG4* cassette. (a)Agarose gel electrophoresis showing the release of *mRFP* from *mRFP-ARG4*. The cloning was done into *pJET-ARG4* vector. Lane 1: undigested plasmid, lane 2: Restriction sigestion showing release of *mRFP* (~700 bp) upon digestion with BamHI and XhoI. **(b)** Vector map showing the construction of *mRFP-ARG4* cassette. **(c)** Schematic diagram showing the homologous recombination strategy for tagging any gene with *mRFP* at the C terminus using the *mRFP-ARG4* cassette(modified from Thermo Scientific Inc.).

This *mRFP-ARG4* cassette was then amplified with gene specific primers having sequences

homologous to the 3' end of the gene. This PCR product was then purified and transformed

into *Candida albicans* as described in the Materials and Methods section. This transformation

replaced the stop codon of the gene with the *mRFP-ARG4* cassette, thereby adding the

fluorescent tag at the C-terminus of the protein. We tagged *CaGPI2* with *mRFP* using this

approach in the wild type BWP17 (WT) and the *Cagpi19* null backgrounds. A representative

image of the tagging done in the wild type is shown below (Figure A3.3). Similarly,

CaGPI19 was also tagged with *mRFP* in the wild type strain (Figure A3.3).
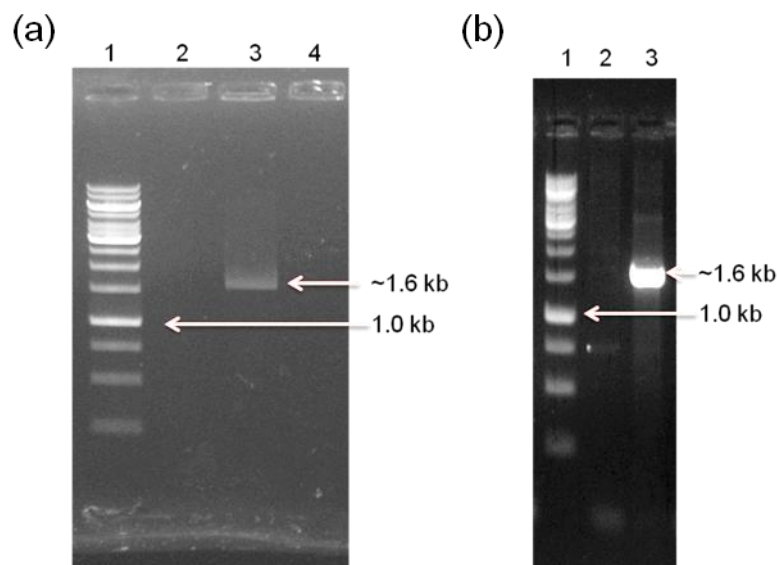
Figure A3.3: Generation of *CaGPI2-mRFP* and *CaGPI19-mRFP* strains. (a) Confirmation of *CaGPI2-mRFP* in the wild type (WT) background. PCR amplification from the genomic DNA of the colonies obtained after transformation using gene specific GPI2FP and RFP RP. Lane 1: 1 kb DNA ladder, lanes 2: negative colony, lane 3: Positive colony showing the expected size of ~1.6 kb, lane 5: Negative control (untransformed wild type cells). **(b)**Confirmation of *CaGPI19-mRFP* in the wild type (WT) background.PCR amplification from the genomic DNA of the colonies obtained after transformation using gene specific *CaGPI19* forward primer and mRFP reverse primer. Lane 1: 1 kb DNA ladder, lane 2: Negative control (untransformed wild type cells), lane 3: Positive colony showing the expected size of ~1.6 kb.

These strains were checked to ensure that tagging with mRFP did not alter their filamentation

phenotype (Figure A3.4)
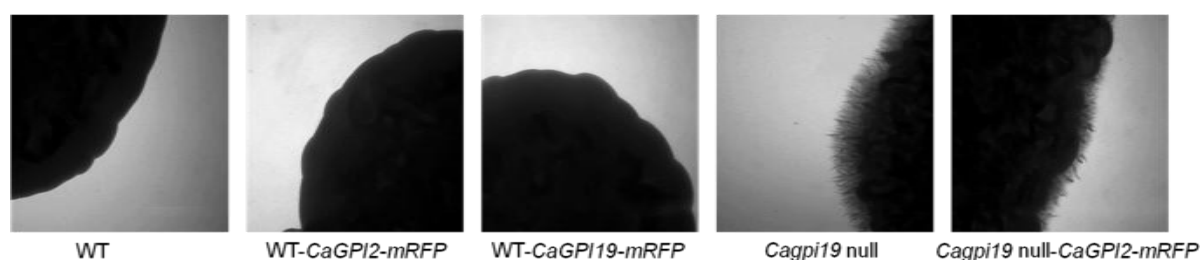
Figure A3.4: Filamentation study of mRFP tagged strains. The filamentation pattern of the strains in which *CaGPI2* and *CaGPI19* was tagged with *mRFP* were studied to ensure that tagging with *mRFP* did not alter their filamentation pattern. The cells were grown in hyphae inducing Spider medium and images were captured after 8 days.

We observed that even after tagging with mRFP, there was no change in the filamentation

pattern of these strains compared to the untagged strains. The *Cagpi19* null-*CaGPI2-*

*mRFP*strain continued to be hyperfilamentous than the WT-*CaGPI2-mRFP* strain. We then proceeded to study the dynamics of the subunits of the GPI-GnT complex in these strains (Figure A3.5). FCS measurements were recorded as described in the Materials and Methods section. The same 2D2C equation was used to fit the correlation curves.
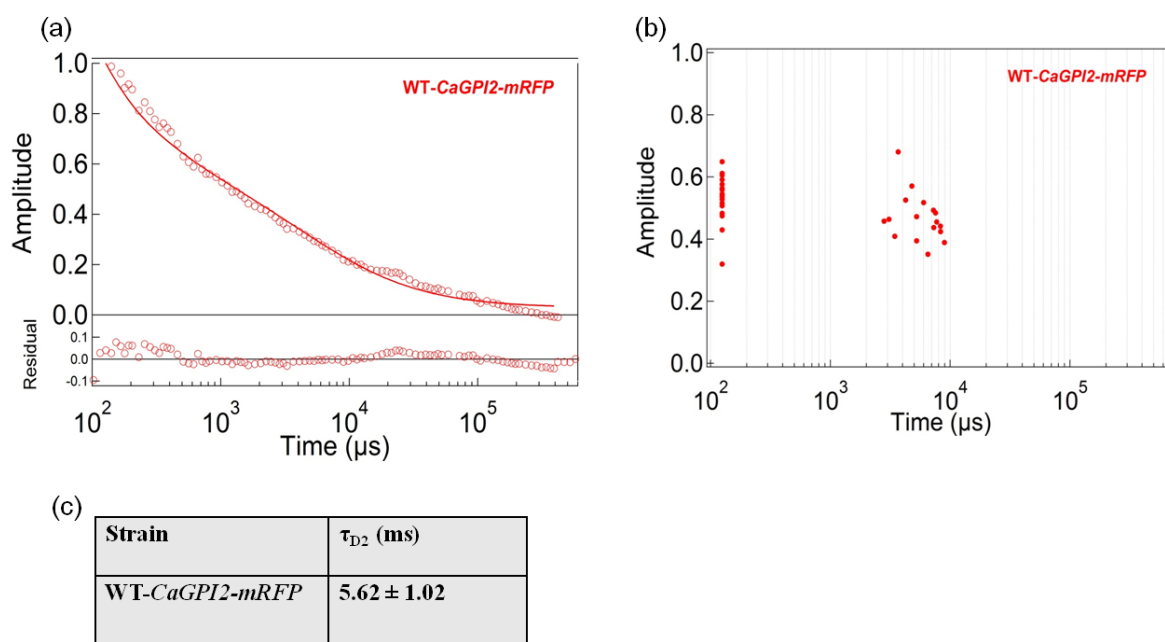

Strain	τ_{D2} (ms)
WT-*CaGPI2-mRFP*	5.62 ± 1.02

Figure A3.5: Dynamics of the GPI-GnT complex. (a) Average fluorescence autocorrelation $G(\tau)$ curves for WT-*CaGPI2-mRFP* strain **(b)** Plot of amplitude versus diffusion times for the same FCS data obtained for individual cells. The data were collected for 20-30 cells. **(c)** Table showing the diffusion times of the indicated strains as obtained after fitting the FCS traces to the 2D2C model. Values are given ± S.D.

We studied the autocorrelation of these proteins in the WT-*CaGPI2-mRFP* strain and obtained a diffusion time of 5.62 ms. We also did similar studies in the ER microsomes prepared from these strains, but were unable to get any correlation. Considering that wecalibrated the FCS setup using Rhodamine-6-G, which gave a single diffusion time of 63 µs, the diffusion coefficient of CaGpi2-mRFPin theWT-*CaGPI2-mRFP* is 0.04×10^{-6} µm^2/sec. FCS studies for the WT-*CaGPI19-mRFP*and the*Cagpi19* null-*CaGPI2-mRFP*strains are currently in progress. These studies will tell us about the similarities or differences in the dynamics obtained when different subunits of the same complex are tagged with mRFP and

one of the subunits of the complex is missing. This would give us an idea about the size of the functional GPI-GnT complex and also about the stoichiometry of the complex, i.e. how many units of each subunits are there in the GPI-GnT complex.

A4. *Construction of fluorescent tagging cassettes for Candida albicans*

We also did some clonings to prepare cassettes that could be used to tag the desired genes with fluorescent markers or place any gene under a regulatable promoter to control its expression.

A4.1 *Construction of pGFP-ARG4 cassette*

We constructed the *pGFP-ARG4* cassette (Figure A4.1) which could be used to tag any protein with GFP at its N-terminus.
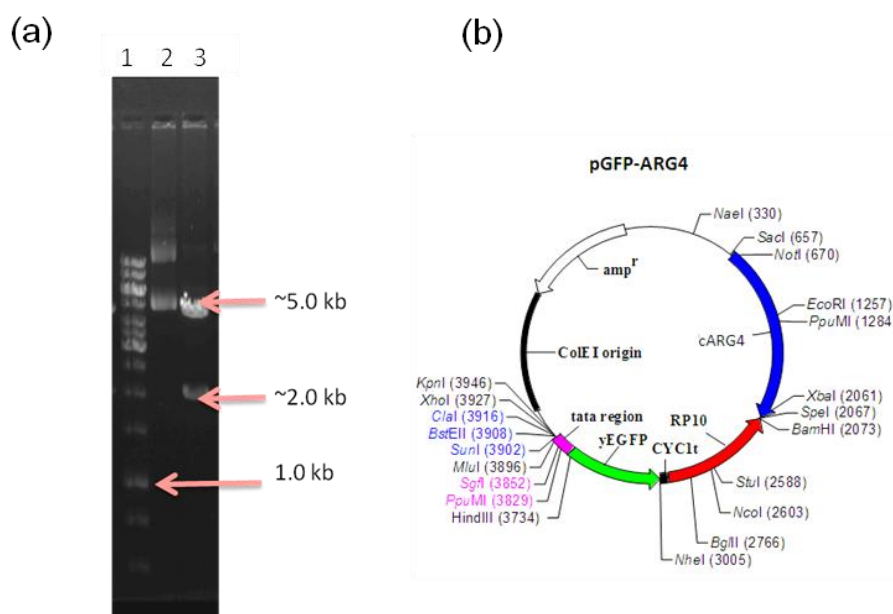

Figure A4.1: Cloning of *pGFP-ARG4*. (a)Restriction digestion showing the release of *ARG4* marker. Lane1: 1 kb DNA ladder. Lane 2: Uncut plasmid. Lane3: Positive colony showing the release of *ARG4*(~2.0 kb) upon digestion with BamHI and NotI. **(b)**Vector map of *pGFP-ARG4*(modified from Thermo Scientific Inc.).

This construct can be amplified with primers homologus to the upstream region of the gene which will place the gene under the basal ADH1 promoter. This construct can be used to study the localization of any protein of interest.

A4.2 *Construction of MET3-GFPvectors*

GFP tagging vectors with *MET3* promoter were made having *HIS1/URA3* markers (Figure A4.2) . *pMET3-GFP-URA3* was cloned after which the *URA3* marker was replaced with the HIS1 marker to get *pMET3-GFP-HIS1*. *pGEX-HIS1* vector already available in the lab was used as a template for *HIS1*.
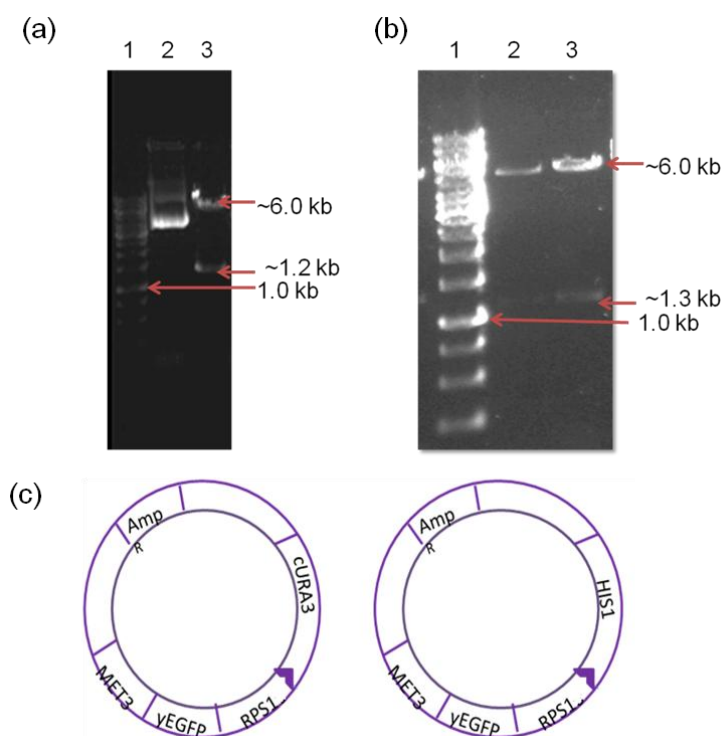
Figure A4.2:Construction of *pMET3-GFP-URA3 and pMET3-GFP-HIS1.vectors*(a)Restriction diggestion showing the release of *MET3*. Lane 1: 1kb DNA ladder. Lane2: Uncut plasmid. Lane3: Release of *MET3*(~1.2 kb) after digestion with KpnI and HindIII. **(b)**Restriction diggestion showing the release of *HIS1*. Lane 1: 1kb DNA ladder. Lane2: Release of *HIS1*(~1.3 kb) after digestion with BamHI and NotI. **(c)** Cartoon showing the schematic representation of *pMET3-GFP-URA3 and pMET3-GFP-HIS1*.

These vectors could be used to tag any gene with GFP at the N-terminus and the expression of the gene could be regulated by addition of methionine and cysteine to the growth medium. They can also be used to clone any gene under the *MET3* promoter and integrated at the *RPS1* locus.We transformed the *pMET3-GFP-URA3* vector into the wild type (WT) anddid fluorescence microscopy to show the expression of GFP in the absence of methionine and cysteine to the growth medium (Figure A4.3).
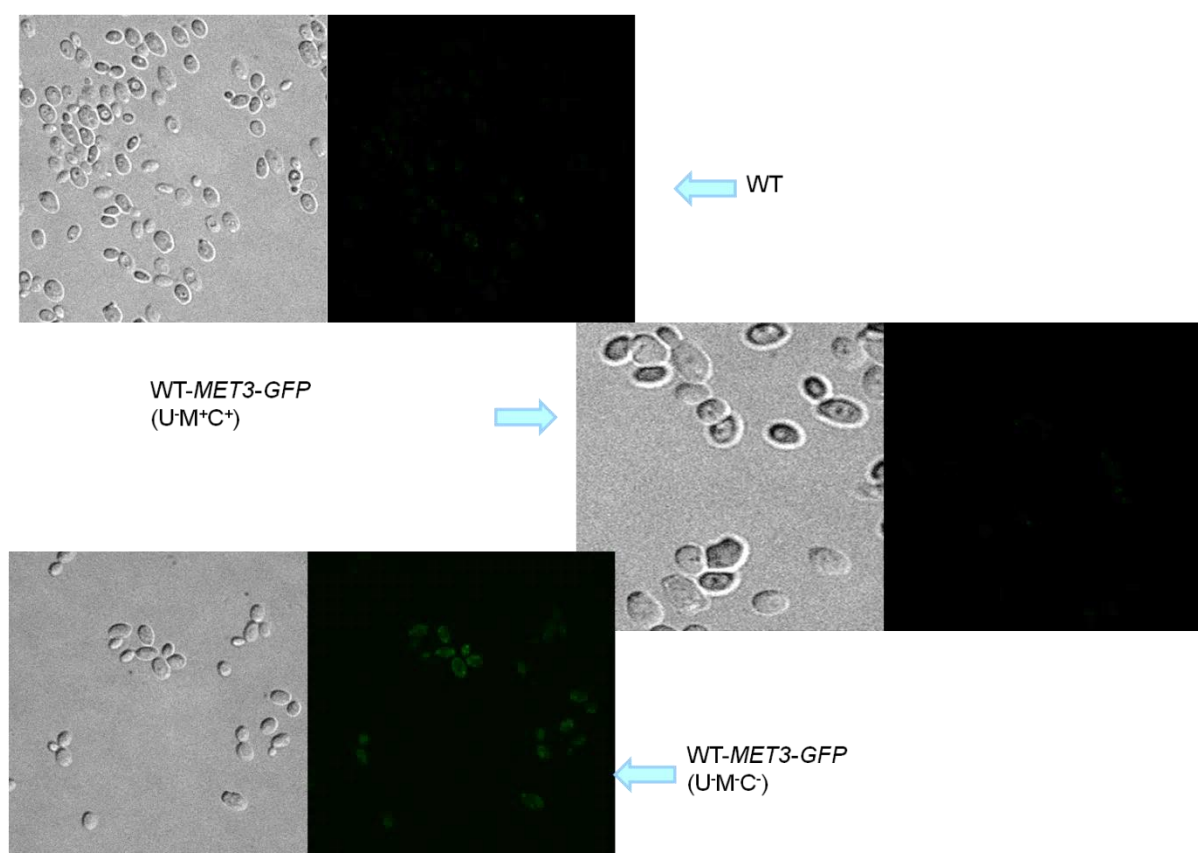
Figure A4.3: Repressible expression of *MET3* promoter. Microscopic images to show the repressible expression of *MET3* promoter. Wild type cells were transformed with*pMET3-GFP-URA3 vector* andGFP is expressed in the absence of methionine and cysteine showing the regulatable expression of *MET3* promoter.

A4.3Construction of pARG4-MET3 vector

We also made another cassette which would place any gene under the *MET3* promoter (Figure A4.4).
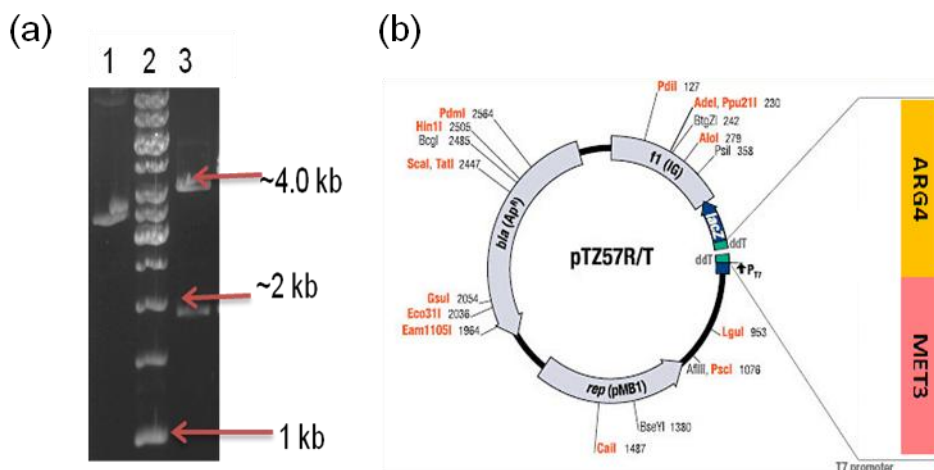
Figure A4.4:Cloning of *pARG4-MET3*. **(a)** Restriction digestion showing the release of *ARG4* marker. Lane 1: Uncut plasmid. Lane2: 1 kb DNA ladder. Lane3: Positive colony showing the release of *ARG4*(~2.0 kb) upon digestion with KpnI and HindIII. **(b)** Vector map of *pARG4-MET3*(modified from Thermo Scientific Inc.).

The expression of the gene can be repressed by addition of methionine and cysteine to the growth medium. This cassette was made with the *ARG4* marker so that the *URA3* marker that is commonly present in *Candida albicans* tagging cassettes could be used for other transformations. *MET3* promoter was initially cloned in the TA vector pTZ57R/T and the *ARG4* marker was cloned between KpnI and HindIII sites.

References

Abankwa, D., Gorfe, A.A., and Hancock, J.F. (2007). Ras nanoclusters: molecular structure and assembly. Semin. Cell Dev. Biol. *18*, 599–607.

Abrahamsson, T. (1979). Axonal transport of adrenaline, noradrenaline and phenylethanolamine-N-methyl transferase (PNMT) in sympathetic neurons of the cod, *Gadus morhua.* Acta Physiol. Scand. *105*, 316–325.

Ahmad, A., and Khan, A.U. (2009). Prevalence of *Candida* species and potential risk factors for vulvovaginal candidiasis in Aligarh, India. Eur. J. Obstet. Gynecol. Reprod. Biol. *144*, 68–71.

Alvarez, F.J., Douglas, L.M., and Konopka, J.B. (2007). Sterol-Rich Plasma Membrane Domains in Fungi. Eukaryot. Cell *6*, 755–763.

Amberg, D.C., Burke, D.J., and Strathern, J.N. (2006). Isolation of Yeast Genomic DNA for Southern Blot Analysis. Cold Spring Harb. Protoc. *2006*, pdb.prot4149.

Apolloni, A., Prior, I.A., Lindsay, M., Parton, R.G., and Hancock, J.F. (2000). H-ras but not K-ras traffics to the plasma membrane through the exocytic pathway. Mol. Cell. Biol. *20*, 2475–2487.

Arthington-Skaggs, B.A., Warnock, D.W., and Morrison, C.J. (2000). Quantitation of *Candida albicans* Ergosterol Content Improves the Correlation between In Vitro Antifungal Susceptibility Test Results and In Vivo Outcome after Fluconazole Treatment in a Murine Model of Invasive Candidiasis. Antimicrob. Agents Chemother. *44*, 2081–2085.

Ashida, H., Hong, Y., Murakami, Y., Shishioh, N., Sugimoto, N., Kim, Y.U., Maeda, Y., and Kinoshita, T. (2005). Mammalian PIG-X and yeast Pbn1p are the essential components of glycosylphosphatidylinositol-mannosyltransferase I. Mol. Biol. Cell *16*, 1439–1448.

Ashok, A., and Hegde, R.S. (2008). Retrotranslocation of prion proteins from the endoplasmic reticulum by preventing GPI signal transamidation. Mol. Biol. Cell *19*, 3463–3476.

Ashraf, M., Yadav, B., Perinthottathil, S., Kumar, K.S., Vats, D., Muthuswami, R., and Komath, S.S. (2011). N-acetyl-D-glucosaminylphosphatidylinositol de-N-acetylase from

Entamoeba histolytica: metal alters catalytic rates but not substrate affinity. J. Biol. Chem. *286*, 2543–2549.

Ashraf, M., Sreejith, P., Yadav, U., and Komath, S.S. (2013). Catalysis by N-acetyl-D-glucosaminylphosphatidylinositol de-N-acetylase (PIG-L) from *Entamoeba histolytica*: new roles for conserved residues. J. Biol. Chem. *288*, 7590–7595.

Braun, P.C., and Calderone, R.A. (1978). Chitin synthesis in *Candida albicans*: comparison of yeast and hyphal forms. J. Bacteriol. *133*, 1472–1477.

Cao, X., Jin, X., Zhang, X., Li, Y., Wang, C., Wang, X., Hong, J., Wang, X., Li, D., and Zhang, Y. (2015). Morphogenesis of Endoplasmic Reticulum Membrane-Invaginated Vesicles during Beet Black Scorch Virus Infection: Role of Auxiliary Replication Protein and New Implications of Three-Dimensional Architecture. J. Virol. *89*, 6184–6195.

Cardoso de Almeida, M.L., and Turner, M.J. (1983). The membrane form of variant surface glycoproteins of *Trypanosoma brucei*. Nature *302*, 349–352.

Chaffin, W.L. (2008). *Candida albicans* Cell Wall Proteins. Microbiol. Mol. Biol. Rev. *72*, 495–544.

Chander, J., Singla, N., Sidhu, S.K., and Gombar, S. (2013). Epidemiology of *Candida* blood stream infections: experience of a tertiary care centre in North India. J. Infect. Dev. Ctries. *7*.

Cheng, S., Nguyen, M.H., Zhang, Z., Jia, H., Handfield, M., and Clancy, C.J. (2003). Evaluation of the Roles of Four *Candida albicans* Genes in Virulence by Using Gene Disruption Strains That Express URA3 from the Native Locus. Infect. Immun. *71*, 6101–6103.

Chow, D., Guo, L., Gai, F., and Goulian, M. (2012). Fluorescence Correlation Spectroscopy Measurements of the Membrane Protein TetA in Escherichia coli Suggest Rapid Diffusion at Short Length Scales. PLoS ONE *7*, e48600.

Christian, A.E., Haynes, M.P., Phillips, M.C., and Rothblat, G.H. (1997). Use of cyclodextrins for manipulating cellular cholesterol content. J. Lipid Res. *38*, 2264–2272.

De Backer, M.D., Maes, D., Vandoninck, S., Logghe, M., Contreras, R., and Luyten, W.H. (1999). Transformation of *Candida albicans* by electroporation. Yeast Chichester Engl. *15*, 1609–1618.

Eisenhaber, B., Maurer-Stroh, S., Novatchkova, M., Schneider, G., and Eisenhaber, F. (2003). Enzymes and auxiliary factors for GPI lipid anchor biosynthesis and post-translational transfer to proteins. BioEssays News Rev. Mol. Cell. Dev. Biol. *25*, 367–385.

Elson, E.L., and Magde, D. (1974). Fluorescence correlation spectroscopy. I. Conceptual basis and theory. Biopolymers *13*, 1–27.

Epp, E., Nazarova, E., Regan, H., Douglas, L.M., Konopka, J.B., Vogel, J., and Whiteway, M. (2013). Clathrin- and Arp2/3-Independent Endocytosis in the Fungal Pathogen *Candida albicans*. MBio *4*, e00476-13-e00476-13.

Fan, J.-Y., Cui, Z.-Q., Wei, H.-P., Zhang, Z.-P., Zhou, Y.-F., Wang, Y.-P., and Zhang, X.-E. (2008). Split mCherry as a new red bimolecular fluorescence complementation system for visualizing protein–protein interactions in living cells. Biochem. Biophys. Res. Commun. *367*, 47–53.

Fedor-Chaiken, M., Deschenes, R.J., and Broach, J.R. (1990). SRV2, a gene required for RAS activation of adenylate cyclase in yeast. Cell *61*, 329–340.

Fernandez-Medarde, A., and Santos, E. (2011). Ras in Cancer and Developmental Diseases. Genes Cancer *2*, 344–358.

Ferrando-Miguel, R., Cheon, M.S., Yang, J.W., and Lubec, G. (2003). Overexpression of transcription factor BACH1 in fetal Down syndrome brain. J. Neural Transm. Suppl. 193–205.

Fraering, P., Imhof, I., Meyer, U., Strub, J.M., van Dorsselaer, A., Vionnet, C., and Conzelmann, A. (2001). The GPI transamidase complex of *Saccharomyces cerevisiae* contains Gaa1p, Gpi8p, and Gpi16p. Mol. Biol. Cell *12*, 3295–3306.

Gabriel, M., Horký, D., Svoboda, A., and Kopecká, M. (1998). Cytochalasin D interferes with contractile actin ring and septum formation in *Schizosaccharomyces japonicus* var. versatilis. Microbiol. Read. Engl. *144 (Pt 8)*, 2331–2344.

Garai, K., Sahoo, B., Kaushalya, S.K., Desai, R., and Maiti, S. (2007). Zinc Lowers Amyloid-β Toxicity by Selectively Precipitating Aggregation Intermediates †. Biochemistry (Mosc.) *46*, 10655–10663.

Gerami-Nejad, M., Hausauer, D., McClellan, M., Berman, J., and Gale, C. (2004). Cassettes for the PCR-mediated construction of regulatable alleles in *Candida albicans*. Yeast Chichester Engl. *21*, 429–436.

Gerami-Nejad, M., Dulmage, K., and Berman, J. (2009). Additional cassettes for epitope and fluorescent fusion proteins in *Candida albicans*. Yeast *26*, 399–406.

Gourlay, C.W., and Ayscough, K.R. (2006). Actin-Induced Hyperactivation of the Ras Signaling Pathway Leads to Apoptosis in *Saccharomyces cerevisiae*. Mol. Cell. Biol. *26*, 6487–6501.

Gow, N.A., and Hube, B. (2012). Importance of the *Candida albicans* cell wall during commensalism and infection. Curr. Opin. Microbiol. *15*, 406–412.

Grab, D.J., Webster, P., Ito, S., Fish, W.R., Verjee, Y., and Lonsdale-Eccles, J.D. (1987). Subcellular localization of a variable surface glycoprotein phosphatidylinositol-specific phospholipase-C in African trypanosomes. J. Cell Biol. *105*, 737–746.

Grahl, N., Demers, E.G., Lindsay, A.K., Harty, C.E., Willger, S.D., Piispanen, A.E., and Hogan, D.A. (2015). Mitochondrial Activity and Cyr1 Are Key Regulators of Ras1 Activation of *C. albicans* Virulence Pathways. PLOS Pathog. *11*, e1005133.

Grimme, S.J. (2004). Deficiencies in the Endoplasmic Reticulum (ER)-Membrane Protein Gab1p Perturb Transfer of Glycosylphosphatidylinositol to Proteins and Cause Perinuclear ER-associated Actin Bar Formation. Mol. Biol. Cell *15*, 2758–2770.

Grimme, S.J., Westfall, B.A., Wiedman, J.M., Taron, C.H., and Orlean, P. (2001). The Essential Smp3 Protein Is Required for Addition of the Side-branching Fourth Mannose during Assembly of Yeast Glycosylphosphatidylinositols. J. Biol. Chem. *276*, 27731–27739.

Hall, B.E., Bar-Sagi, D., and Nassar, N. (2002). The structural basis for the transition from Ras-GTP to Ras-GDP. Proc. Natl. Acad. Sci. *99*, 12138–12142.

Hancock, J.F. (2003). Ras proteins: different signals from different locations. Nat. Rev. Mol. Cell Biol. *4*, 373–384.

Hendrix, J., Flors, C., Dedecker, P., Hofkens, J., and Engelborghs, Y. (2008). Dark states in monomeric red fluorescent proteins studied by fluorescence correlation and single molecule spectroscopy. Biophys. J. *94*, 4103–4113.

van der Hoeven, D., Cho, K. -j., Ma, X., Chigurupati, S., Parton, R.G., and Hancock, J.F. (2013). Fendiline Inhibits K-Ras Plasma Membrane Localization and Blocks K-Ras Signal Transmission. Mol. Cell. Biol. *33*, 237–251.

Holzinger, A. (2009). Jasplakinolide: an actin-specific reagent that promotes actin polymerization. Methods Mol. Biol. Clifton NJ *586*, 71–87.

Hong, Y., Ohishi, K., Watanabe, R., Endo, Y., Maeda, Y., and Kinoshita, T. (1999). GPI1 Stabilizes an Enzyme Essential in the First Step of Glycosylphosphatidylinositol Biosynthesis. J. Biol. Chem. *274*, 18582–18588.

Howard, M.F., Murakami, Y., Pagnamenta, A.T., Daumer-Haas, C., Fischer, B., Hecht, J., Keays, D.A., Knight, S.J.L., Kölsch, U., Krüger, U., et al. (2014). Mutations in PGAP3 impair GPI-anchor maturation, causing a subtype of hyperphosphatasia with mental retardation. Am. J. Hum. Genet. *94*, 278–287.

Huyer, G., Liu, S., Kelly, J., Moffat, J., Payette, P., Kennedy, B., Tsaprailis, G., Gresser, M.J., and Ramachandran, C. (1997). Mechanism of inhibition of protein-tyrosine phosphatases by vanadate and pervanadate. J. Biol. Chem. *272*, 843–851.

Inglis, D.O., and Sherlock, G. (2013). Ras signaling gets fine-tuned: regulation of multiple pathogenic traits of *Candida albicans*. Eukaryot. Cell *12*, 1316–1325.

Inoue, N., Watanabe, R., Takeda, J., and Kinoshita, T. (1996). PIG-C, one of the three human genes involved in the first step of glycosylphosphatidylinositol biosynthesis is a homologue of *Saccharomyces cerevisiae* GPI2. Biochem. Biophys. Res. Commun. *226*, 193–199.

Jones, L.A., and Sudbery, P.E. (2010). Spitzenkorper, Exocyst, and Polarisome Components in *Candida albicans* Hyphae Show Different Patterns of Localization and Have Distinct Dynamic Properties. Eukaryot. Cell *9*, 1455–1465.

Kaksonen, M., Toret, C.P., and Drubin, D.G. (2005). A Modular Design for the Clathrin- and Actin-Mediated Endocytosis Machinery. Cell *123*, 305–320.

Kamitani, T., Chang, H.M., Rollins, C., Waneck, G.L., and Yeh, E.T. (1993). Correction of the class H defect in glycosylphosphatidylinositol anchor biosynthesis in Ltk- cells by a human cDNA clone. J. Biol. Chem. *268*, 20733–20736.

Keppler-Ross, S., Noffz, C., and Dean, N. (2008). A new purple fluorescent color marker for genetic studies in *Saccharomyces cerevisiae* and *Candida albican*s. Genetics *179*, 705–710.

Kostova, Z., Rancour, D.M., Menon, A.K., and Orlean, P. (2000). Photoaffinity labelling with P3-(4-azidoanilido)uridine 5'-triphosphate identifies gpi3p as the UDP-GlcNAc-binding subunit of the enzyme that catalyses formation of GlcNAc-phosphatidylinositol, the first glycolipid intermediate in glycosylphosphatidylinositol synthesis. Biochem. J. *350 Pt 3*, 815–822.

Krawitz, P.M., Murakami, Y., Hecht, J., Krüger, U., Holder, S.E., Mortier, G.R., Delle Chiaie, B., De Baere, E., Thompson, M.D., Roscioli, T., et al. (2012). Mutations in PIGO, a member of the GPI-anchor-synthesis pathway, cause hyperphosphatasia with mental retardation. Am. J. Hum. Genet. *91*, 146–151.

Lakowicz, J.R. (1999). Principles of fluorescence spectroscopy (New York: Kluwer Academic/Plenum).

Leach, M.D., Klipp, E., Cowen, L.E., and Brown, A.J.P. (2012). Fungal Hsp90: a biological transistor that tunes cellular outputs to thermal inputs. Nat. Rev. Microbiol. *10*, 693–704.

Leidich, S.D., and Orlean, P. (1996). Gpi1, a Saccharomyces cerevisiae protein that participates in the first step in glycosylphosphatidylinositol anchor synthesis. J. Biol. Chem. *271*, 27829–27837.

Leidich, S.D., Drapp, D.A., and Orlean, P. (1994). A conditionally lethal yeast mutant blocked at the first step in glycosyl phosphatidylinositol anchor synthesis. J. Biol. Chem. *269*, 10193–10196.

Leidich, S.D., Kostova, Z., Latek, R.R., Costello, L.C., Drapp, D.A., Gray, W., Fassler, J.S., and Orlean, P. (1995). Temperature-sensitive yeast GPI anchoring mutants gpi2 and gpi3 are

defective in the synthesis of N-acetylglucosaminyl phosphatidylinositol. Cloning of the GPI2 gene. J. Biol. Chem. *270*, 13029–13035.

Lenardon, M.D., Munro, C.A., and Gow, N.A. (2010). Chitin synthesis and fungal pathogenesis. Curr. Opin. Microbiol. *13*, 416–423.

Lin, W.-C., Iversen, L., Tu, H.-L., Rhodes, C., Christensen, S.M., Iwig, J.S., Hansen, S.D., Huang, W.Y.C., and Groves, J.T. (2014). H-Ras forms dimers on membrane surfaces via a protein-protein interface. Proc. Natl. Acad. Sci. *111*, 2996–3001.

Maeda, Y., Tashima, Y., Houjou, T., Fujita, M., Yoko-o, T., Jigami, Y., Taguchi, R., and Kinoshita, T. (2007). Fatty Acid Remodeling of GPI-anchored Proteins Is Required for Their Raft Association. Mol. Biol. Cell *18*, 1497–1506.

Magde, D., Elson, E.L., and Webb, W.W. (1974). Fluorescence correlation spectroscopy. II. An experimental realization. Biopolymers *13*, 29–61.

Maiti, S., Haupts, U., and Webb, W.W. (1997). Fluorescence correlation spectroscopy: diagnostics for sparse molecules. Proc. Natl. Acad. Sci. U. S. A. *94*, 11753–11757.

Mann, P.A., McLellan, C.A., Koseoglu, S., Si, Q., Kuzmin, E., Flattery, A., Harris, G., Sher, X., Murgolo, N., Wang, H., et al. (2015). Chemical Genomics-Based Antifungal Drug Discovery: Targeting Glycosylphosphatidylinositol (GPI) Precursor Biosynthesis. ACS Infect. Dis. *1*, 59–72.

Martins, N., Ferreira, I.C.F.R., Barros, L., Silva, S., and Henriques, M. (2014). Candidiasis: Predisposing Factors, Prevention, Diagnosis and Alternative Treatment. Mycopathologia *177*, 223–240.

Masterson, W.J., Doering, T.L., Hart, G.W., and Englund, P.T. (1989). A novel pathway for glycan assembly: biosynthesis of the glycosyl-phosphatidylinositol anchor of the trypanosome variant surface glycoprotein. Cell *56*, 793–800.

McCarthy, A.A., Peterson, N.A., Knijff, R., and Baker, E.N. (2004). Crystal structure of MshB from *Mycobacterium tuberculosis*, a deacetylase involved in mycothiol biosynthesis. J. Mol. Biol. *335*, 1131–1141.

Mendes Giannini, M.J.S., Bernardi, T., Scorzoni, L., Fusco-Almeida, A.M., and Sardi, J.C.O. (2013). *Candida* species: current epidemiology, pathogenicity, biofilm formation, natural antifungal products and new therapeutic options. J. Med. Microbiol. *62*, 10–24.

Miller, J.P., Lo, R.S., Ben-Hur, A., Desmarais, C., Stagljar, I., Noble, W.S., and Fields, S. (2005). Large-scale identification of yeast integral membrane protein interactions. Proc. Natl. Acad. Sci. *102*, 12123–12128.

Murakami, Y. (2005). The Initial Enzyme for Glycosylphosphatidylinositol Biosynthesis Requires PIG-Y, a Seventh Component. Mol. Biol. Cell *16*, 5236–5246.

Nakamura, K., Osaka, H., Murakami, Y., Anzai, R., Nishiyama, K., Kodera, H., Nakashima, M., Tsurusaki, Y., Miyake, N., Kinoshita, T., et al. (2014). PIGO mutations in intractable epilepsy and severe developmental delay with mild elevation of alkaline phosphatase levels. Epilepsia *55*, e13-17.

Nakamura, N., Inoue, N., Watanabe, R., Takahashi, M., Takeda, J., Stevens, V.L., and Kinoshita, T. (1997). Expression cloning of PIG-L, a candidate N-acetylglucosaminyl-phosphatidylinositol deacetylase. J. Biol. Chem. *272*, 15834–15840.

Newman, H.A., Romeo, M.J., Lewis, S.E., Yan, B.C., Orlean, P., and Levin, D.E. (2005). Gpi19, the *Saccharomyces cerevisiae* homologue of mammalian PIG-P, is a subunit of the

initial enzyme for glycosylphosphatidylinositol anchor biosynthesis. Eukaryot. Cell *4*, 1801–1807.

Oberholzer, U., Marcil, A., Leberer, E., Thomas, D.Y., and Whiteway, M. (2002). Myosin I Is Required for Hypha Formation in Candidaalbicans. Eukaryot. Cell *1*, 213–228.

Ohad, N., and Yalovsky, S. (2010). Utilizing bimolecular fluorescence complementation (BiFC) to assay protein-protein interaction in plants. Methods Mol. Biol. Clifton NJ *655*, 347–358.

Ohishi, K., Inoue, N., Maeda, Y., Takeda, J., Riezman, H., and Kinoshita, T. (2000). Gaa1p and Gpi8p Are Components of a Glycosylphosphatidylinositol (GPI) Transamidase That Mediates Attachment of GPI to Proteins. Mol. Biol. Cell *11*, 1523–1533.

Orlean, P., and Menon, A.K. (2007). Thematic review series: Lipid Posttranslational Modifications. GPI anchoring of protein in yeast and mammalian cells, or: how we learned to stop worrying and love glycophospholipids. J. Lipid Res. *48*, 993–1011.

Piispanen, A.E., Bonnefoi, O., Carden, S., Deveau, A., Bassilana, M., and Hogan, D.A. (2011). Roles of Ras1 membrane localization during *Candida albicans* hyphal growth and farnesol response. Eukaryot. Cell *10*, 1473–1484.

Piispanen, A.E., Grahl, N., Hollomon, J.M., and Hogan, D.A. (2013). Regulated proteolysis of *Candida albicans* Ras1 is involved in morphogenesis and quorum sensing regulation. Mol. Microbiol. *89*, 166–178.

Pittet, M., and Conzelmann, A. (2007). Biosynthesis and function of GPI proteins in the yeast *Saccharomyces cerevisiae*. Biochim. Biophys. Acta *1771*, 405–420.

Plaine, A., Walker, L., Da Costa, G., Mora-Montes, H.M., McKinnon, A., Gow, N.A.R., Gaillardin, C., Munro, C.A., and Richard, M.L. (2008). Functional analysis of *Candida albicans* GPI-anchored proteins: Roles in cell wall integrity and caspofungin sensitivity. Fungal Genet. Biol. *45*, 1404–1414.

Prior, I.A., and Hancock, J.F. (2012). Ras trafficking, localization and compartmentalized signalling. Semin. Cell Dev. Biol. *23*, 145–153.

Prior, I.A., Lewis, P.D., and Mattos, C. (2012). A Comprehensive Survey of Ras Mutations in Cancer. Cancer Res. *72*, 2457–2467.

Prusiner, S.B. (1998). Prions. Proc. Natl. Acad. Sci. U. S. A. *95*, 13363–13383.

Rajalingam, K., Schreck, R., Rapp, U.R., and Albert, Š. (2007). Ras oncogenes and their downstream targets. Biochim. Biophys. Acta BBA - Mol. Cell Res. *1773*, 1177–1195.

Rigler, R., Mets, U., Widengren, J., and Kask, P. (1993). Fluorescence correlation spectroscopy with high count rate and low background: analysis of translational diffusion. Eur. Biophys. J. *22*.

Roe, S.M., Prodromou, C., O'Brien, R., Ladbury, J.E., Piper, P.W., and Pearl, L.H. (1999). Structural basis for inhibition of the Hsp90 molecular chaperone by the antitumor antibiotics radicicol and geldanamycin. J. Med. Chem. *42*, 260–266.

Roy, S., Luetterforst, R., Harding, A., Apolloni, A., Etheridge, M., Stang, E., Rolls, B., Hancock, J.F., and Parton, R.G. (1999). Dominant-negative caveolin inhibits H-Ras function by disrupting cholesterol-rich plasma membrane domains. Nat. Cell Biol. *1*, 98–105.

Sambrook, J., and Russell, D.W. (2006). The Hanahan Method for Preparation and Transformation of Competent *E. coli:* High-efficiency Transformation. Cold Spring Harb. Protoc. *2006*, pdb.prot3942.

Schenk, A., Ivanchenko, S., Röcker, C., Wiedenmann, J., and Nienhaus, G.U. (2004). Photodynamics of Red Fluorescent Proteins Studied by Fluorescence Correlation Spectroscopy. Biophys. J. *86*, 384–394.

Sengupta, P., Balaji, J., and Maiti, S. (2002). Measuring diffusion in cell membranes by fluorescence correlation spectroscopy. Methods San Diego Calif *27*, 374–387.

Sengupta, P., Garai, K., Sahoo, B., Shi, Y., Callaway, D.J.E., and Maiti, S. (2003). The Amyloid β Peptide (Aβ $_{1-40}$) Is Thermodynamically Soluble at Physiological Concentrations [†]. Biochemistry (Mosc.) *42*, 10506–10513.

Senn, H., Shapiro, R.S., and Cowen, L.E. (2012). Cdc28 provides a molecular link between Hsp90, morphogenesis, and cell cycle progression in Candida albicans. Mol. Biol. Cell *23*, 268–283.

Shapiro, R.S., Uppuluri, P., Zaas, A.K., Collins, C., Senn, H., Perfect, J.R., Heitman, J., and Cowen, L.E. (2009). Hsp90 orchestrates temperature-dependent *Candida albicans* morphogenesis via Ras1-PKA signaling. Curr. Biol. CB *19*, 621–629.

Shapiro, R.S., Zaas, A.K., Betancourt-Quiroz, M., Perfect, J.R., and Cowen, L.E. (2012). The Hsp90 co-chaperone Sgt1 governs *Candida albicans* morphogenesis and drug resistance. PloS One *7*, e44734.

Shields, J.M., Pruitt, K., McFall, A., Shaub, A., and Der, C.J. (2000). Understanding Ras: 'it ain't over 'til it's over'. Trends Cell Biol. *10*, 147–154.

Shima, F., Okada, T., Kido, M., Sen, H., Tanaka, Y., Tamada, M., Hu, C.D., Yamawaki-Kataoka, Y., Kariya, K., and Kataoka, T. (2000). Association of yeast adenylyl cyclase with

cyclase-associated protein CAP forms a second Ras-binding site which mediates its Ras-dependent activation. Mol. Cell. Biol. *20*, 26–33.

Shukla, S., Saini, P., Smriti, Jha, S., Ambudkar, S.V., and Prasad, R. (2003). Functional Characterization of *Candida albicans* ABC Transporter Cdr1p. Eukaryot. Cell *2*, 1361–1375.

Singh, S.L., Rai, R.C., Sah, S.K., and Komath, S.S. (2016). The catalytic subunit of the first mannosyltransferase in the GPI biosynthetic pathway affects growth, cell wall integrity and hyphal morphogenesis in *Candida albicans*. Yeast Chichester Engl. *33*, 365–383.

Sobering, A.K., Romeo, M.J., Vay, H.A., and Levin, D.E. (2003). A Novel Ras Inhibitor, Eri1, Engages Yeast Ras at the Endoplasmic Reticulum. Mol. Cell. Biol. *23*, 4983–4990.

Sobering, A.K., Watanabe, R., Romeo, M.J., Yan, B.C., Specht, C.A., Orlean, P., Riezman, H., and Levin, D.E. (2004). Yeast Ras regulates the complex that catalyzes the first step in GPI-anchor biosynthesis at the ER. Cell *117*, 637–648.

Spangler, B., Morgan, C.W., Fontaine, S.D., Vander Wal, M.N., Chang, C.J., Wells, J.A., and Renslo, A.R. (2016). A reactivity-based probe of the intracellular labile ferrous iron pool. Nat. Chem. Biol. *12*, 680–685.

Stynen, B., Van Dijck, P., and Tournu, H. (2010). A CUG codon adapted two-hybrid system for the pathogenic fungus *Candida albicans*. Nucleic Acids Res. *38*, e184–e184.

Sudbery, P.E. (2011). Growth of *Candida albicans* hyphae. Nat. Rev. Microbiol. *9*, 737–748.

Sütterlin, C., Horvath, A., Gerold, P., Schwarz, R.T., Wang, Y., Dreyfuss, M., and Riezman, H. (1997). Identification of a species-specific inhibitor of glycosylphosphatidylinositol synthesis. EMBO J. *16*, 6374–6383.

Tanaka, S. (2004). Inositol Deacylation of Glycosylphosphatidylinositol-anchored Proteins Is Mediated by Mammalian PGAP1 and Yeast Bst1p. J. Biol. Chem. *279*, 14256–14263.

Tanaka, Y., Minami, Y., Mine, S., Hirano, H., Hu, C.D., Fujimoto, H., Fujii, K., Saito, K., Tsukada, J., van Kooyk, Y., et al. (1999). H-Ras signals to cytoskeletal machinery in induction of integrin-mediated adhesion of T cells. J. Immunol. Baltim. Md 1950 *163*, 6209–6216.

Tsukahara, K., Hata, K., Nakamoto, K., Sagane, K., Watanabe, N.-A., Kuromitsu, J., Kai, J., Tsuchiya, M., Ohba, F., Jigami, Y., et al. (2003). Medicinal genetics approach towards identifying the molecular target of a novel inhibitor of fungal cell wall assembly. Mol. Microbiol. *48*, 1029–1042.

Urbaniak, M.D., Crossman, A., Chang, T., Smith, T.K., van Aalten, D.M.F., and Ferguson, M.A.J. (2005). The N-Acetyl-D-glucosaminylphosphatidylinositol De-N-acetylase of Glycosylphosphatidylinositol Biosynthesis Is a Zinc Metalloenzyme. J. Biol. Chem. *280*, 22831–22838.

Vainauskas, S. (2003). A Conserved Proline in the Last Transmembrane Segment of Gaa1 Is Required for Glycosylphosphatidylinositol (GPI) Recognition by GPI Transamidase. J. Biol. Chem. *279*, 6540–6545.

Verma, S.D., Pal, N., Singh, M.K., Shweta, H., Khan, M.F., and Sen, S. (2012). Understanding ligand interaction with different structures of G-quadruplex DNA: evidence of kinetically controlled ligand binding and binding-mode assisted quadruplex structure alteration. Anal. Chem. *84*, 7218–7226.

Victoria, G.S., Kumar, P., and Komath, S.S. (2010). The *Candida albicans* homologue of PIG-P, CaGpi19p: gene dosage and role in growth and filamentation. Microbiol. Read. Engl. *156*, 3041–3051.

Victoria, G.S., Yadav, B., Hauhnar, L., Jain, P., Bhatnagar, S., and Komath, S.S. (2012). Mutual co-regulation between GPI-N-acetylglucosaminyltransferase and ergosterol biosynthesis in *Candida albicans.* Biochem. J. *443*, 619–625.

Vossen, J.H., Müller, W.H., Lipke, P.N., and Klis, F.M. (1997). Restrictive glycosylphosphatidylinositol anchor synthesis in cwh6/gpi3 yeast cells causes aberrant biogenesis of cell wall proteins. J. Bacteriol. *179*, 2202–2209.

Walther, A., and Wendland, J. (2003). An improved transformation protocol for the human fungal pathogen *Candida albicans*. Curr. Genet. *42*, 339–343.

Wang, D.-K., Liu, Y., Myers, E.J., Guo, Y.-M., Xie, Z.-D., Jiang, D.-Z., Li, J.-M., Yang, J., Liu, M., Parker, M.D., et al. (2015). Effects of Nt-truncation and coexpression of isolated Nt

domains on the membrane trafficking of electroneutral Na+/HCO3– cotransporters. Sci. Rep. *5*.

Wang, Y., Zou, H., Fang, H.-M., and Zhu, Y. (2010). Linking cellular actin status with cAMP signaling in *Candida albicans*. Virulence *1*, 202–205.

Watanabe, N. -a., Miyazaki, M., Horii, T., Sagane, K., Tsukahara, K., and Hata, K. (2012). E1210, a New Broad-Spectrum Antifungal, Suppresses *Candida albicans* Hyphal Growth through Inhibition of Glycosylphosphatidylinositol Biosynthesis. Antimicrob. Agents Chemother. *56*, 960–971.

Watanabe, R., Ohishi, K., Maeda, Y., Nakamura, N., and Kinoshita, T. (1999). Mammalian PIG-L and its yeast homologue Gpi12p are N-acetylglucosaminylphosphatidylinositol de-N-

acetylases essential in glycosylphosphatidylinositol biosynthesis. Biochem. J. *339 (Pt 1)*, 185–192.

Watanabe, R., Murakami, Y., Marmor, M.D., Inoue, N., Maeda, Y., Hino, J., Kangawa, K., Julius, M., and Kinoshita, T. (2000). Initial enzyme for glycosylphosphatidylinositol biosynthesis requires PIG-P and is regulated by DPM2. EMBO J. *19*, 4402–4411.

Weiner, M.P., Costa, G.L., Schoettlin, W., Cline, J., Mathur, E., and Bauer, J.C. (1994). Site-directed mutagenesis of double-stranded DNA by the polymerase chain reaction. Gene *151*, 119–123.

Wilson, R.B., Davis, D., and Mitchell, A.P. (1999). Rapid hypothesis testing with *Candidaalbicans* through gene disruption with short homology regions. J. Bacteriol. *181*, 1868–1874.

Wojtera-Kwiczor, J., Groß, F., Leffers, H.-M., Kang, M., Schneider, M., and Scheibe, R. (2013). Transfer of a Redox-Signal through the Cytosol by Redox-Dependent Microcompartmentation of Glycolytic Enzymes at Mitochondria and Actin Cytoskeleton. Front. Plant Sci. *3*.

Yadav, A., Singh, S.L., Yadav, B., and Komath, S.S. (2014a). Saccharomycescerevisiae Gpi2, an accessory subunit of the enzyme catalyzing the first step of

glycosylphosphatidylinositol (GPI) anchor biosynthesis, selectively complements some of the functions of its homolog in *Candida albicans*. Glycoconj. J. *31*, 497–507.

Yadav, B., Bhatnagar, S., Ahmad, M.F., Jain, P., Pratyusha, V.A., Kumar, P., and Komath, S.S. (2014b). First step of glycosylphosphatidylinositol (GPI) biosynthesis cross-talks with ergosterol biosynthesis and Ras signaling in *Candida albicans*. J. Biol. Chem. *289*, 3365–3382.

Yan, B.C., Westfall, B.A., and Orlean, P. (2001). Ynl038wp (Gpi15p) is the *Saccharomyces cerevisiae* homologue of human Pig-Hp and participates in the first step in glycosylphosphatidylinositol assembly. Yeast Chichester Engl. *18*, 1383–1389.

Yapar, N. (2014). Epidemiology and risk factors for invasive candidiasis. Ther. Clin. Risk Manag. 95.

Zhao, R., Leung, E., Grüner, S., Schapira, M., and Houry, W.A. (2010). Tamoxifen enhances the Hsp90 molecular chaperone ATPase activity. PloS One *5*, e9934.

Zhou, X., Zhang, H., Li, G., Shaw, B., and Xu, J.-R. (2012). The Cyclase-Associated Protein Cap1 Is Important for Proper Regulation of Infection-Related Morphogenesis in Magnaporthe oryzae. PLoS Pathog. *8*, e1002911.

Zhu, Y., Fraering, P., Vionnet, C., and Conzelmann, A. (2005). Gpi17p does not stably interact with other subunits of glycosylphosphatidylinositol transamidase in *Saccharomyces cerevisiae*. Biochim. Biophys. Acta *1735*, 79–88.

Zhu, Y., Fang, H.-M., Wang, Y.-M., Zeng, G.-S., Zheng, X.-D., and Wang, Y. (2009). Ras1 and Ras2 play antagonistic roles in regulating cellular cAMP level, stationary-phase entry and stress response in *Candida albicans*. Mol. Microbiol. *74*, 862–875.

Zou, H., Fang, H.-M., Zhu, Y., and Wang, Y. (2009). Candida albicans Cyr1, Cap1 and G-actin form a sensor/effector apparatus for activating cAMP synthesis in hyphal growth: A sensor/effector for *C. albicans* hyphal growth. Mol. Microbiol. *75*, 579–591.

(1996). Lipids of pathogenic fungi /: edited by Rajendra Prasad, Mahmoud A. Ghannoum (Boca Raton: CRC Press).

(2014). Ras superfamily small g proteins:: biology and mechanisms. 1: General features, signaling (Cham: Springer).

Ph.D Thesis

Kumar. P., (2010). A study of proteins involved in the first step of GPI anchor biosynthesis in *Candida albicans*. JNU, New Delhi, India.

Jain. P., (2016). Interaction between Ras signaling and GPI anchor biosynthesis in *Candida albicans*. JNU, New Delhi, India.

Victoria. S., (2010). Investigating the role of PIG-P in GPI anchor biosynthesis of*Candida albicans*. JNU, New Delhi, India.

Yadav. B., (2013). Study of N-acetylglucosaminyltransferase complex in GPI anchor biosynthesis: Role of *CaGPI1* and *CaGPI2* in *Candida albicans*. JNU, New Delhi, India.

Yadav. U., (2016). Functional characterization of *Candida albicans*GPI12. JNU, New Delhi, India.

Websites

Candida Genome Database*(www.candidagenome.org)*

NCBI BLAST*(https://blast.ncbi.nlm.nih.gov)*

Publications

Yadav, B., Bhatnagar, S., Ahmad, M.F., Jain, P., **Pratyusha, V.A.**, Kumar, P., and Komath, S.S. (2014). First step of glycosylphosphatidylinositol (GPI) biosynthesis cross-talks with ergosterol biosynthesis and Ras signaling in *Candida albicans*. J. Biol. Chem. *289*, 3365–3382.